12-2012

Post-transcriptional Regulation of Mammalian Gene Expression in Non-coding Region of Target RNA

Jing Lin

Post-transcriptional Regulation of Mammalian Gene Expression in Non-coding Region of Target RNA

By
Jing Lin, M.S.

APPROVED:

_____
Lin Ji, Ph.D.
Supervisory Professor

_____
Jack A. Roth, M.D.

_____
Bingliang Fang, M.D. Ph.D.

_____
Wei Zhang, Ph.D.

_____
Xiaofeng Le, M.D. Ph.D.

Approved:

_____
Dean, The University of Texas,
Graduate School of Biomedical Sciences at Houston

Post-transcriptional Regulation of Mammalian Gene Expression in Non-coding Region of Target RNA

A
DISSERTATION

Presented to the Faculty of

The University of Texas

Health Science Center at Houston

and

The University of Texas

M. D. Anderson Cancer Center

Graduate School of Biomedical Sciences

in Partial Fulfillment

of the Requirements

for the degree of

DOCTOR OF PHILOSOPHY

By

Jing Lin, M.S.

Houston, Texas

December, 2012

DEDICATION

To my family:

For their love and support

ACKNOWLEDGEMENTS

First of all, I would like to thank my mentor, Dr. Ji Lin, for giving me an opportunity to work on such exciting and important projects in his laboratory, and especially for his constant support and guidance during my Ph.D. training. Dr. Ji has constantly challenged me to think logically and hone my presentation skills; both of these lessons have benefited me a great deal. Thanks very much for Dr. Ji, I will forever appreciate.

I would like to thank Dr. Jack Roth for scientific inspiration in my academic career. When I first joined Department of Thoracic and Cardiovascular Surgery, I was still naive in regard to lung cancer biology. After 5 years of training, I have harvested not only my own scientific knowledge but also a sense of what constitutes excellent science. Since joining his Monday seminar and Wednesday lab meeting, I have been inspired and cheered by every speech. In addition, I look forward to another success for post-doctor training under his guidance.

Special thanks to Kai Xu for all the assistance and experiments discussions. He has encouraged my scientific development and shared every aspect of science with me.

I would also like to thank my committee members, my Advisory committee: Dr. Bingliang Fang, Dr. Paul Chiao, Dr. Ralph B Arlinghaus, as well as my Supervisory committee: Dr. Wei Zhang and Dr. Xiaofeng Le, for their constructive suggestions during each of my committee meetings. I would also like to thank all the staff of GSBS for their excellent work in making GSBS a wonderful training environment.

I must also thank all the past and present members in Dr. Ji's laboratory, including Bingbing Wang, Gitanjali Jayachandran, Shaoyu Yan, Hongjiang Wang, Sakai Ryo, Watanabe Yuichi, Qing Liu, Kuroda Shinji and Wismach Marnie for their friendship and

help in the past several years. In addition, I would like to thank Wang Li, Shaopin Ruo, Shuhong Wu, Bingbing Dai, Jieru Meng, Humberto Lara-Guerra in our department.

Last but certainly not least, I would like to extend my deepest appreciation to my beloved family, my parents and my lovely son. Especially thanks very much for my husband, Wenjun Ying, who quit his job in China and came to USA to accompany me to finish my Ph.D. study. Without his support, I cannot have a wonderful 5 year Ph.D. journey. In addition, I must thank my parents for their endless love and encouragement

Post-transcriptional Regulation of Mammalian Gene Expression in Non-coding Region of Target RNA

Publication No. _____

Jing Lin, M.S.

Supervisory Professor: Lin Ji, Ph.D.

Tumor Suppressor Candidate 2 (TUSC2) is a novel tumor suppressor gene located in the human chromosome 3p21.3 region. TUSC2 mRNA transcripts could be detected on Northern blots in both normal lung and some lung cancer cell lines, but no endogenous TUSC2 protein could be detected in a majority of lung cancer cell lines. Mechanisms regulating TUSC2 protein expression and its inactivation in primary lung cancer cells are largely unknown. We investigated the role of the 5'- and 3'-untranslated regions (UTRs) of the TUSC2 gene in the regulation of TUSC2 protein expression. We found that two small upstream open-reading frames (uORFs) in the 5'UTR of TUSC2 could markedly inhibit the translational initiation of TUSC2 protein by interfering with the "scanning" of the ribosome initiation complexes. Site-specific stem-loop array reverse transcription-polymerase chain reaction (SLA-RT-PCR) verified several micoRNAs (miRNAs) targeted at 3'UTR and directed TUSC2 cleavage and degradation.

In addition, we used the established let-7-targeted high mobility group A2 (Hmga2) mRNA as a model system to study the mechanism of regulation of target mRNA by miRNAs in mammalian cells under physiological conditions. There have been no evidence of direct link between mRNA downregulation and mRNA cleavages mediated by miRNAs. Here we showed that the endonucleolytic cleavages on mRNAs were

initiated by mammalian miRNA in seed pairing style. Let-7 directed cleavage activities among the eight predicted potential target sites have varied efficiency, which are influenced by the positional and the structural contexts in the UTR. The 5' cleaved RNA fragments were mostly oligouridylated at their 3'-termini and accumulated for delayed 5'–3' degradation. RNA fragment oligouridylation played important roles in marking RNA fragments for delayed bulk degradation and in converting RNA degradation mode from 3'–5' to 5'–3' with cooperative efforts from both endonucleolytic and non-catalytic miRNA-induced silencing complex (miRISC). Our findings point to a mammalian miRNA-mediated mechanism for the regulation of mRNA that miRNA can decrease target mRNA through target mRNA cleavage and uridine addition.

TABLE OF CONTENTS

LIST OF FIGURES

ABBREVIATIONS

AMOs	anti-miRNA oligonucleotides
ASOs	antisense oligonucleotides
BRCA1	breast cancer 1
EMT	epithelial-to-mesenchymal transition
GFP	green fluorescent protein
HBE	human bronchial epithelial cell
Hmga2	high mobility group A2
Hox	human homeobox loci
IRES	ribosome entry site
LNAs	locked nucleic acids
miRISC	miRNA-induced silencing complex
miRNA	microRNA
mRNA	messenger RNA
mRNP	messenger ribonucleoprotein
ncRNA	non-coding RNA
NSCLC	non-small cell lung cancer cell
NTS	nucleotides
PCR	polymerase chain reaction
PDGFR	platelet-derived growth factor receptors
piRNA	PIWI-interacting RNA
pre-miRNA	precursor microRNA

pri-miRNA	primary microRNA
RACE	rapid amplification of cDNA ends
RE	restriction enzyme
RT	reverse transcriptase reaction
SLA-RT-PCR	stem-loop array reverse transcription polymerase chain reaction
snoRNAs	small nucleolar RNAs
TBE	tris-borate-EDTA
TUSC2	tumor suppressor candidate 2
TUTase	terminal uridylyl transferase
uORF	upstream open-reading frames
UTR	un-translated regions of transcripts

Chapter 1. Overview

RNAs are divided into two classes: messenger RNAs (mRNAs), which are translated into proteins, and non-coding RNAs (ncRNAs), which does not encode protein. However, this does not mean that such ncRNAs do not contain information nor have function. Although it has been traditionally thought that most important genetic information is translated to proteins, recent evidence suggests that the majority of the genomes is transcribed into ncRNAs. The total fraction of protein-coding transcripts is about 1.4% in humans, whereas about 27% is transcribed as introns and UTRs (untranslated regions) but not translated [1, 2], which further increase the space for potential novel ncRNAs.

Most genomic DNA can be regulated at either the transcriptional level, controlling whether a gene is transcribed or not, or at the post-transcriptional level, controlling the fate of the transcribed RNA molecules, including their stability, the efficiency of their translation and their subcellular localization. The past few years have seen a rapid expansion in the identification and characterization of mRNA regulatory elements in UTRs.

1.1 Post-transcriptional regulation of gene expression in UTRs of mRNA

UTRs play crucial roles in the post-transcriptional regulation of gene expression, which control mRNA stability [3], translation efficiency [4], and subcellular localization [5]. The turnover of mRNAs is a crucial step in post-transcriptional regulation of gene expression. The rate of mRNA synthesis is not the sole determinant of mRNA, and the

mRNA decay rate is also a major determinant. Several mechanisms have been proposed to describe how mRNA degradation takes place: decay can be preceded by shortening or removal of the poly (A) tail at the 3' end or by removal of the m7G cap at the 5' end [6]. The turnover of an mRNA is widely regulated by cis-acting elements located in the 3' UTR, such as the AU-rich elements (AREs), which promote mRNA decay in response to cell signals. Degradation of mRNAs can also take place by endonuclease activity. Endonucleolytic cleavage has been identified in the 3' UTR region which is targeted by miRNAs. It has been recently reported that let-7 miRNA results in degradation of lin-41 target mRNA in *C. elegans* [7].

UTRs have a fundamental role in the control of RNA subcellular location, which is particularly important during organism development. In many cases, mRNAs are localized as ribonucleoprotein complexes along with proteins of the translational apparatus, thus ensuring efficient localized translation. One example is 21-nucleotide element in the 3' UTR of MBP mRNA, which are required for MBP mRNA transport and localization [8].

In addition, UTRs play an important role in controlling mRNA translation efficiency, in which 5’ UTR play a major role. Several cis-acting elements within 5’UTR, such as upstream ORFs (uORFs), secondary structures or binding by specific proteins could be involved in translation efficiency regulation. Recently, it was demonstrated that uORFs reduce protein translation initiation levels by 30-80 %. After translation of the uORFs, the large (60S) ribosomal subunit will be detached and the 40S small ribosomal subunit may resume scanning, reinitiating with impaired translation efficiency of the main ORF. An example has been reported for the yeast transcription factors GCN4 and YAP1 down-

regulation by uORFs [9]. Another alternative mechanism for translation initiation, which allows translation of the RNAs in a cap-independent manner, is an internal ribosome entry site (IRES). Cell may use IRES to increase translation of certain proteins during mitosis. In mitosis, the cell dephosphorylates eIF-4E so that it has little affinity for the 5'cap. As a result, the pre-initiation mRNA loop is not formed, and the translational machinery is diverted to IRES within the mRNA. Many proteins involved in mitosis are encoded by IRES mRNA.

1.2 Biogenesis and Functions of miRNA

miRNAs are small ncRNAs that have been shown to function as key regulators of gene expression and modulate many crucial biological processes, such as cell proliferation, differentiation, and apoptosis in multicellular organisms [12-14]. miRNA genes are transcribed as long primary microRNA (pri-miRNA), which is processed by Drosha and its co-factor DGCR8 to generate precursor miRNA (pre-miRNA). Pre-miRNA is rapidly exported to the cytoplasm by exportin-5 in a Ran–GTP-dependent manner, where it is cut by Dicer to generate a mature approximately ~22 nucleotides long miRNA [10, 11]. Mature miRNAs are incorporated into argonaute proteins as guide sequence in the assembling of miRNA-induced silencing complex (miRISC) for target-specific gene silencing [15].

Small RNA Lin-4 was first reported miRNA as gene regulatory molecule in 1993 [16]. Plant miRNAs match their mRNA target complementarily to ensure irreversible cleavage of target mRNAs and this is thought to be the predominant mode of miRNA mechanism in plants [17]. In mammalian cells, miRNA: target pairing are rare and miRNA

recognizes mRNA targets with much shorter base pairs usually located at highly conserved nucleotides at position 2 -7 of miRNA 5' termini [18]. In mammalian cells, the mechanistic details for miRNAs in repressing protein synthesis are still poorly understood. miRNAs can affect both the translation and stability of mRNAs, but the results from studies conducted in different laboratories have often been contradictory. Earlier studies suggest that the miRNA-induced gene expression interference is through binding to the 3'UTR of target mRNA and repressing translation. Recent studies suggest that the mammalian miRNAs predominantly act to decrease target mRNA levels. However, no direct evidence for miRNA-mediated target mRNA cleavage and degradation has been demonstrated in mammalian cells [19]. The detection methods used in those studies, i.e., 5'-RACE, PARE, Ribosome profiling, lacked the necessary sensitivity to address the short lived nature of mRNA intermediates in detail especially when there were only small portion of mRNA cleavages. With improved detecting methods, those few cases of miRNA cleavages could just be the tip of iceberg.

Animal AGO proteins are essential for miRNA-directed target mRNA destabilization, but insufficient for silencing. The study of the mechanism of miRNA-mediated mRNA destabilization has been demonstrated in *D. melanogaster*. P‑body protein GW182, which interacts with the miRNP Argonaute1, is a key factor that marks mRNAs for decay [20, 21].

The CCR4-NOT complex and PAN2-PAN3 complex are two major enzyme complex, which are responsible for mRNA deadenylation. Depletion of CCR4–NOT complex prevents the decay-promoting activity of GW182, suggesting that GW182 plays a role in recruiting CCR4–NOT to destabilize mRNAs [22]. It has also been reported that GW182

recruits the PAN2-PAN3 deadenylase complex through PAM2 motif [23]. In addition, accelerated deadenylation results in a miRNA-induced degraded mRNAs in mammalian cells. Widespread miRNA-mediated deadenylation of mRNAs occurs during zebrafish embryogenesis, in which miR‑430 facilitates the destabilization of hundreds of mRNAs by inducing their deadenylation and subsequent decay at the onset of zygotic transcription [24, 25].

1.3 Roles of non-coding RNAs in Regulation of Gene expression

There are some other ncRNAs, which play important roles in cells. piRNAs (PIWI-interacting RNAs) are ncRNAs of 24–30 nt in length, binding the PIWI subfamily of AGO proteins that are involved in target RNA repression. The complex, formed by piRNAs and PIWI proteins, suppresses transposable element expression and mobilization. snoRNAs (small nucleolar RNAs) are 60–300 nt in length ncRNAs, which guide the site-specific modification of nucleotides in target RNAs through short regions of base-pairing. SnoRNAs are composed of two major classes, the box C/D snoRNAs which guide 2'-O-ribose-methylation, and the box H/ACA snoRNAs which guide pseudouridylation of target RNAs [26, 27].

There is still considerable debate as to whether ncRNAs are functional or merely some kind of 'transcriptional noise'. It appears that the human genome express an enormous repertoire of ncRNAs, which had been previously overlooked. We may have fundamentally misunderstood the nature of genetic programming. Although the functions of these ncRNAs are likely to be varied, the evidences strongly suggest that their main role is to regulate and direct the complex pathways in cells [28].The extent of ncRNAs

conservation is also much higher than mRNAs, perhaps as high as 10% [29]. This conservation includes ultra-conserved sequences [30] and long transposon-free regions that have remained refractory to transposon insertions during evolution [31]. There are probably many other functions of ncRNAs awaiting discovery. For example, the observation that many ncRNAs are located in the cytoplasm suggests that they might have undiscovered roles. There is increasing interest in the potential involvement of ncRNAs in disease development, owing to aberrant function of ncRNAs in differentiation and developmental processes. For example, an antisense ncRNA transcribed from the p15 tumor suppressor locus regulate local heterochromatin and DNA methylation status, thereby down-regulating p15 expression, which is involved in oncogenesis in leukemia [40].

1.4 Therapeutic Applications of miRNAs and miRNA-target Sites in Human Cancers

miRNA is the most widely studied group of ncRNAs in human cancer. miRNA expression profiles differ between normal cells and tumor cells, acting as oncogenes or tumor suppressors [41]. One of the first reported associations between miRNAs and cancer was miR‑15 and miR‑16 dysregulation in most B cell chronic lymphocytic leukaemias as a result of chromosome 13q14 deletion [42]. Another intriguing example is miR-200. CpG island hypermethylation-associated silencing of miR-200 in tumors up-regulate the zinc finger E-box-binding homeobox ZEB1 and ZEB2, which, in turn, leads to a down-regulation of E-cadherin, promoting epithelial-to-mesenchymal transition (EMT) in cancer [43].

Antisense oligonucleotides (ASOs) are therapeutically widely used to inhibit miRNA function. ASOs inhibit miRNA targets based on base-pair complementarity. There are three main classes of ASOs, including locked nucleic acids (LNAs), anti-miRNA oligonucleotides (AMOs) and antagomirs with chemical modifications to increase stability and efficacy [44]. For example, the intravenous injection of antagomirs targeting miR-10b prevents the onset of metastasis, suppressing dissemination to the lungs in the mouse [45]. Another recent study reported the use of 'miRNA replacement therapy' strategy, restoring miR-26a expression in hepatocellular carcinoma. miR-26a was delivered by an adenoviral vector in a mouse model of hepatocellular carcinoma, resulting in suppression of proliferation and induction of apoptosis, thereby inhibiting cancer progression [46].

In addition, certain features in UTR have been approved to be associated with tumor genesis. BRCA1 (breast cancer 1) acts as a tumor suppressor and is involved in cell-cycle checkpoints, apoptosis and DNA damage repair. BRCA1 protein expression is controlled by an alternative 5' UTR. BRCA1 has two promoters (α and β), encoding two 5' UTR differing in the length of the 5'UTR.The longer 5'UTR is found in breast cancer tissues, whereas the shorter 5'UTR is found in normal breast tissues. The longer 5'UTR, being more structured and having additional uAUGs, is translated 10-fold less efficiently than the shorter 5'UTR. Thus BRCA1 expression is inhibited in breast cancers by longer 5'UTR. Therefore, BRCA1 promoter α (producing longer 5'UTR) can be an effective target in breast cancer therapy [47].

There are many well characterized examples of UTRs that act as regulatory ncRNAs in disease development. Another intriguing example is the ncRNA HSR1 (heat-shock RNA-

1), which forms a complex with HSF1 (heat-shock transcription factor 1), enabling the transcription factor to induce expression of heat-shock proteins during the cellular heat-shock response [23]. UTRs are the sensors of miRNAs by base-pairing mechanism. For instance, SLITRK1 mRNA 3'UTR sequence variants in the binding site for the miR-189 have been shown to be associated with Tourette's syndrome.

1.4 The purpose of this study

Interests in the contribution of ncRNAs to the genesis and progression of human disorders are booming. However, there are still huge gaps in our study of ncRNAs, including their function and mechanisms by which ncRNAs exert pathological effects. It will be crucial to understand the mechanism how miRNA regulation of target mRNA repression, which is the basis to miRNA research in mammalian cells.

One important challenge will be to identify all functional ncRNAs that are encoded in the human genome. What is required, and is currently developing, is the application of unbiased techniques, such as the Encyclopedia of DNA Elements (ENCODE) project, which will identify all functional elements in the human genome [48]. Bioinformatics tools for identifying potentially functional ncRNAs will also be important. Because ncRNAs fold into complex secondary structures that are crucial to their function, sequence-based alignments alone might not be enough to identify ncRNAs. A number of algorithms have been developed to identify potentially functional ncRNAs (for example, RNAfold, Pfold, CMFinder and Foldalign). To some degree, the studies of ncRNAs have been delayed, which is because of the lack of appropriate laborious techniques to identify these ncRNAs systematically. Identification of novel ncRNA occurred rather by chance than by systematic screens.

With respect to disease, understanding the precise biological roles of ncRNAs is a key challenge. For example, mouse model is a good model to study the specific function of ncRNAs. A recent study of mouse model that conditionally express miR-21, revealed that miR-21 as a genuine oncogenes [49]. Biochemical tools, such as antagomirs, have been useful in elucidating the function of miRNAs, however, having its limitations. Some other techniques have been developed, for example, rapid amplification of cDNA ends (RACE) method was used to define the origin of transcription of T-UCRs, but the process is very time consuming [50]. Therefore, advanced molecular biological and biochemical tools and methods are much needed to efficiently and accurately identify non-coding region RNA. Technical breakthroughs can bridge the gap between ncRNAs knowledge and knowledge-based application in disease diagnosis and treatment.

In our study, we tried to study the transcriptional regulation of TUSC2. TUSC2 is a novel tumor suppressor gene located in the human chromosome 3p21.3 region. TUSC2 mRNA transcripts could be detected on Northern blots in both normal lung and some lung cancer cell lines, but no endogenous TUSC2 protein could be detected in a majority of lung cancer cell lines. Mechanisms regulating TUSC2 protein expression and its inactivation in primary lung cancer cells are largely unknown. We investigated the role of the 5'-UTR and 3'-UTR of the TUSC2 gene in the regulation of TUSC2 protein expression, as TUSC2 have very conservative and complex UTRs. We found that two small uORFs in the 5'UTR of TUSC2 could markedly inhibit the translational initiation of TUSC2 protein by interfering with the "scanning" of the ribosome initiation complexes. In addition, there are miR-98, miR-93 and miR-197 directed cleavage sites on TUSC2 3'TUR, which cause TUSC2 mRNA degradation.

In addition, we tried to study the mechanistic details for miRNAs in repressing protein synthesis. The established let-7 miRNA -targeted Hmga2 mRNA was used as a model system to study the regulation of target mRNA by miRNAs in mammalian cells under physiological conditions. In our study, we pointed out a direct link between mRNA down-regulation and mRNA cleavages mediated by miRNAs, which were confused in many years regarding miRNA mechanism study. The endonucleolytic cleavages on Hmga2 target mRNAs were initiated by let-7 miRNA in seed pairing style have been detected by our new developed SLA-RT-PCR. After that, the 5' cleaved RNA fragments were mostly oligouridylated at their 3'-termini and destroyed by mRNA 5'–3' degradation. These findings warrant further investigation to identify the precise miRNA targets in mammalians in endogenous context.

Chapter 2. Regulation of Novel Tumor Suppressor Gene TUSC2 Expression in Human Lung Cancer Cells

2.1 Introduction

2.1.1 Lung Cancer and tumor suppressor gene

Lung cancer is the most common cancer in the world, with an estimate of 1.35 million new cases per year. Lung cancer kills more than 1.18 million patients each year, as the leading cause of cancer death for both men and women. More than 85 % of lung cancers are caused by tobacco smoke [51-53]. Studies of lung cancers have shown that genetic alterations in the short arm of chromosome 3p are among the most frequent and earliest genomic abnormalities. Moreover, the 3p21.3 region has been frequently detected in smoke-damaged pre-neoplastic lesions. These findings suggest that one or more genes in 3p21.3 region are tumor suppressor genes as molecular gatekeepers in lung cancers. TUSC2 gene, also called FUS1, is one candidate tumor suppressor gene, located in 3p21.3 region [54-55]. Wild-type TUSC2 protein induces tumor cells G1 growth arrest and apoptosis, suppresses tumor growth and inhibits lung metastases in mouse model. TUSC2 induces apoptosis through the activation of the mitochondria-dependent and Apaf-1 associated pathways and inhibits the tyrosine kinases function including EGFR, PDGFR and AKT [56-60]. Enforced expression of TUSC2 in H1299 cells inactivated c-Abl and its tyrosine kinase [61]. It also showed that expression of TUSC2 sensitized the response of lung cancer cells to cisplatin, which was associated with the down-regulation of MDM2 and increase of p53 [62].

Squamous metaplasia and dysplasia express significantly lower levels of TUSC2 than normal and hyperplastic bronchial epithelia. Loss or reduction of TUSC2 protein expression is associated with worse overall patient survival [60]. TUSC2-nanoparticles is used in Phase I clinical trial for patients with chemotherapy refractory stage IV lung cancers at the University of Texas M.D. Anderson Cancer Center. TUSC2 mRNA transcripts could be detected on Northern blots in both normal lung and some lung cancer cell lines, but no endogenous TUSC2 protein could be detected in a majority of lung cancer cell lines. Only a few mutations in TUSC2 gene are found in human lung cancers, and its promoter methylation is a rare phenomenon. Uno *et al.* showed TUSC2 is a myristoylated protein and loss of myristoylation at the N-terminus cause TUSC2 protein rapidly degradation. The defect of the TUSC2 protein was detected in primary lung cancers [58]. However, mechanisms regulating TUSC2 protein expression and its inactivation in lung cancers are largely unknown. Therefore, elucidation of mechanisms regulating TUSC2 protein expression is important to control the loss of TUSC2 in the early pathogenesis of lung cancer.

2.1.2 TUSC2 protein expression regulation

The regulatory events that govern gene expression are implemented at three levels: transcription, post-transcription, and translation. The normal TUSC2 mRNA expression in tumor cells suggests translational control of TUSC2 mRNA might inactivate TUSC2. Although many features of mRNA can contribute to its translation, control elements are mostly found in the un-translated regions of transcripts (UTRs), because UTRs are under less pressure of sequence conservation and easily to form regulatory elements [63]. It is

widely known that 5'UTR is responsible for translation initiation through start-site consensus sequence as well as upstream AUGs [64]. 3'UTR regulates transcripts stability and localization, which contains numerous binding sites for regulatory factors [65]. A highly conserved and long complex TUSC2 UTRs suggests UTRs might play an important role in regulation of TUSC2 protein expression. Here, we investigated the role of the TUSC2 UTRs in the regulation of TUSC2 protein expression and detected the regulatory mechanisms lead to the loss or reduction of TUSC2 expression in lung cancer cell lines.

2.2 Methods and Materials

2.2.1 Cell lines and cell cultures

The human non-small cell lung cancer cell (NSCLC) line H1299, A549, H322 and cervix Hela cells were obtained from American Type Culture Collection. H1299, A549, H322 and Hela cells were grown in RPMI 1640 supplemented with 10% fetal bovine serum in an atmosphere of humidified air containing 5% CO_2. Normal human bronchial epithelial (HBE) cells were obtained from Dr. John Minna's laboratory. HBE cells were grown in Keratinocyte-SFM medium (Invitrogen, Carlsbad, CA).

2.2.2 Preparation of plasmids

A 1772 nucleotides sequence region containing TUSC2 coding region bounded by 5'UTR and 3'UTR was cloned into pKGB2 plasmid. Following the same construction procedure, 433 nucleotides (nts) 5'UTR-TUSC2 coding region, 1672 nts TUSC2 coding region-3'UTR, 333 nts TUSC2 was cloned into each pKGB2 construct. We constructed

four plasmids with the same backbone and different translated regions as follows: 5'UTR-TUSC2-3'UTR, 5'UTR-TUSC2, TUSC2-3'UTR and TUSC2. **Figure** 1 showed schematic drawing of the four plasmids. All constructs were confirmed by DNA sequencing.

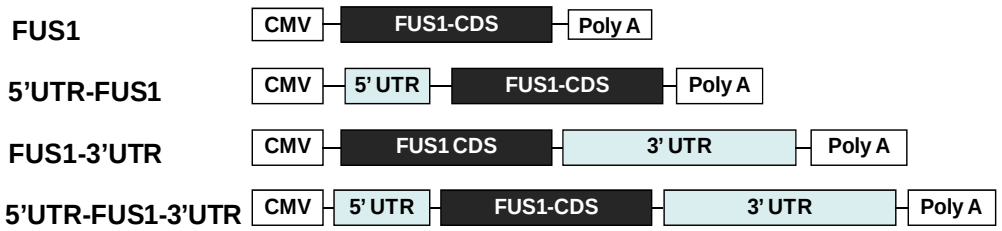

Figure 1. Effects of UTRs of TUSC2 mRNA gene and protein expression in human NSCLC H1299 and normal HBE cells. Schematic representations of TUSC2 expressing constructs with or without intrinsic 5'UTR and 3'UTR. TUSC2 expression plasmid constructs contain an expression cassette with a CMV promoter-FUS1 CDS-BGH polyA signal (Reproduced with permission of BBRC 410(2):235-241).

2.2.3 Plasmid transfection

Cells were plated and cultured overnight, and then transfected with specified expression vectors using DOTAP: cholesterol - encapsulated plasmid DNA nanoparticles. In brief, 2 μL DOTAP: cholesterol reagent and 2 μg plasmid DNA were mixed, and the mixture was added to each well in a six-well plate and incubated for indicated days. The transfection efficiency was assessed by a parallel transfection with an equal amount of green fluorescent protein (GFP)-expressing plasmid vector.

2.2.4 RNA isolation

For total RNA preparation, cells were grown on 6-well plates and approximately 2 x 10^6 cells were used to isolate the total RNA using the TRIzol reagent (Life Technologies,

Grand Island, NY) and phenol:chloroform extraction and ethanol precipitation according to the manufacturer's protocol. The isolated total RNA was stored in 70% ethanol at -80°C.

2.2.5 Reverse-transcription and quantitative Real-time PCR

RNeasy Mini kit was used to isolate total RNA. RNA was treated with DNase I and was reverse-transcribed using High Capacity cDNA Reverse Transcription Kit. Quantitative real-time PCR was performed in triplicate for each reaction. Negative control group using samples without reverse-transcribed was used to see if there is any DNA contaminated in RNA isolation. Melting curve analysis confirmed a single PCR product in each reaction. The nucleotide sequence of the primers as follows:

TUSC2 sense primer: 5'-TCAGAGGCAGCAGGAGCTGA-3', TUSC2 anti-sense primer :5'-CATAGAACATAGAGCCGCGG.

GAPDH sense primer: 5'-TGCACCACCAACTGCTTAGC-3', GAPDH anti-sense primer: 5'-GGCATGGACTGTGGTCATGAG.

GFP sense primer: 5'-TGAGCAAGGGCGAGGAGCTGTT-3', GFP anti-sense primer: 5'- CACGCTGAACTTGTGGCCGT-3'.

2.2.6 Western blotting assay

Cell lysates were prepared by incubating cells in lamin/urea buffer on ice, and centrifuged at 13,000 rpm for 10 min at 4°C. 50 μg cell lysate of each treatment were

resolved by SDS-PAGE and transferred onto a polyvinylidene difluoride membrane. TUSC2 protein was detected with rabbit anti-TUSC2 antibody. The following monoclonal antibodies were used: anti-green fluorescent protein (GFP) antibody and anti-β-actin antibody (Clontech, CA).

2.2.7 Secondary structure prediction of RNA segments

The lowest free-energy secondary structure for TUSC2 RNA was predicted by RNAfold software (www.tbi.unvivie.ac.at).

2.3 Results

2.3.1 Expression of TUSC2 is repressed by its UTR

To determine the UTR regulation for TUSC2 expression, we transfected H1299 cells and HBE-KTR cells with four plasmids, which have the same backbone and different translated region including TUSC2, 5'UTR-TUSC2, TUSC2-3'UTR, 5'UTR-TUSC2-3'UTR. In H1299 and HBE-KTR cell, UTRs down-regulate TUSC2 mRNA expression significantly ($P<0.05$). In H1299 cell, compared with the transcripts from construct only carrying TUSC2 coding sequence, the TUSC2 transcript level decreased significantly 3-fold from 5'UTR-TUSC2 construct ($P<0.05$) and decreased significantly 10-fold from TUSC2-3'UTR construct ($P<0.05$). In HBE-KTR cell, the TUSC2 transcript level decreased about 2-fold from 5'UTR-TUSC2 construct and decreased significantly 4-fold from TUSC2-3'UTR construct ($P<0.05$) (**Figure** 2). These observations indicated that

5’UTR and 3’UTR decreased the abundance of TUSC2 transcripts, which was more significant in tumor cells than in normal cells.

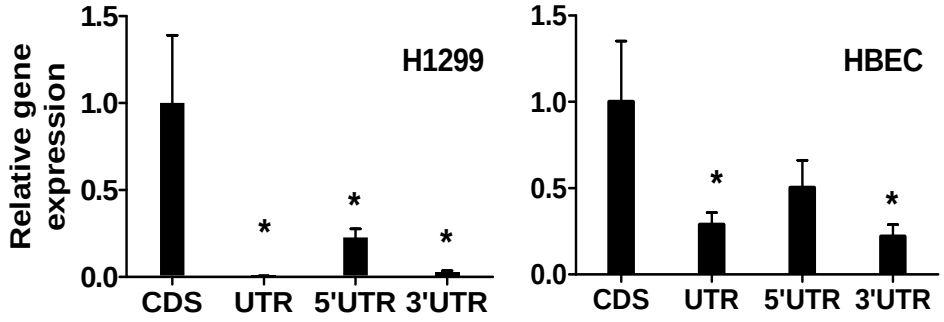

Figure 2. Effects of UTR of TUSC2 mRNA gene expression in human NSCLC H1299 and normal HBE cells. Real-time PCR analysis for effects of TUSC2 5’- and 3’-UTR on the TUSC2 mRNA expression in HBE and H1299 cells. In both cases the TUSC2 RNA expression for cells transfected with TUSC2 expression plasmid without UTR was set to 1. TUSC2 relative gene expressions were normalized to GFP levels. * means $P< 0.05$, error bars denote standard error. (Reproduced with permission of BBRC 410(2):235-241)

After 48h transient transfection, the western blot results showed that both 5’UTR and 3’UTR down-regulated TUSC2 protein expression. 3’UTR inhibitory effect showed more significant in tumor cell line H1299 than in normal cell line HBE-KTR, which is correlated with mRNA transcripts changes regulated by 3’UTR (**Figure** 3). A band close to molecular weight of TUSC2 was observed, however, this is a nonspecific band as it was detected in H1299 which cannot express TUSC2. Thus studies using this TUSC2 antibody should be interpreted with caution.

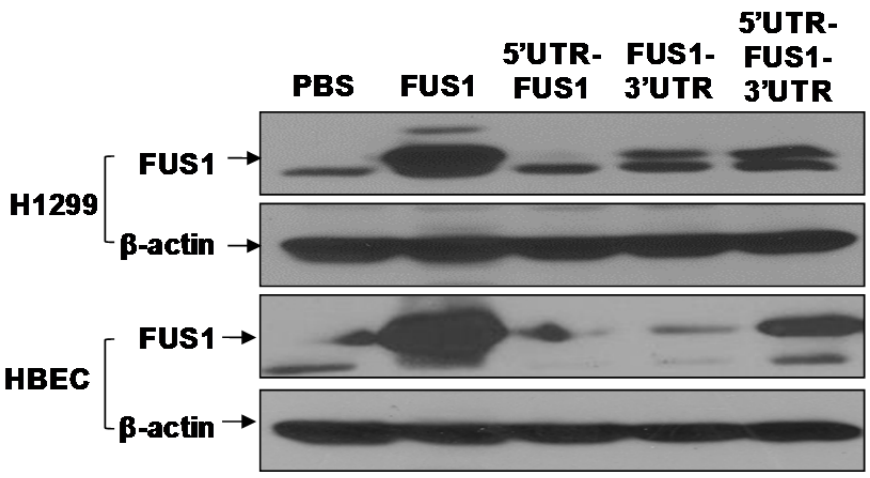

Figure 3. Effects of UTRs on FUS1 protein expression in H1299 and HBE cells by Western-blot analysis. Western blotting analysis for TUSC2 protein expression in HBE and H1299 cells transfected with TUSC2 expression plasmids with or without UTRs. (Reproduced with permission of BBRC 410(2):235-241)

To further confirm these findings, we investigated whether the TUSC2 UTRs exert a similar effect on the translation of GFP. We cloned TUSC2 5'UTR and 3'UTR into GFP reporter plasmid to test regulation of TUSC2 UTRs on GFP translation. H1299 cells were transiently co-transfected with the plasmids carrying GFP coding region with or without TUSC2 UTRs and CMV promoter-RFP plasmid. CMV promoter-RFP plasmid was added to test if plasmid transfection efficiency was the same in these two groups. 48 h later, the presence of TUSC2 UTRs significantly inhibited GFP expression, confirming that TUSC2 UTRs have sequence or secondary structure element inhibition on gene translation (**Figure 4**).

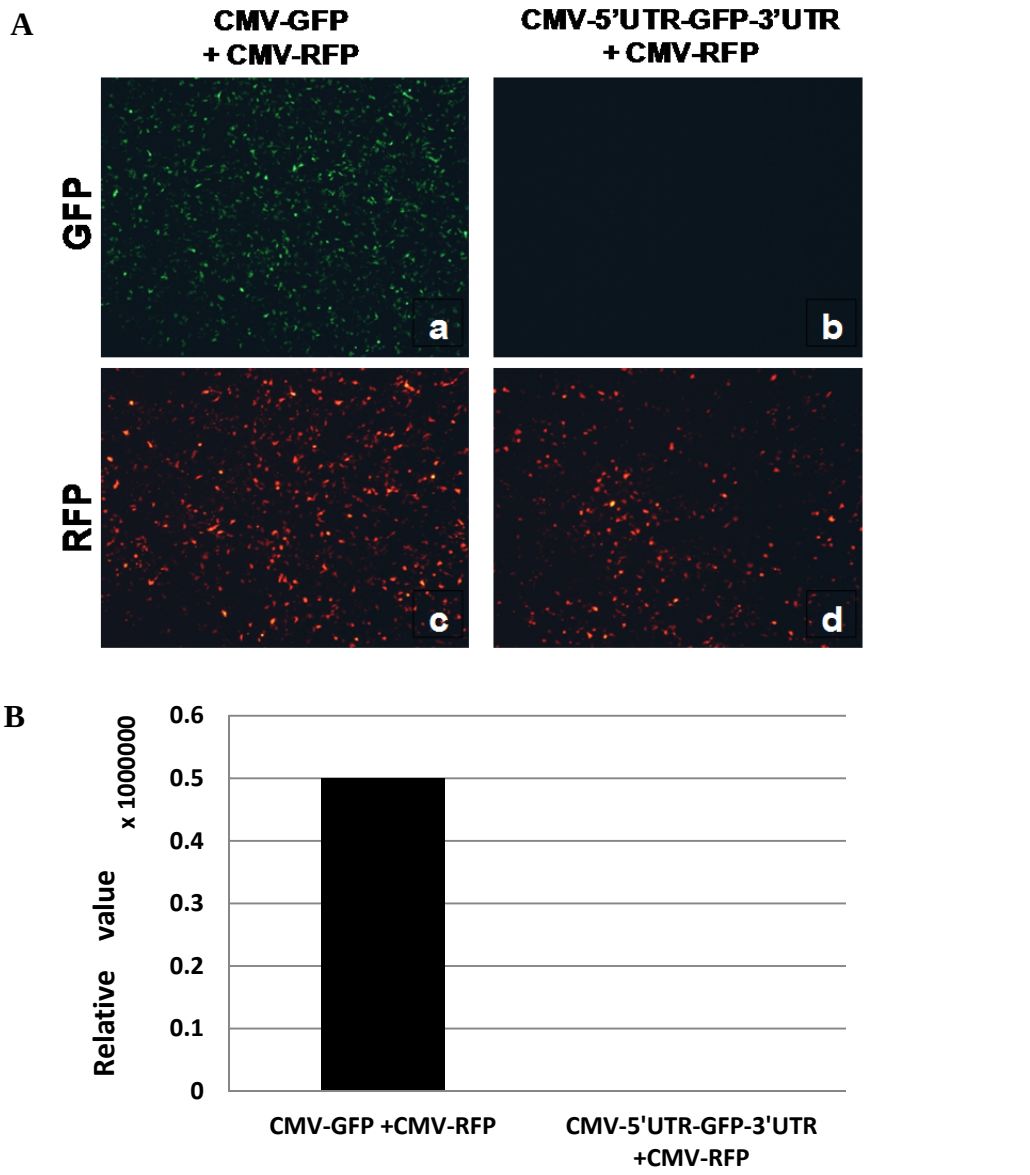

Figure 4. Repression of reporter GFP protein expression by FUS1 UTRs in H1299 cells. **(A)** H1299 cells were co-transfected with either a CMV-GFP [a] or a CMV-5'UTR-GFP-3'UTR [b] expression plasmid, together with a CMV-RFP expression plasmid, to normalize GFP expression in these H1299 transfectants. GFP [a and b] and RFP [c and d] protein expressions were visualized under a fluorescence microscope. **(B)** Quantification of GFP expression in CMV-GFP and CMV-5'UTR-GFP transfectants, which was based on RFP expression as transfection control. (Reproduced with permission of BBRC 410(2):235-241)

2.3.2 TUSC2 translation is repressed by 5'UTR

TUSC2 5'UTR contains two small uORFs encoding an 8-amino-acid peptide (uORF1) and another 6-amino-acid peptide (uORF2), which could inhibit the main ORF translation initiation by interfering with the "scanning" of the ribosome subunit. Therefore, we made three site-directed point mutation plasmids in 5'UTR-TUSC2 to detect the funtction for these two uORF: the first plasmid is to mutate the first ATG to AAG in uORF1 for eliminating uORF1; the second plasmid is to mutate the second ATG to AAG in uORF2 for eliminating uORF2; the third plasmid is to mutate both ATG to AAG in two uORFs for eliminating both uORFs (**Figure 5**).

Figure 5. Regulation of TUSC2 5'UTR on FUS1 expression. Schematic representation of TUSC2 expressing constructs with 5'UTR site-directed eliminations of uORFs. The positions of the uORFs and their corresponding point-mutation constructs are indicated by arrows. (Reproduced with permission of BBRC 410(2):235-241)

We transfected these plasmids into H1299 cells and HBE-KTR cells. Mutation of uORFs significantly abolished the 5'UTR down-regulation function in TUSC2 protein expression but not in mRNA transcripts, which suggests these two uORFs inhibit TUSC2

expression through translational influence, but not transcriptional influence (**Figure 6** and **Figure 7**). The two uORFs inhibitory effect is constant in normal cell line HBE-KTR and tumor cell line H1299, suggesting TUSC2 cannot express extensively in tumor and normal cells, otherwise excessive TUSC2 give rise to cell cycle arrest and apoptosis.

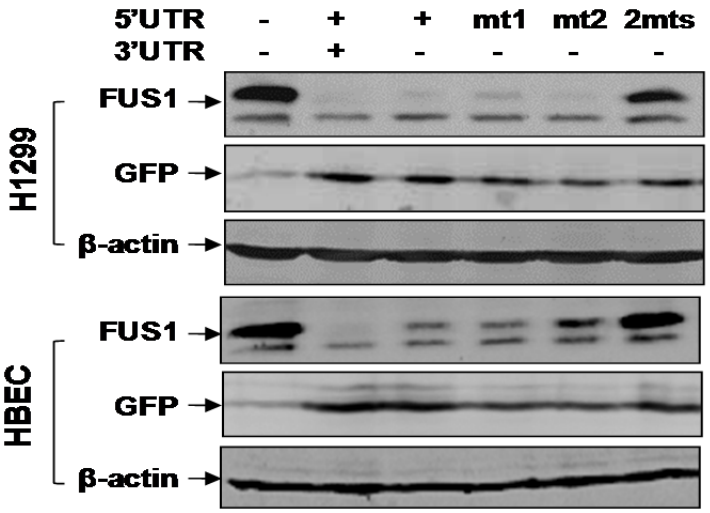

Figure 6. Effects of uORFs in 5'UTR on TUSC2 protein expression in H1299 cell and HBE cell. Western blot analysis of TUSC2 protein expression in HBE and H1299 cells transfected with TUSC2 expression plasmids with or without uORFs (Reproduced with permission of BBRC 410(2):235-241).

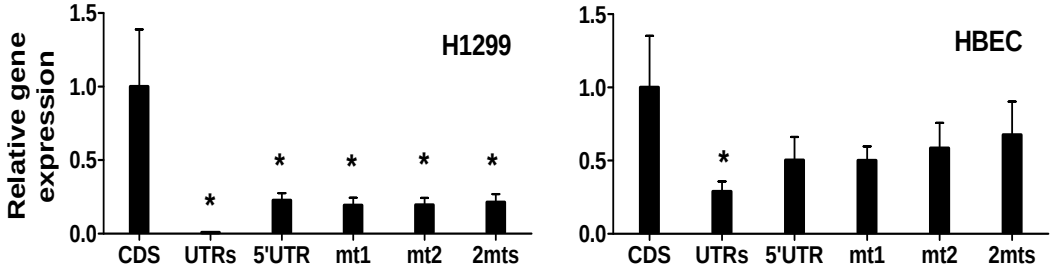

Figure 7. Effects of uORFs in 5'UTR on TUSC2 RNA expression in H1299 cell and HBE cell. * means P< 0.05, error bars denote standard error. Real-time PCR analysis of TUSC2 protein expression in HBE and H1299 cells transfected with TUSC2 expression plasmids with or without uORFs (Reproduced with permission of BBRC 410(2):235-241).

2.3.3 3'UTR regulation of TUSC2 expression

To elucidate which region of 3'UTR down-regulate TUSC2 expression, we performed a series of deletion mutants of the 3'UTR. The mRNA structure prediction program RNAfold software revealed that there are several hairpin-like stem elements in 3'UTR with potential to form stable secondary structure. As shown in Figure 8, we deleted a series of stable secondary structure: 334-504 nt, 764-1479 nt, 776-1102 nt, 1080 -1461 nt, 1183-1248 nt (**Figure 8**).

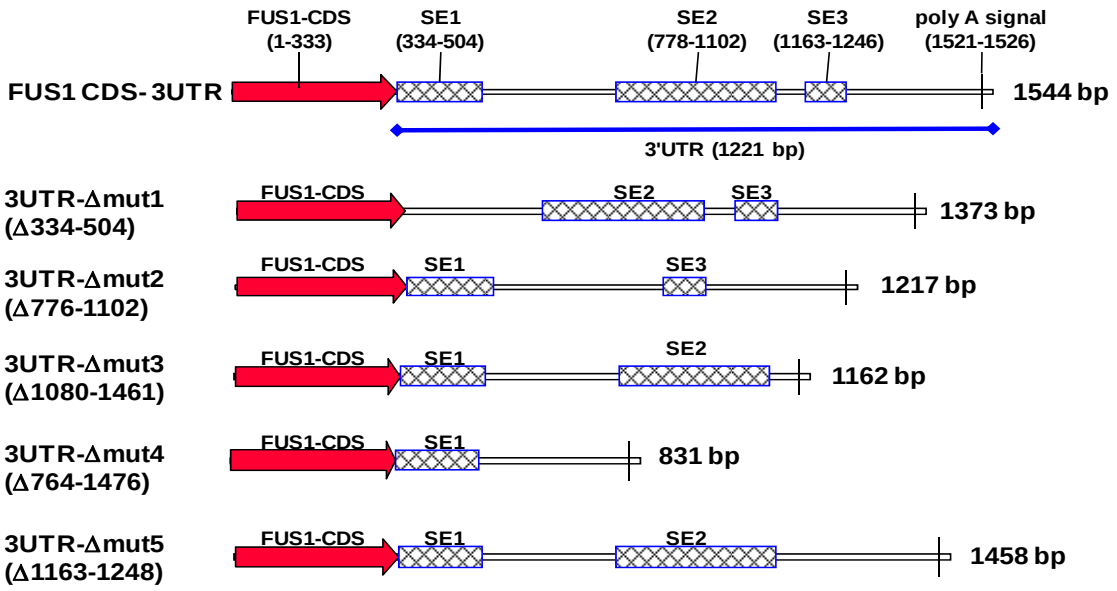

Figure 8. Effects of 3'UTR regulatory elements on TUSC2 expression in NSCLC H1299 and normal HBE cells. Constructs of deletion mutants of TUSC2 3'UTR. Names, relative locations, nucleotide sequence lengths, and putative regulatory 3'UTR sequence elements of the deletion mutants in TUSC2 3'UTR are schematically illustrated. (Reproduced with permission of BBRC 410(2):235-241)

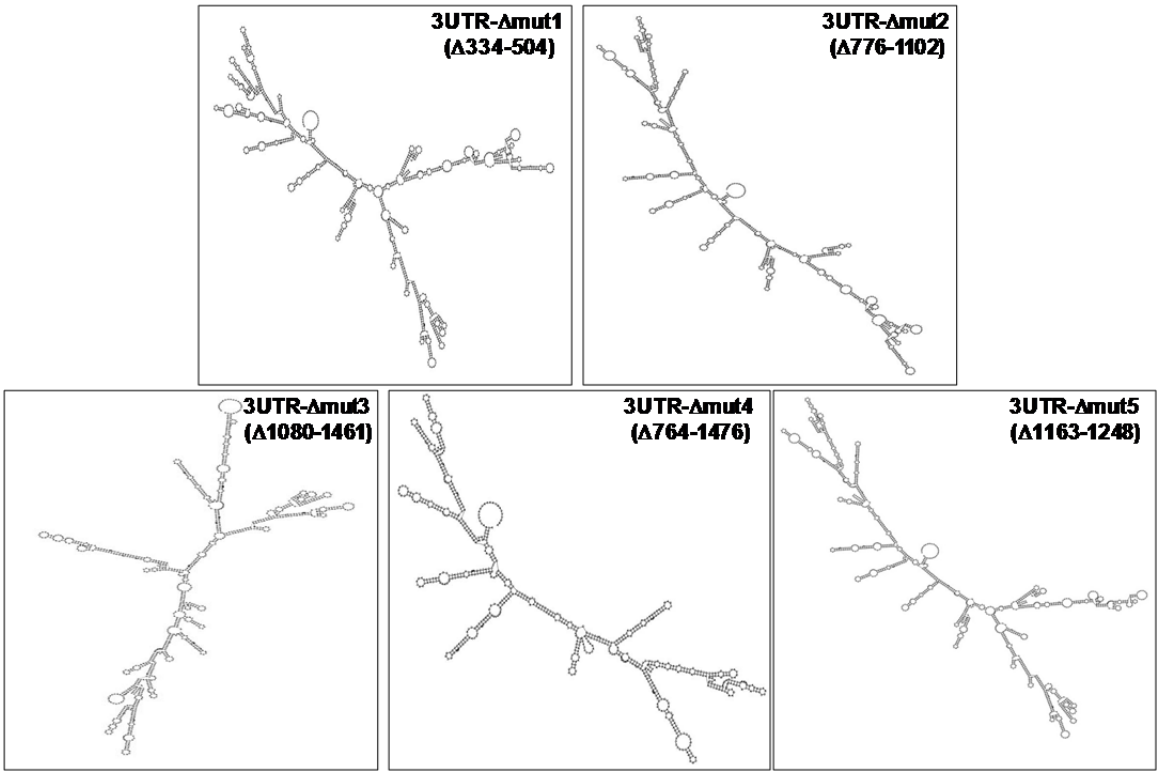

Figure 9. TUSC2 3'UTR and mutants secondary structure analyzed by RNAfold software. (Reproduced with permission of BBRC 410(2):235-241)

Figure 9 indicated the 3'UTR secondary structure after a specific stem loop deletion. After transfection of TUSC2-3'UTR containing 764-1479 nucleotides deletions in H1299 cell, TUSC2 protein expression was significantly increased, indicating that elements in 764-1479 nt are important for TUSC2 translation inhibition (**Figure 10**).

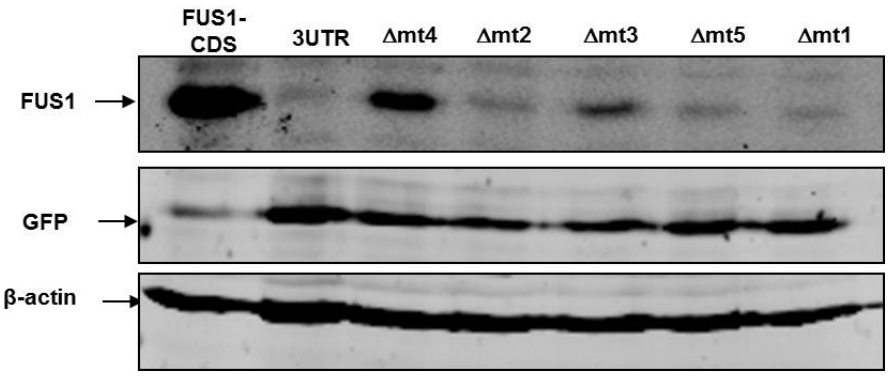

Figure 10. Effects of the 3'UTR mutations on TUSC2 protein expression by western-blot analysis. Expression of GFP was used to normalize the transfection efficiency in H1299 cells co-transfected with a GFP expression plasmid and individual FUS1-3'UTR deletion mutants. (Reproduced with permission of BBRC 410(2):235-241)

We also observed TUSC2 mRNA level was increased after 764-1479 nt deletion (Figure 11), which suggest 764-1479 nt affected TUSC2 mRNA expression. In addition, deletion of 1080 -1461 nt can also increase TUSC2 protein expression, which indicated that 1080 -1461 nt might have regulatory elements, contributing to 764-1479 nt inhibitory function. TUSC2 3'UTR in H1299 cell shows more significant inhibition on TUSC2 expression than in HBE-KTR cell. Interestingly, Figure 10 showed removals of 764-1479 nucleotides in 3'UTR abolishes TUSC2 protein expression inhibition and RNA synthesis inhibition by 3' UTR in H1299 cell, but has no effect in HBE-KTR cell. This result suggests 3'UTR repress TUSC2 expression in H1299 through 764-1479 nucleotides, but has no effect in HBE-KTR cells (**Figure 11**). Thus we speculate that 764-1479 nucleotides in 3'UTR might have unique regulatory elements in tumor cells, which contribute to reduction of TUSC2 protein expression in tumor cells compared to normal cells.

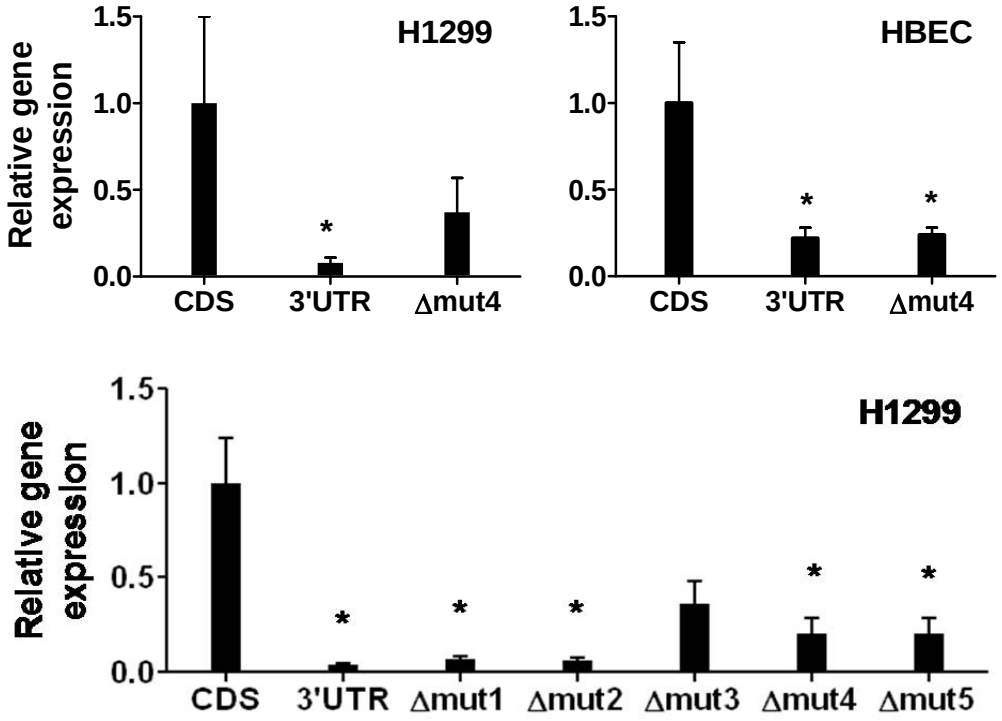

Figure 11. TUSC2 mRNA expression in H1299 and HBE cells transfected with TUSC2 3'UTR deletion mutants. Real-time PCR analysis of TUSC2 protein expression in HBE and H1299 cells transfected with TUSC2 3' UTR deletion plasmids. Effects of the deletion at position 764–1476 (mut4) in the FUS1 30UTR region on FUS1 mRNA transcription in the H1299 and HBE cells. * means $P < 0.05$, error bars denote standard error. (Reproduced with permission of BBRC 410(2):235-241)

2.4 Discussion

Translation can be divided into three stages: initiation, elongation, and termination. 5'UTR is responsible for initiation of translation, which is the primary target of translation regulation. Selection of the translation initiation site occurs via "scanning mechanism", which postulates that the small ribosome subunit scans linearly from the 5' end of the mRNA; stopping when the first AUG codon is reached and forming an 80S ribosome to start translation [66]. Several cis-acting elements within 5'UTR, such as

uORFs, secondary structures or binding motifs bound by specific RNA binding proteins could be involved in translational regulation. Recently, it was demonstrated that uORFs reduce protein levels by 30-80 %. The translation repression by uORFs is associated with: strong uAUG context, evolutionary conservation, increased distance from the cap, and multiple uORFs in the 5'UTR. The 5'UTR of TUSC2 contains two uORFs; both of the uORFs are nearly identical in mice, chimpanzee and humans, which suggests good reservation. In addition, the uAUG of uORFs are far from the cap; and the 1st uAUG is flanked by a guanine at position -3 and a guanine at position +4, and the 2nd uAUG is flanked by a guanine at position -3 and a cytosine at position +4, and thus is in 'adequate' consensus context for uORF translation initiation start [67]. In agreement with this prediction, the two uORFs influences significantly TUSC2 translation. Mutation of uAUGs to uAAGs significantly up-regulate TUSC2 translation.

In addition, it was reported that stable stem loops with a free energy of -30 to -61 kcal/mol are sufficient to block ribosomal scanning in 5'UTR and therefore inhibit translation. Based on RNAfold analysis, TUSC2 5'UTR display highly stable secondary structure with the free energy of -72.18 kcal/mol, which might impede ribosome scanning. As shown in Figure 6, the inhibitory function of 5'UTR cannot be all attributable to uORFs. The 5'UTR stable secondary structure might contribute to the TUSC2 translation initiation through blocking ribosomal scanning.

3'UTR regulate gene expression through mRNA 3'end processing, sub-cellular localization and its stability. We also identified several regulatory elements or motifs in the 3'UTR region of TUSC2 transcripts by serial deletions and biological characterization of these 3'UTR deletion mutants in normal lung and lung cancer cells. It

was reported that 3'UTR is "a molecular hotspot for pathology", if disrupted, leads to life threatening disease. TUSC2 has a highly conserved and long complex 3'UTR, suggesting 3'UTR might play a critical role in regulating TUSC2 expression. However, TUSC2 3'UTR lacks typical AU-rich elements, which are well-known targets for degradation. It was reported that RNA binding proteins are involved in translational control of certain gene by binding to secondary structure elements like stem loops in 3'UTR. Sequence analysis revealed TUSC2 3'UTR has a series of stable secondary structure might be involved in TUSC2 expression regulation. Our findings indicate that nucleotides 764-1479 nt in 3'UTR are decisive in the control of TUSC2 RNA expression in tumor cells and normal cells. However, precise structural elements and mechanism of repressive action in 3'UTR remained to be clarified. The 3'UTR of TUSC2 has been shown to be a target of other miRNAs including miR-93, miR-98, and miR-197 [136]. Down-regulation of TUSC2 expression in both SCLC and NSCLC cell lines and primary tumors correlates with elevated miR-93 and miR-197 expression [136]. The predicted miR-98 targeting site is located in $\Delta 334-504$ region of 3'UTR. These results suggest that differentially expressed miRNAs may target the 3'UTR of TUSC2 mRNA and act as negative regulators of TUSC2 expression in lung cancers.

The results indicate that TUSC2 expression is tightly regulated. Because too much TUSC2 could lead cell death and too little TUSC2 could promote tumor formation, it is extremely important that TUSC2 expression needs to be strictly controlled. Firstly, for the 5'UTR, two uORFs inhibitory effect is constant in normal cell HBE-KTR and tumor cell H1299, suggesting TUSC2 cannot express extensively otherwise excessive TUSC2 give rise to cell cycle arrest and apoptosis. Secondly, for the 3'UTR, the stem loops

down-regulate TUSC2 protein expression through affecting mRNA stability in H1299 cells, but not in HBE cells, which is responsible for the low-expression of TUSC2 protein in tumor cells.

Chapter 3. Detection of intermediates and end products of microRNA processing in human cells by a novel Stem-loop Array RT-PCR

3.1 Introduction

3.1.1 microRNA biogenesis

MicroRNAs (miRNAs) are small non-coding RNAs that have been shown to function as key regulators of gene expression at the posttranscriptional level and modulate many crucial biological processes, such as cell proliferation, differentiation, and apoptosis in multicellular organisms [68-75]. MiRNA genes are transcribed as long primary microRNA (pri-miRNA), which is processed by Drosha and its co-factor DGCR8 to generate precursor miRNA (pre-miRNA). Pre-miRNA is rapidly exported to the cytoplasm by exportin-5 in a Ran–GTP-dependent manner, where it is cut by Dicer to generate a mature miRNA [73,76-79] . The processed miRNA species are the production of phased small RNA reads that consist of the most abundant form of the 22 nt-long mature miRNAs, the less abundant miRNA isoforms, and other miRNA gene transcript-originated miRNA and transient miRNA sequences [76]. Despite the complex compositions of these small RNA reads, there should be little variation in the RNA ends corresponding to Drosha and Dicer processing sites and, in particular, it should have a nearly uniform position at the 5′ ends of the RNA reads and a unique 2-nt overhang at the 3′ ends of miRNA duplexes [75]. An in depth analysis of tremendous amounts of these small RNA reads could provide an opportunity for miRNA gene discovery but also poses the big challenge in distinguishing authentic miRNAs from other types of small RNA

species and in quantifying the abundance and verifying the accurate sequence of a given mature miRNA species in living cells [76,80,81].

3.1.2 Current methods used for detection of miRNAs

A number of methods are employed for sequence determination and expression profiling of endogenous miRNAs. Cloning and Northern blotting are the standard methods for miRNA sequence analysis, but such approaches require a large amount of input RNAs [81,82]. Recently, microarray and bead based assays are used for high-throughput miRNA profiling for fast screening and comparative expression analysis of miRNAs in biological samples, but have a limited sensitivity and specificity due to the potential non-specific annealing inherent for hybridization-based methods [84-87]. Recent applications of deep sequence technology have greatly facilitated and simplified the analysis of miRNAs and made the investigation of small RNA repertoires of cells possible at the unprecedented resolution of hundreds of millions of reads [80, 81]. However the cost-intensive equipment and reagents and the complicated data process and bioinformatics analysis of deep RNA sequencing may not practical or affordable for routine miRNA analysis in majority of research laboratories. RT-PCR is a gold standard for gene expression analysis [88] and exhibits a high degree of sensitivity and specificity [89]. Chen *et al.* developed a TaqMan based stem-loop RT-PCR for a real-time quantification of miRNAs and demonstrated a high sensitivity and specificity [90]. This method, however, was designed to quantify a given miRNA with only one stem-loop RT primer based on the predicted mature miRNA sequence but cannot verify and detect processed mature miRNA species with variations or modifications at their 3' and 5' ends.

Furthermore, the recent studies have revealed amazing complexity in the miRNA-mediated regulatory mechanisms and biological functions, which involves multiple steps of miRNA processing, target recognition, binding, and cleavage, and interactions with other miRNAs, protein cofactors, and signaling pathways [72, 74-76]. To determine the precise mechanism of action and better understand the regulatory function of endogenous miRNAs in a complex biological system such as in mammalian cells, advanced molecular biological and biochemical tools and methods are much needed to efficiently and accurately identify and quantitatively measure intermediates and end-products resulted from the miRNA action in multicellular organisms under physiological conditions.

For these purposes, we developed a novel stem-loop array reverse transcription polymerase chain reaction (SLA-RT-PCR) approach to systematically verify and detect the endogenous miRNAs and the target mRNA and DNA cleavage fragments by accurately identifying their unique nucleotide ends generated during miRNA processing and molecular action of siRNA and restriction enzymes (REs) in human cells. We used the endogenous miRNA, the synthetic siRNA with an ectopically expressed mRNA target template, and the REs with DNA templates as testing models to evaluate sensitivity, specificity, and efficiency of the SLA-RT-PCR assay. Our results demonstrated the great potential and broad applications of using the SLA-RT-PCR as a sensitive, cost-efficient, and high-throughput tool to systematically determine the biogenesis and expression of endogenous miRNAs and their mechanisms of action in multicellular organisms under physiological conditions.

3.2 Methods and Materials

3.2.1 SLA-Reverse-transcription

Reverse transcriptase reaction (RT) contains total RNA samples prepared from human lung and cervix cancer cell lines and normal HBE cells. The RNA sample was briefly treated with (0.04U/ µl as final concentration) RNAase-free DNAase I. RNA was reversed transcribed using the High Capacity Reverse Transcription kit (Life Technologies, Applied Biosystems) in combination with an array of stem-loop RT-primers. The 20 µl of RT reaction contains 50 ng of total RNA, 5×10^{-12} mol of SLA-RT primer, 2 µl 10x RT buffer (Applied Biosystems), 1 µl Multiscribe reverse transcriptase (Applied Biosystems), and 0.8 µl 100 mM of dNTP mix (Applied Biosystems). To increase reverse transcription efficiency, a pulsed RT reaction was performed on a DNAEngine Peltier Thermal Cycler (BIO-RAD) with 60 cycles at 18 °C for 1 min and 37 °C for 1 second, followed by 60 cycles at 20 °C for 1 min, 37 °C for 1 second, 37 °C for 30min, 42 °C for 20 min, 85 °C for 10 min, and then held at 4 °C.

3.2.2 SLA-PCR

For regular PCR, each cDNA sample generated from the SLA-RT reactions was diluted 500 fold. The 20 µl of PCR reaction contains 1µl diluted RT product, 2 µl 10×standard PCR buffer, 0.8 µl 10mM dNTP, 0.5 µl 100mM MgSO4, 0.2 µl Taq polymerase, 1µl 10nm of forward primer and 1µl 10nm of reverse primer. PCR reactions were conducted as at 95 °C for 5 min followed by 35 cycles at 95 °C for 15 s, 61 °C for 30s, and 37 °C for 30s, and 72 °C 10 min, on DNAEngine Peltier Thermal Cycler (BIO-RAD).

3.2.3 miRNA detection real-time PCR

For real-time RT-PCR, a Taqman® Real-time RT-PCR for miRNA detection kit was used (Applied Biosystems). The 15 µl of RT reaction consisted of 7 µl master mix, 3 µl 5×RT stem-loop RT primer, and 5 µl RNA sample (20 ng). The 7 µl of master mix contained 1.5 µl 10× RT buffer, 0.15 µl 100 mM dNTPs, 1µl 50 U/µl MultiScribe reverse transcriptase, and 0.19 µl 20 U/µl RNase inhibitor. RT reactions were incubated for 30 min at 16°C, 30 min at 42°C, 5 min at 85°C, and then held at 4°C. The 20 µl of real-time PCR included 1.33 µl RT product, 10 µl 2× TaqMan® Universal PCR Master Mix, 1 µl TaqMan® small RNA assay, and 7.67 µl H_2O. The reactions were incubated at 95°C for 10 min, followed by 40 cycles at 95°C for 15 s and 60°C for 1 min. The threshold cycle (C_T) is defined as the cycle number at which the FAM fluorescence signal passes the fixed threshold, and were converted into relative miRNA expression by using U6 small RNA as endogenous control.

3.2.4 SLA-RT-PCR product detection by agarose gel electrophoresis

PCR products resulting from SLA-RT-PCR were analyzed by agarose gel electrophoresis in 1x Tris-borate-EDTA (TBE) buffer containing 89 mM Tris Base, 89 mM Boric Acid, and 2 mM EDTA, pH 8.0. TBE buffer was useful for separation of smaller DNA fragments because it has a greater buffering capacity and gives a sharper resolution than that of TAE buffer.

3.2.5 Fluorescence-based DNA fragment size analysis

In many of our SLA-RT-PCR products the sizes of non-specific primer dimmers are similar to PCR products and it is difficult to distinguish them by size from agarose gel.

Therefore, a fluorescence-based DNA fragment size analysis (FBFSA) [41] was performed to accurately determine differences between non-specific and specific PCR products. Fluorescently labeled fragments were detected using the Applied Biosystems 3730 Genetic Analyzer and the size of each PCR fragment was determined using Genotyper analysis software by comparing it with the standard curve for that specific fragment lane. Accuracy of less than one base difference could be seen between sample replicates. Higher throughput can be achieved by multiplexing different dyes and fragment sizes together.

3.3 Results

3.3.1 SLA-RT-PCR

We developed a novel SLA-RT-PCR technique to systematically verify and detect the endogenous mature miRNAs and the intermediate mRNA fragments cleaved by siRNA by accurately identifying their unique nucleotide ends generated during miRNA processing and by siRNA-mediated target cleavage in human cells. The SLA-RT-PCR assay includes two steps: SLA-RT and PCR. The principle of works, experimental design, and assay procedures are illustrated in **Figure** 12. The stem-loop-array RT-primers comprise two unique sequence components: a short single-stranded stretch (6 bases) at the 3' end of the primer oligonucleotide that is miRNA-specific and hybridizes to the end of mature miRNA and a double stranded stem at the 5' end that forms stem-loop to function as a forceps to stabilize the secondary structure of the primer. The specific sequences of the mature miRNA is recognized by the six-nucleotide

complementary extension at the 3'ends of the RT-primer array, which can efficiently reverse transcribe the miRNA into cDNA (**Figure 12**, Step 1). The use of an array of stem-loop RT primers allows to accurately recognizing and verifying unique ends of the RNA or DNA fragments processed by endonucleases. If the SLA-RT primers have no perfect match, on both the length and the base, to the sequence of the 3' or 5' end of a RNA fragment the efficiency of RT reaction will be dramatically reduced. The size and relative amount of SLA-RT-PCR products can be detected by agarose gel electrophoresis or a quantitative real-time RT-PCR. For subsequent PCR (**Figure 12**, Step 2) it is proceeded with a pair of forward and reverse primers that contain antisense sequence complementary to the 5'-end of miRNA and to the 3'-end of the stem loop of RT- primer, respectively.

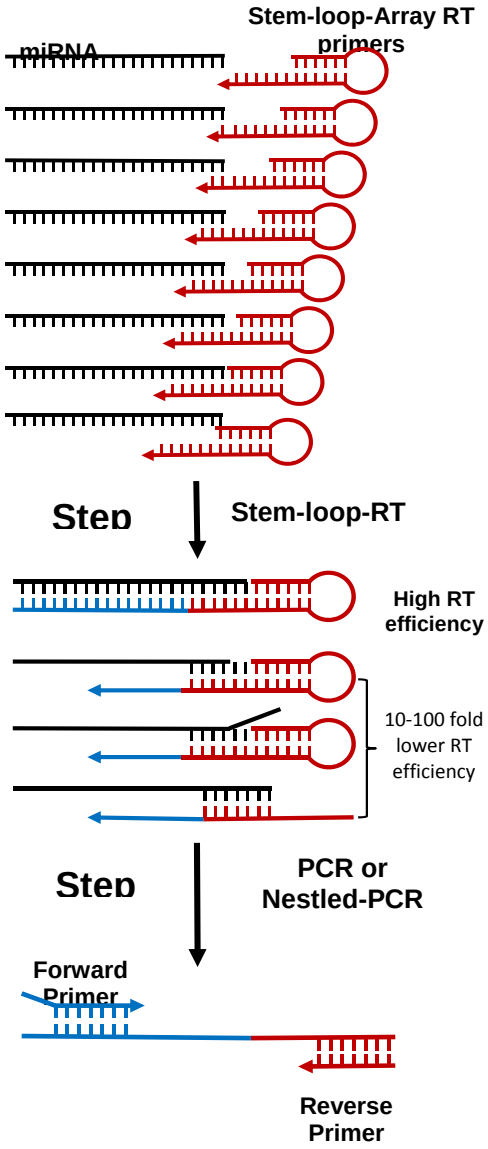

Figure 12. Schema of SLA-RT-PCR assays for miRNA detection and verification. The SLA-RT PCR assay includes two steps: SLA-RT and PCR. The stem-loop-array (SLA) RT-primers bind to the ends of mature miRNAs. Specific sequences of mature miRNA species are recognized by the six-nucleotide (nt) complementary extension at the 3'- or 5'-ends of SLA-RT primers, which can reverse transcribe the miRNA into cDNA with varied efficiency (Step 1). The highest RT efficiency and specificity will be detected in RT reactions with SLA-RT primers containing 6-nt stem sequences perfectly matched to those at ends of the mature miRNA will exhibit and a dramatically reduced efficiency (10-100 fold less) and specificity will be noticed in RT reactions with SLA-RT primers having no perfect matches or mutations. The subsequent PCR (Step 2) is preceded with a pair of forward and reverse primers that contain antisense sequence complementary to the 3' or 5' end of miRNA and to the 5' or 3'-end of SLA-RT primer, respectively.

3.3.2 Verification of 3’ ends of synthetic RNU44 RNA and DNA fragments by SLA-RT-PCR

We first used synthetic small RUN44 RNA or DNA templates as model systems to evaluate the SLA-RT-PCR for detection and verification of the 3’ end of RUN44 RNA and DNA fragments. RNU44 is a member of abundant intronic small-nucleolar RNAs that were frequently used as reference genes for measuring endogenous miRNA expression [75]. It has a predicted RNA sequence of 66 nucleotides (**Figure 13**). We designed 12 SLA-RT-primers that are different by one nucleotide from each other (**Figure 13**) and performed SLA-RT-PCR reactions using synthetic RNU44 RNA and DNA as templates and analyzed SLA-RT-PCR and SLA-PCR products, respectively, by agarose gel electrophoresis (**Figure 14**).

Predicted RUN44 RNA Sequence

5′-CCUGGAUGAUGAUAGCAAAUGCUGACUGAACAUGAAGGUCUUAAUUAGCUCUAACUGACU-3′

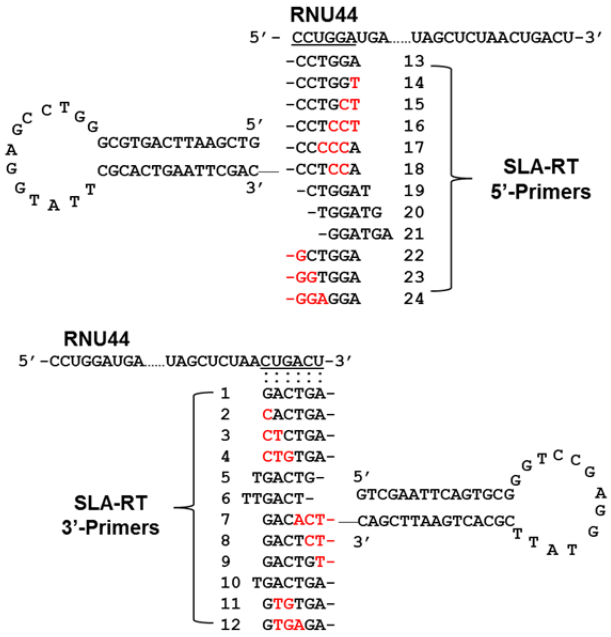

Figure 13. Detection and verification of 3' and 5' ends of synthetic and endogenous small nucleolar RNU44 RNAs by SLA-RT-PCR. A, The predicted full length RNU44 RNA sequences with 5' and 3' end sequences (underlined) targeted by SLA-RT-5'-primers and SLA-RT-3'- primers, respectively.

As expected, the SLA-RT primers ending in AGTCAG (primer 1), GTCAGT (primer 5), TCAGTT (primer 6), TGTCAG (primer 9), and AGTCAGT (primer 10) that process perfect or near perfect match to the 3'end sequences of RUN44 successfully reverse-transcribed RNU44 RNA with a high efficiency. However, the RT primers with mutations at 3' end or in the middle of RT-primer sequences, including AGTCAC (primer 2), AGTCTC (primer 3), AGTGTC (primer 4), TCACAG (primer 7), AGTGTG (primer 11) and AGAGTG (primer 12), could not reverse-transcribe RNU44 or showed dramatically reduced efficiency (Figure 14, panel I). Similar results were also demonstrated in PCR reactions with same primer sets using RNU44 DNA as a template

with either the same nucleic acid sequences corresponding to RNA sequences (Figure 14, panel II) or with one base (T) added at the 3'-end (Figure 14, panel III). The predicted sizes and sequences of the SLA-RT-PCR products with primers 1 (AGTCAG), 5 (GTCAGT), 6 (TCAGTT), 9 (TGTCAG), and 10 (AGTCAGT) (primer 10) were further confirmed by fluorescence-based fragment size analysis (FBFSA) (Figure 16, Array I) and DNA sequencing (Figure 16), respectively. These results indicate the high specificity of the designed SLA-RT primers to the 3' end sequences of RNA or DNA fragments.

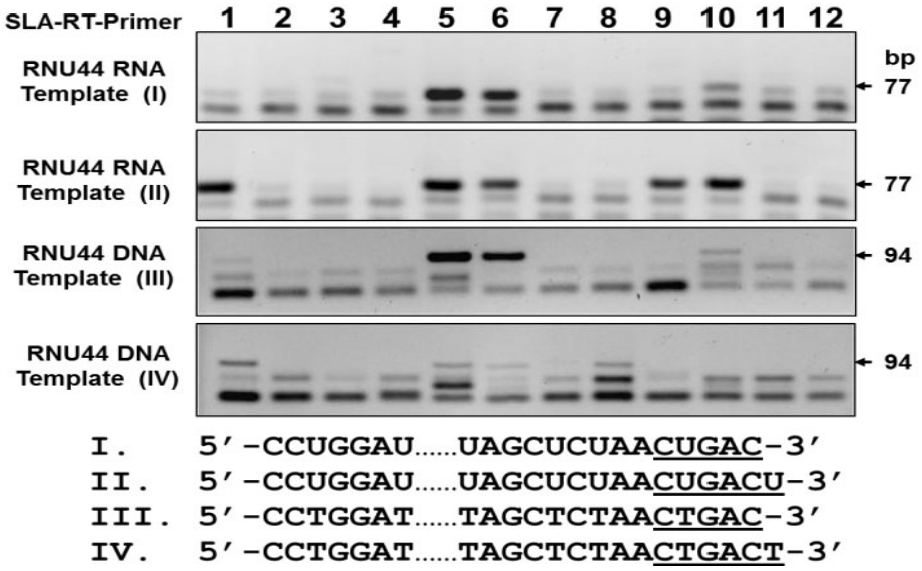

Figure 14. Detection and verification of 3' ends of synthetic RNU44 RNA (I, 44nt) and (II, 45 nt) and DNA (III, 61 bp) and (IV, 62 bp) templates by SLA-RT-3'-primers (Fig 13) on agarose gels. Sequences of synthetic RNU44 RNA and DNA templates are described at the bottom of gel graphs and the predicted specific SLA-RT-PCR products are indicated by arrows on the left sides of gels.

3.3.3 Detection and verification of 3' and 5' ends of endogenous RNU44 RNAs in H1299 Cells

We used two sets of SLA-RT-primers to detect and verify the 3' and 5' ends of endogenous RNU44 RNAs in H1299 cells (Figure 15). The same set of 3' SLA-RT

primers as shown in Figure 13 (SLA-RT 3'-primers) was used to detect the 3' end of RUN44 RNA in H1299 cells (**Figure 15**, panel I). Similarly, the RT products of RNU44 were detected with a high efficiency in RT reactions containing primers 1, 5, 6, 9, and 10 but were not detectable in RT reactions with mutation-bearing primers 2, 3, 7, 11, and 12 or detected in dramatically reduced efficiency with primers 4 and 8, respectively (**Figure 15**). The sizes and sequences of these 3'-SLA-RT products amplified from endogenous RNU44 RNAs were further confirmed and verified by both FBFSA and DNA sequencing (data not shown). These results indicate that a large population of RNU44 RNAs expressed in H1299 cells is ended with sequences of ACUGAC at their 3' ends but without the predicted U (Figure 13) at their termini.

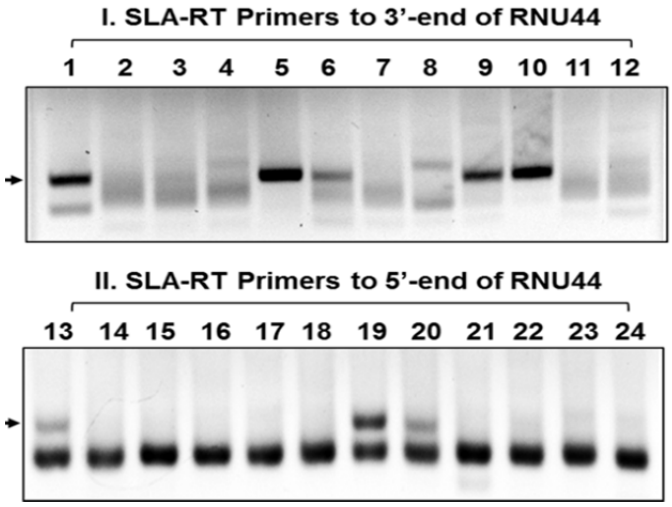

Figure 15. Detection of 3' and 5' ends of endogenous RNU44 RNAs in H1299 cells by SLA-RT-PCR on agarose gels, using two sets of SLA-RT primers shown in Figure 13 and run in TBE buffer. The predicted specific SLA-RT-PCR fragments are indicated by arrows on the left sides of gels.

We also used a set of 5'-SLA-RT primers to detect and verify the 5' ends of endogenous RNU44 RNAs in H1299 cells (**Figure 15**, panel II). The 5'-RT-PCR products amplified from endogenous RNU44 RNAs were detected with a high efficiency in RT reactions containing 5'-SLA-RT primers 13 (CCTGGA), 19 (CTGGAT), and 20

(TGGATG) with perfectly matched complementary sequences to the 5' ends of RNU44, but were not detectable in RT reactions containing RT primers 14 to 18 and 21 to 24 with mutations at 3' end or in the middle of the RT primer (**Figure 15**). The 5'-SL-RT primer #19 ending in CTGGAT reversely transcribed RNU44 with the highest efficiency (**Figure 15**, panel II). The sizes and sequences of these 5'-SLA-RT products amplified from endogenous RNU44 RNAs were further confirmed and verified by both FBFSA (Figure 16, FDFSA profiles/5'-SLA-RT-PCR) and DNA sequencing. These results suggest that a large population of RNU44 RNAs in H1299 cells is ended with sequences of CUGGAU at their 5' ends but without the predicted nucleotide "C" (**Figure 13**) at their 5'-termini. Together, these results indicate the high specificity and efficiency of SLA-RT-PCR in detection of both 3' and 5' ends of endogenously expressed or processed RNA fragments.

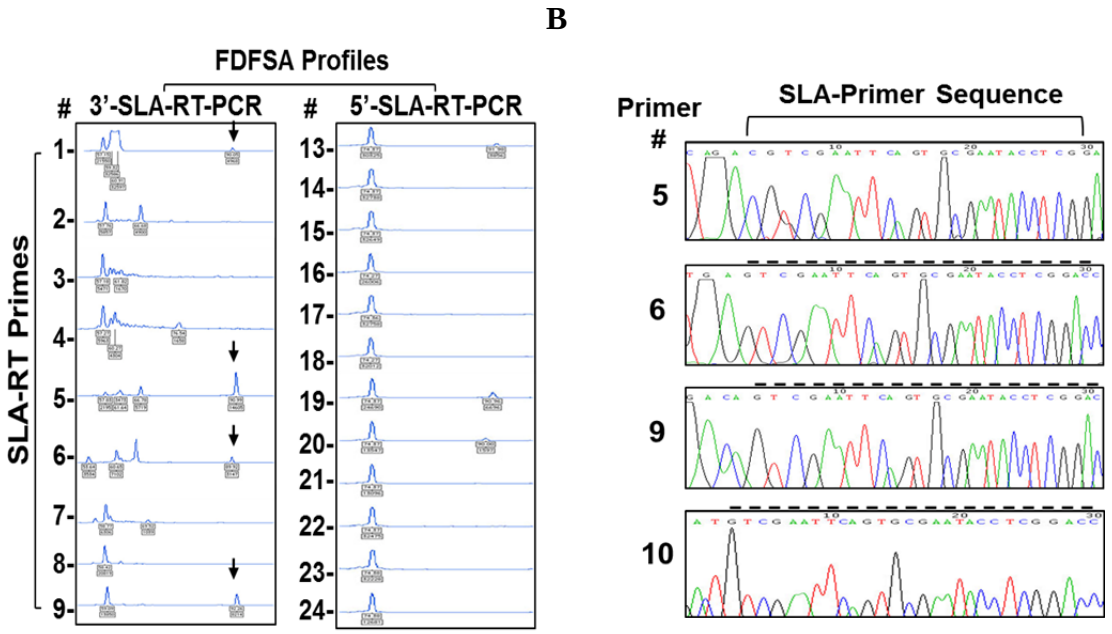

Figure 16. Verification of SLA-RT-PCR products. **(A)** Verification of sizes of SLA-RT-PCR products by fluorescence-based fragment size analysis (FBFSA). Representative FBFSA profiles corresponding to individual 3' SLA-RT primers (left panels) and 5' SLA-RT primers (right panels). The verified sizes of specific SLA-RT-PCR DNA fragments are indicated by arrows. **(B)** Confirmation of identities of specific SLA-RT-PCR fragments by DNA sequencing. Representative DNA sequencing histograms are shown in SLA-RT-PCR reactions with synthetic RNU44 RNA templates and corresponding SLA-RT primers as indicated on the top.

3.3.4 The dynamic range and sensitivity of SLA-RT-PCR

To evaluate the dynamic range and sensitivity of the SLA-RT-PCR assay, we used two synthetic small RUN44 RNAs as templates. The RNU44 RNA template I (**Figure 17**) contains the predicted full 66-base sequences ending with "U" at the 3' terminal and the template II (**Figure 17**) contains the verified RNU44 RNA sequences without "U" at the 3' end. SLA-RT primer was used to specifically detect the 3'-end of RNU44 RNA templates I and II. Synthetic RUN44 RNAs were quantified based on the A_{260} reading

and made a series of dilution over a range of eleven orders of magnitude from 10^{-18} to 10^{-28} mole (**Figure 17**). SLA-RT primer could successfully reverse-transcribe the RNU44 RNA template A (**Figure 17**). However, as expected, a reduced RT efficiency was observed in SLA-RT-PCR reactions because of the one-base over the reach by this stem-loop primer at the 3'end of RNU44 RNA template II (**Figure 17**). These results further demonstrated the specificity of SLA-RT-PCR assay.

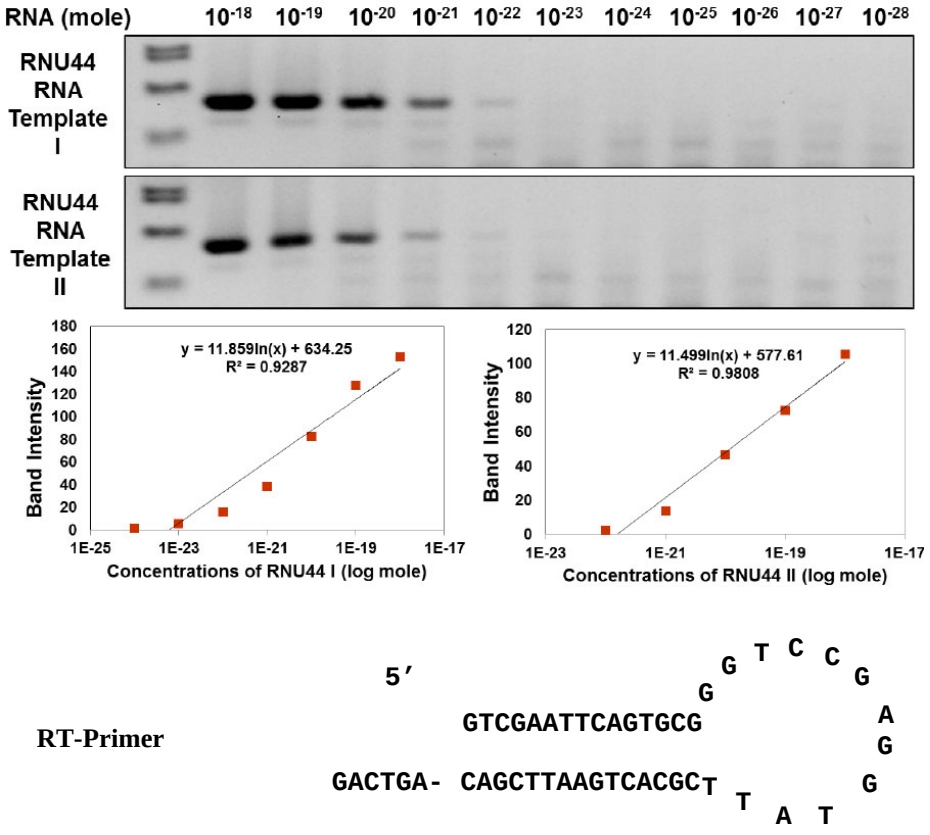

Figure 17. Dynamic range and sensitivity of the SLA-RT-PCR assay. The SLA-RT-PCR reactions were performed using SLA-RT primers and known concentrations of input synthetic RNU44 RNA templates I and II over ten orders of magnitude from 10^{-18} to 10^{-28} mole. The specific SLA-RT-PCR products were analyzed by agarose gel electrophoresis (upper panels) and corresponding liner regression plots of the log RNA template input (mole) vise the relative output of SLA-RT-PCR products are presented in lower two panels.

The SLA-RT-PCR assay showed an excellent linear output of RT-PCR products corresponding to the input of RNA templates over a dynamic detection range at lease of five orders of magnitudes (from 10^{-18} to 10^{-22} mole) and demonstrated an extremely high sensitivity that is capable of detecting as few as 10^{-22} mole in PCR reactions with both RNU44 RNA templates and specific SLA-RT primers on agarose gel (**Figure 17**).

3.3.5 Detection and verification of 3'-end of mammalian miR-98 in mammalian cells

We used a human hsa-miR-98 as a model miRNA molecule to evaluate the SLA-RT-PCR assay for detecting and verifying the 3'-ends of endogenous miRNAs in human cells (**Figure 18**). The hsa-miR-98 is a member of let-7 miRNA family and its structure and function have been extensively investigated in multi-organisms. The predicted secondary structure and mature sequences of pri-miR-98 from miRBase data base (http://www.mirbase.org) [94] is shown in Figure 18A. We designed 9 SLA-RT-primers, which are complementary to the 3' end of miR-98 (**Figure 18B**).

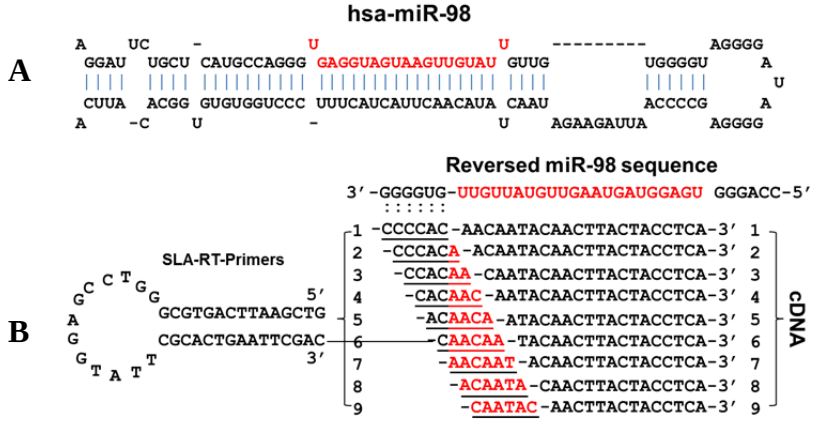

Figure 18. Detection and verification of mature miR-98 species in human cells by SLA-RT-PCR. **(A)** Predicted secondary structure of has-miR-98. The mature miR-98 sequences are presented in red. **(B)** SLA-RT 3'-primers for detection of 3'-ends of mature miR-98 and corresponding sequences of cDNA fragments by RT reactions.

The endogenously expressed and processed mature miR-98 RNAs showed predicted sequence reads at their 3' ends with varied levels of distribution in H1299 cells, as demonstrated by specific SLA-RT-PCR fragments in RT-PCR reactions containing SLA-RT primers 6, 7, 8, and 9 and by an increased level of distribution of mature miR-98 species detected in reactions containing SLA-RT primers 6 to 9 (**Figure 19**). Similar results to those shown in Figure 19 were also obtained in exogenously expressed and endogenously processed mature miR-98 RNAs in H1299 cells, using the same set of SLA-RT primers (**Figure 19**). These results demonstrate the reliability and accuracy of the SLA-RT-PCR in detection and verification of end reads and levels of processed mature miRNA species in mammalian cells.

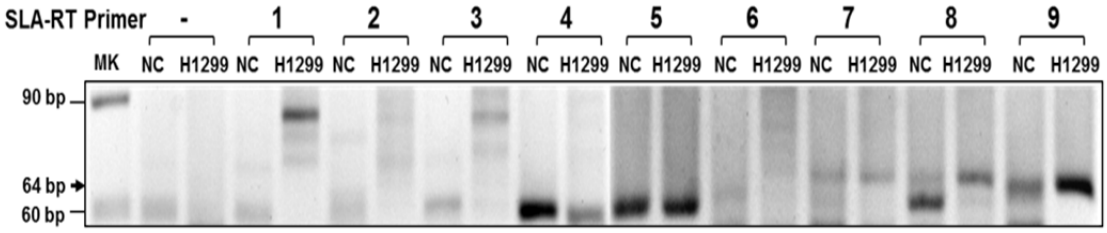

Figure 19. SLA-RT-PCR detection of miR-98 in H1299 cell. PCR corresponding to individual SLA-RT primers was shown in Figure 18. The predicted size of specific SLA-RT-PCR is indicated by arrow on the left side. **MK**, molecular marker, **NC**, negative control. SLA-RT-PCR reactions without SLA-RT primer was used as a control.

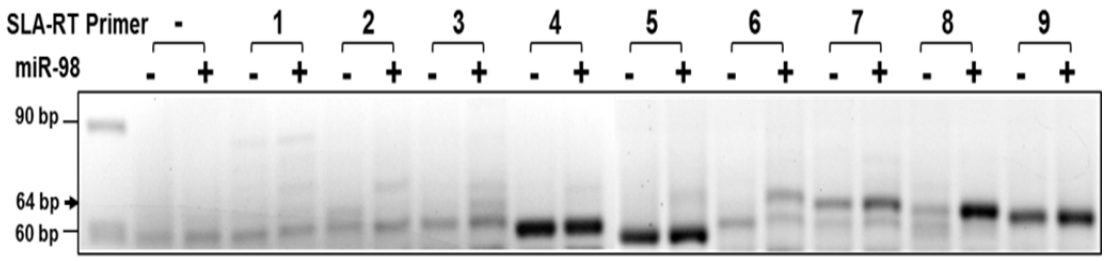

Figure 20. SLA-RT-PCR detection of miR-98 in Hela cells with (+) or without (-) exogenous transfection of miR-98 gene expressing plasmid. PCR corresponding to individual SLA-RT primers was shown in Figure 18. The predicted size of specific SLA-RT-PCR is indicated by arrow on the left side.

Based on these SLA-RT-PCR results of the distribution of mature miR-98 RNAs in H1299 cells, we compared the distribution and expression levels of endogenous miR-98 RNAs among normal bronchial epithelial HBE, NSCLC H1299, and cervix cancer Hela cells with or without the ectopic expression of miR-98, using above tested SLA-RT primers 6-9 (**Figure 21A**). Different levels of expression and distributions of mature miR-98 species were observed in different cells and cell lineages (**Figure 21A**). Particularly, the mature miR-98 species with 3'-end in "CAACAA" detected by RT primer #6 showed lowest distribution across all these cell lines and a highest level of miR-98 expression could be detected in RT-PCR reaction using RT primer #9 in H1299 cells, whereas the highest level of mature miRNA species were detected using primer #8 in HBE and Hela cells (**Figure 21A**). For comparison, we also performed a quantitative real-time SL-RT-PCR to determine the expression of miR-98 in these cells using an Applied Biosystems SL-qRT-PCR miRNA detection kit, which contains one SL-RT primer with similar sequences to those of our SLA-RT primer #6 (**Figure 21B**). The quantitative real-time SL-RT-PCR results exhibited a similar trends and magnitudes of

miR-98 expression in these cells to those detected by SLA-RT-PCR using RT primer #6 (**Figure 21B** and **C**).

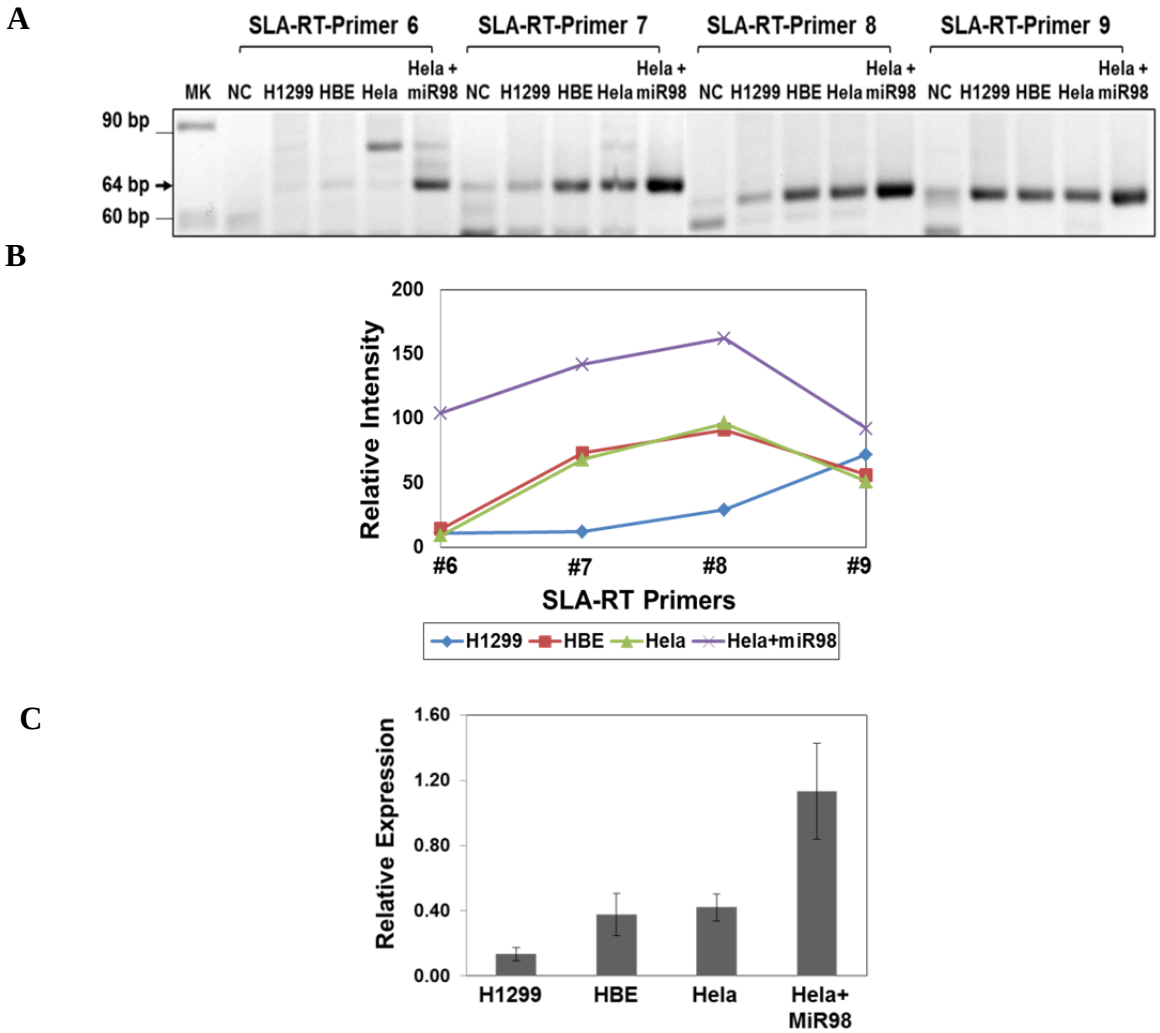

Figure 21. The distribution and expression levels of endogenous miR-98 RNAs among normal HBE, H1299, and Hela cells. **(A)** A highest level of miR-98 expression could be detected in using RT primer #9 in H1299 cells, whereas the highest level of mature miRNA species were detected using primer #8 in HBE and Hela cells. **(B)** Relative distribution of mature miR-98 species detected by SLA-RT primers #6, 7, 8, and 9, respectively, in human HBE, H1299 and Hela cells**. (C)** Detection and quantification of endogenous miR-98 by a quantitative real-time SL-RT-PCR miRNA detection assay (Applied Biosystem).

These results further confirmed by FBFSA and DNA sequencing (data not shown) and clearly demonstrated the accuracy and advantage of SLA-RT-PCR assay in verification and detection of different mature miRNA species in different cell lines or organisms over the current SL-RT-PCR assay with a fixed SL-RT primer for a given miRNA.

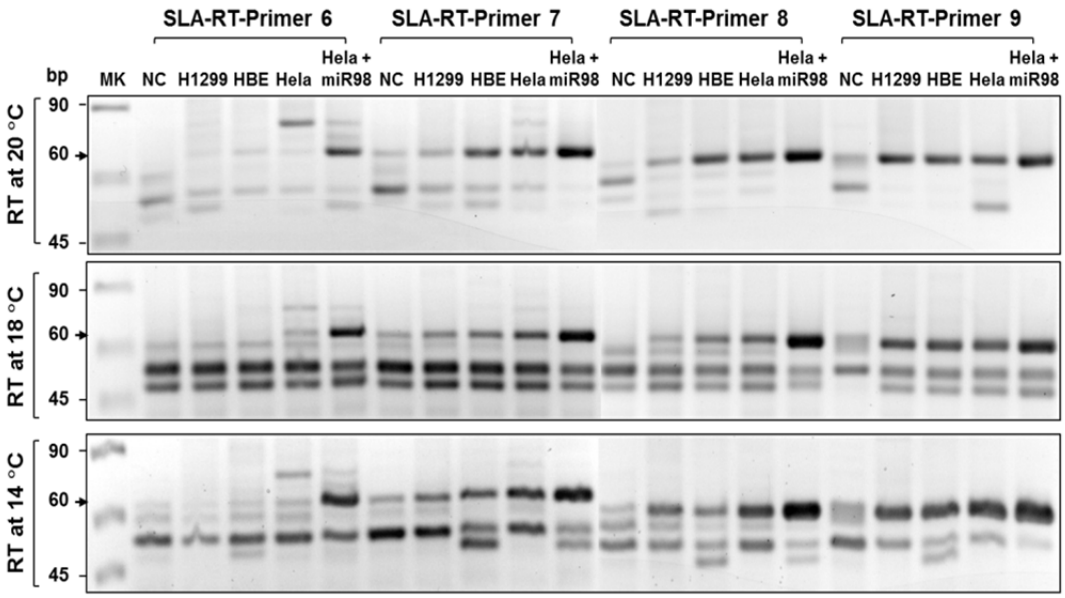

Figure 22. Effects of RT temperature on the specificity and efficiency of SLA-RT-PCR reactions in detection of mature miR-98 species in HBE, Hela and H1299 cells. PCR corresponding to individual SLA-RT primers was shown in Figure 18. SLA-RT reaction was performed at 20 °C (A), 18 °C (B) and 14 °C (C).

Furthermore, we evaluate the effects of RT temperature on the specificity and efficiency of SLA-RT-PCR reactions in detection of mature miR-98 species in human normal bronchial epithelia and tumor cells (**Figure 22**). We generally performed a SLA-RT reaction at 20 °C as a standard RT temperature. An increased amplification of both the specific and the non-specific RT-PCR products was observed when RT temperature was lowered from 20 °C to 18 °C or 14 °C. The patterns of SLA-RT-PCR corresponding to individual SLA-RT primers, however, remained unchanged in reactions with varied

RT temperatures. These results further confirmed the specificity and reproducibility of the SLA-RT-PCR assay.

3.3.6 Verification and detection of the site-specific DNA cleavage by restriction endonucleases

Restriction endonucleases (REs) are endonuclease that can cleave double-stranded (ds) DNAs at specific sites and generate cleaved DNA fragments with unique 3' and 5' overhangs with defined length and bases. We used the well-defined restriction cleavage sites and patterns on DNA templates as model systems to evaluate the potential of using SLA-PCR assay to determine and verify the actual cleavage sites and the cleaved DNA fragments by endonuclease RE activities. The RE Kpn I recognizes the palindromic double-stranded DNA sequence 5'-GGTACC-3' and cleaves DNA by generating a 4-base 3'-overhang; and the Acc651 is an isoschizomer of Kpn I, recognizes the same DNA sequence but produces DNA fragments that have a strictly 4-base 5'-overhang (**Figure 23A**). We used a SLA-PCR strategy, which applies the same principle of works as the SLA-RT-PCR, to precisely map the actual cleavage sites by Kpn I and Acc651 by detecting and verifying the 3'- and 5' overhangs of the intermediates and final products of RE reactions on DNA templates (**Figure 23B** and **C**). The Acc651 exhibited a stringent RE cleavage pattern that generates RE DNA fragments predominantly with 5'-AGCTCG overhangs, as amplified by the specific SLA-primer ending in "CGAGCT" (Figure **23B**, primer 10 and **Figure 23C**). In contrast, the Kpn I showed a promiscuous RE activity, generating a mixture of RE DNA fragments with random cleavage sites (**Figure 22B** and **C**). These results clearly demonstrate the sensitivity and specificity of

SLA-PCR in detecting and verifying the intermediates and products of endonuclease activities.

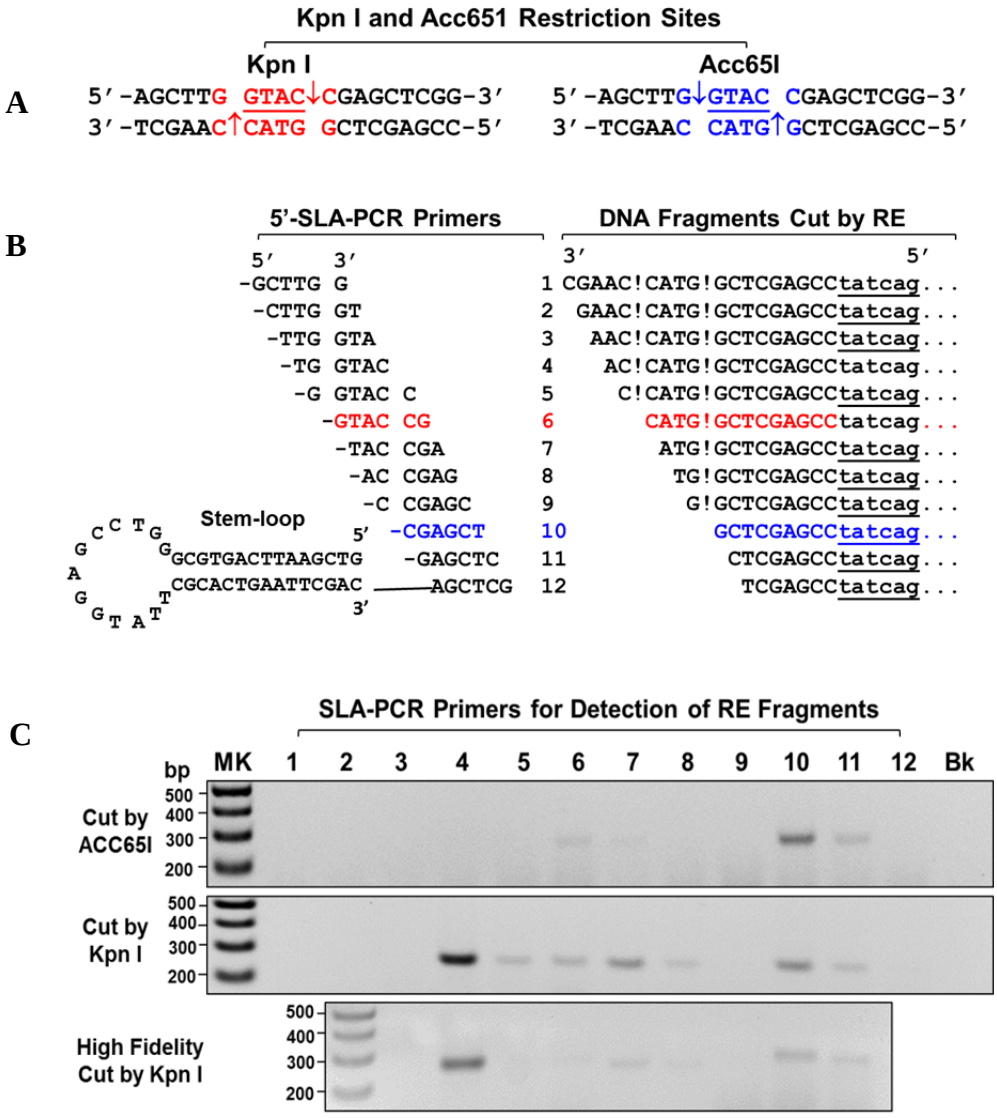

Figure 23. Detection of the site-specific DNA cleavage by restriction endonucleases KpnI and ACC65I. **(A)** The restriction endonuclease map by KpnI and ACC65I. **(B)** SLA -PCR strategy to detect the actual cleavage sites by KpnI and ACC65I. **(C)** SLA -PCR precisely map the actual cleavage sites by Kpn I and Acc651 by detecting and verifying the 3'- and 5' overhangs of the intermediates and final products of RE reactions on DNA templates

3.3.7 Detection and verification of siRNA-mediated mRNA cleavage site by SLA-RT-PCR

To further evaluate the potential application of SLA-RT-PCR assay in identifying novel miRNA targets and molecular mechanisms of action, we used the siRNA-mediated target mRNA cleavage as a model system to precisely detect and verify the intermediates and end products of the siRNA activity in mammalian cells under physiological conditions. It has been shown that mammalian siRNAs (21 and 22 nt) silence gene expression by cleaving their target mRNAs for the sequential degradation and the siRNA cleavage site on the mRNA target is usually located in the middle of the region spanned by the siRNA duplex, following a canonical pattern of 10 bp from the 5′-end of siRNA in the RNA-induced silencing complex (RISC) [95]. The RISC-associated argonaute 2 (Ago 2) protein cleaves the target mRNA into two distinct fragments: a 5′ fragment with a 3′ hydroxyl group, and a 3′ fragment with a 5′ phosphate. The 5’ fragment can be amplified using SLA-RT-PCR with 3’-SLA-RT primers. We used a Dharmacon siRNA transfection reagent (Dharmacon, Chicago, IL) to deliver a synthetic siRNA that was derived from mature hsa-miR-98 and transfected a plasmid vector expressing hsa-miR-98 gene as the siRNA target template into H1299 cells to determine the siRNA cleavage products by SLA-RT-PCR (**Figure 24**). The miR-98-siRNA-mediated cleavage site on the miR-98 mRNA target was precisely detected by the SLA-RT-PCR in the middle of mature miR-98 region at the predicted position “G”, which is 10 bp from the 5′-end of siRNA duplex, as shown in **Figure 24A** and indicated by arrow. The identity of the SLA-RT-PCR products was further verified by DNA sequencing (**Figure 24B** and **24C**).

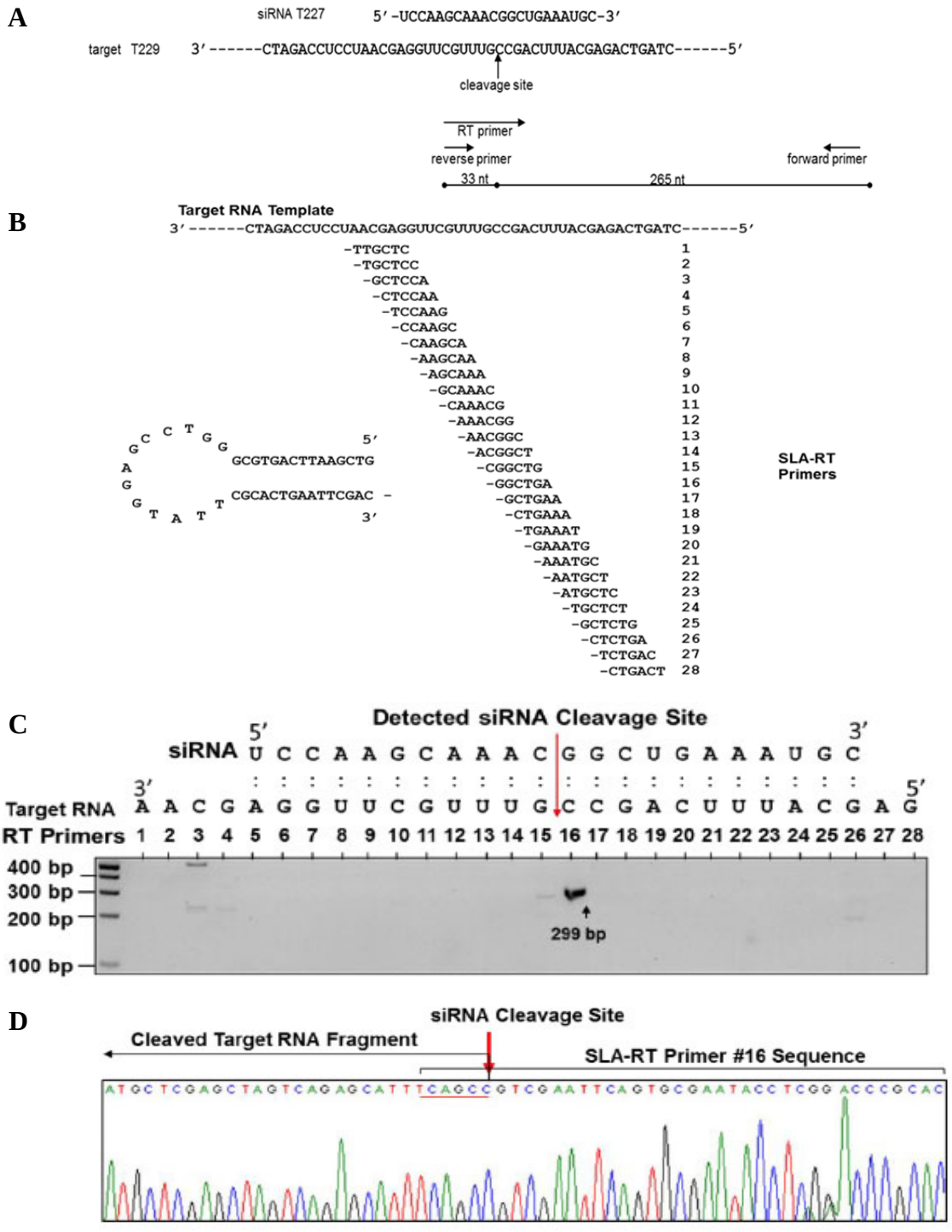

Figure 24. Detection of siRNA cleavage site by SLA-RT-PCR assay. **(A)** The predicted size of SLA-RT-PCR fragment amplified by SLA-RT primer #16. **(B)** sequences of siRNA and its target and SLA-RT primers. The sequences of the SLA-RT primer (#16) anticipated for efficiently detecting the predicted siRNA cleavage site on target RNA template is underlined. **(C)** Detection of siRNA cleavage site in H1299 cells co-transfected with siRNA and target RNA expressing plasmids by SLA-RT-PCR. **(D)** DNA

sequencing confirmation of the siRNA cleavage site and the cleaved RNA fragment detected by SAL-RT-PCR.

These result clearly demonstrated the potential applications of SLA-RT-PCR in identifying authentic miRNA targets and determine their mechanisms of action by precisely detecting and verifying the cleavage sites on target mRNAs mediated by miRNAs in the Ago 2-mRISC in mammalian cells under physiological conditions.

3.4 Discussion

Since the initial discovery, more than 1000 miRNAs have been experimentally identified or predicted by computational methods in human genome (http://www.mirbase.org) [94]. Different sets of miRNAs have been found to be expressed in different organisms, tissue and cell types [76,82,96] and they may target about 60% of mammalian genes [74, 97]. Consequently, great efforts have currently been attributed to identify miRNA biomarkers and signatures associated with various human diseases including cancer and to explore their biological roles and therapeutic potentials [77, 98, 99]. These studies will greatly benefit from accurate identification and quantification of endogenous miRNAs and determination of precise mechanisms of their action.

The mature miRNA molecules have been shown to be varied in length and base compositions or have modifications at their ends [100]. Accurate determination, verification and quantification of miRNAs in a complex biological system are technically challenging but essential for a better understanding of biological roles of miRNAs in regulation of gene expression and disease pathogenesis. The currently used approaches for miRNA profiling, detection, and quantification rely on the miRNA sequence data

presented in various miRNA databases such as miRBase, which are neither accurate nor complete in representing variations and modifications of endogenous miRNAs in a specific organism and cell type. The small size and the complexity of mature miRNA reads present a unique challenge for the conventional RT-PCR-based miRNA detection and quantification methods. Chen and colleagues developed a TaqMan based stem-loop RT-PCR for a real-time quantification of miRNAs and demonstrated a high sensitivity and specificity [90]. This method was, however, designed to quantify a given miRNA with only one pair of primers based on the predicted mature miRNA sequence but it cannot verify and detect processed mature miRNA species with the unique and specific 3' end and 5' ends directly processed from their pre-miRNA sequences and overlooked the critical distribution patterns of processed miRNA repertoires in a given biological system. As demonstrated in this study, mature miR-98 species showed different distribution and levels in different cell types and lineages and the different miRNA molecules with different processed ends could clearly be identified and detected by SLA-RT-PCR assay with miRNA end-sequence specific SLA-RT primers. The miR-98 molecules with 3'-end in "CAACAA" showed a lowest distribution while miR-98 molecules with 3'-end in "CAATAC" exhibited highest level in H1299 cells. In contrast, a very low level of miR-98 expression was detected by a commercially available quantitative real-time SL-RT-PCR because its fixed SL-RT primer can only detect the miR-98 species that showed the lowest distribution in H1299 cells, as detected by one of SLA-RT primers. Such results from conventional SL-RT-PCR can be misleading in data interpretation regarding to the miRNA expression status. Our results clearly demonstrated the accuracy and advantage of SLA-RT-PCR assay in verification and detection of

different mature miRNA species in different cell lines or organisms over the current SL-RT-PCR assay with a fixed SL-RT primer for a given miRNA, which overlooks the importance of the significantly-varied distribution of mature miRNA species in different cell types or organisms. The SLA-RT-PCR assay also showed an excellent linear output of RT-PCR products corresponding to the input of RNA templates over a dynamic detection range at lease of four orders of magnitudes (from 10^{-15} to 10^{-18} mole) and demonstrated an extremely high sensitivity that is capable of detecting as few as 10^{-21} mole in PCR reactions.

We used an agarose gel electrophoresis and gel staining with ethidium bromide to separate and detect the SLA-RT-PCR products. However, it is very difficult to use this method to distinguish non-specific bands from specific RT-PCR products when their sizes are small and similar. Thus, we used a fluorescent-based fragment size analysis (FBFSA) to more accurately measure the size of PCR products. The FBFSA demonstrated that the SLA-RT-PCR could successfully verify sizes of SLA-RT-PCR products by precisely detecting 3' and 5'-ends of mature miRNAs based on pre-miRNA sequences. Many current studies addressing the role of miRNAs in various human diseases including cancer have emphasized the need for accurately determining the sequences of large numbers of miRNAs [97, 100]. However, it has been a persisted challenge to verify sequences of small miRNAs with an averaging ~ 22 nt in length. Our study convincingly demonstrated the potential of using SLA-RT-PCR method as a sensitive and efficient biochemical and molecular tool to verify end sequences and authentic species of endogenous miRNAs in mammalian cells.

Endonucleases such as restriction enzymes (REs) are widely-used molecular biology tools. We used the SLA-PCR assay to detect and verify RE activities of two RE isoschizomers, Kpn I and Acc651, under stringent and relaxed restriction reaction conditions. The SLA-PCR results provided first-handed molecular evidence confirming those previous findings shown that the Kpn I could introduce unpredicted cuts in the plasmid vector and the DNA insert and that the Acc65I offered more stringent restriction cutting patters than the Kpn I and are more desirable for conditional cloning [103]. Our results clearly demonstrate the sensitivity and specificity of SLA-PCR in detecting and verifying the intermediates and products of endonuclease activities.

The cleavage and process of dsRNAs, such as siRNA, pre-miRNAs, and siRNA- or miRNA-target mRNA duplexes, have been shown to be mediated by an intrinsic endonuclease activity of argonauta (Ago) enzymes [94-109]. However, no confirmative evidence has been commonly reported to demonstrate the actual mRNA cleavage events mediated by siRNA-Ago2 activities in the RISC. Such efforts might partly been hindered by technic difficulties in detecting and verifying the cleavage sites and the cleaved mRNA intermediates and end products. The therapeutic applications of using siRNAs to silence the pathogenic genes in clinical practice have also been hampered by their off-target effects and difficulties in confirming that the observed mRNA knockdown is the direct result of an RNAi-mediated event [110]. RACE (rapid amplification of cDNA ends)-PCR and molecular cloning are commonly used to study the siRNA-Ago2 mediated target mRNA cleavage activities but these methods are very time-consuming and labor-intensive [111]. The new SLA-RT-PCR technique presented in this study takes advantages of the high fidelity of SLA-RT primers in recognizing the specific ends of

DNA and RNA fragments generated by REs and siRNA-Ago2 activities, respectively, and the sensitivity of PCR to efficiently and precisely detect target mRNA cleavage sites by siRNAs, suggesting that the SLA-RT-PCR could be used to confirm that the siRNA-mediated mRNA cleavage mechanisms.

In summary, we have developed a novel SLA-RT-PCR assay to efficiently and accurately detect the distribution and relative quantity of the endogenously or exogenously expressed miRNAs in mammalian cells by determining the authentic 3'end and 5' ends of mature miRNAs processed from their pre-miRNA sequences. We also used the SLA-RT-PCR to accurately detect the specific sites and intermediate nucleic acid fragments of DNA and mRNA targets cleaved by the restriction endonucleases in solution and by the siRNA-Ago2 activity in the RISC in human cells, respectively. Our results demonstrated the great potential and broad applications of using the SLA-RT-PCR as a sensitive, cost-efficient, and high-throughput tool to systematically determine the biogenesis and expression of endogenous miRNAs and to identify authentic miRNA targets and determine mechanisms of siRNA and miRNA action by precisely detecting and verifying the cleavage sites on target mRNAs mediated by siRNA or miRNAs in the Ago2-RISCs in mammalian cells under physiological conditions.

Chapter 4. Target mRNA cleavage and degradation mediated by endogenous mammalian miRNAs

4.1 Introduction

Small RNA Lin-4 was first reported miRNA as gene regulatory molecule in 1993 [112] and miRNA was later identified as a large class of short, single stranded RNAs presented naturally in most eukaryotic cells [113,114,115]. Mature miRNAs are incorporated into argonaute proteins as guide sequence in the assembling of miRNA-induced silencing complex (miRISC) for target-specific gene silencing [116]. Plant miRNAs match their mRNA target complementarily to ensure irreversible cleavage of target mRNAs and this is thought to be the predominant mode of miRNA mechanism in plants [117]. In mammalian cells, extended miRNA: target pairing are rare and miRNA recognizes mRNA targets with much shorter base pairs usually located at highly conserved nucleotides (nt) at position 2 -7 of miRNA 5' termini with compensatory support from 3' supplementary pairing [118]. The algorithm of mammalian miRNA: target recognition makes it possible that a single miRNA might target hundreds of potential mRNA transcripts genome-wide. Over the past few years, remarkable progress has been made in our understanding of miRNA biogenesis and function; however, the mechanism that miRNA use to regulate gene expression remains unclear. Earlier studies suggest that the miRNA-induced gene expression interference is through binding to the 3'UTR of target mRNA and repressing translation. Recent studies suggest that the mammalian miRNAs predominantly act to decrease target mRNA levels. However, no direct evidence for miRNA-mediated target mRNA cleavage and degradation has been demonstrated in mammalian cells [119-121].

Previous studies indicated that miRNA participate in the regulation of many crucial cellular process. It was also predicted that mammalian miRNAs can regulate ~30% of all protein coding genes by bioinformatics groups. The mechanism for miRNAs in repressing protein synthesis is still poorly understood. miRNAs can affect both the translation and stability of mRNAs, but the results from different studies have often been contradictory. The recent development of ribosome profiling has provided a sensitive method to verify that regulation by miRNA is mainly through mRNA destabilization.

In plants, miRNA pair to mRNAs with nearly perfect complementarity and trigger endonucleolytic mRNA cleavage. In mammalians, there are rare examples of near-perfect complementarity between miRNA and target site that enables cleavage of the mRNA, such as in the case of miR-196 and HoxB8 mRNA [124]. Most cases, however, involve duplexes that contain mismatches and multiple nucleotide bulges. Therefore, it is difficult to predict and validate the target cleavage sites. In human somatic cells, argonaute protein superfamily is composed of endonucleolytic-capable Ago2 protein and non-catalytic Ago1, Ago3 and Ago4 proteins [122]. Ago2 is the only Ago that functions in the RNAi because the RNase H-like-P-element induced PIWI domain, but not other Agos, can cleave mRNA at the center of the siRNA-mRNA duplex. Ago2 is the only AGO that partially because of the difference of catalytic capability of Ago2 and the noncatalytic nature of other argonaute proteins, translational suppression and mRNA degradation were both proposed as possible mechanisms in mammalian cells [123].

Later, a limited number of mRNA cleavages were mapped to near perfectly matched miRNA:target with deep sequencing approaches. Owing to the limited cases of cleavages observed and prerequisite of extensive base pairing between miRNA:target, miRNA-

mediated mRNA cleavages were regarded to be exceptional rather than a general rule for mammalian gene silencing machinery [125,126,127]. We felt the detection methods used in those studies, i.e., 5'-RACE, PARE, Ribosome profiling, lacked the necessary sensitivity to address the short lived nature of mRNA intermediates in detail especially when there were only small portion of mRNA cleavages overlapped among those reports. With improved detecting methods, those few cases of miRNA cleavages could just be the tip of iceberg.

miRNA-target interactions also stimulate miRNA degradation. It has been reported that pairing between miRNA and targets can induce 3'end degradation of the miRNA, which is followed by the addition of non-template uridines [104]. Uridine addition at the 3'end of miRNAs leads to miRNA destabilization.

One of the many challenges for studying mechanism of target regulation by miRNA is the limited availability of miRNA-target interaction that has been validated in the endogenous context. Often, target predictions are validated by fusing sequence that contain the target sites to a reporter gene and assaying for regulation in the presence or absence of the cognate miRNA. Here, the natural regulatory context is lost, both at the level of the target sequence within its mRNA as well as at the level of cellular context. However, it is possible now to identify endogenous miRNA-directed cleavage sites through SLA-RT-PCR. Here, we used this method to examine whether Hmga2 mRNA was a natural target of let-7 [128]. Hmga2 is a very good system to study endogenous miRNA regulation mechanism, which has one perfect seed region base pairing in 5' UTR and seven perfect seed region base pairings to seed region of let-7 in 3'UTR, predicted by bioinformatics computer program (**Figure 25A** and **25B**). Additionally, we set out to

discover the mechanism by which the target RNA is recognized and cleaved by endogenous miRNA in physiological context. In the endogenous context, many factors influence the ability of the miRNA targeting at mRNA targets.

A

B

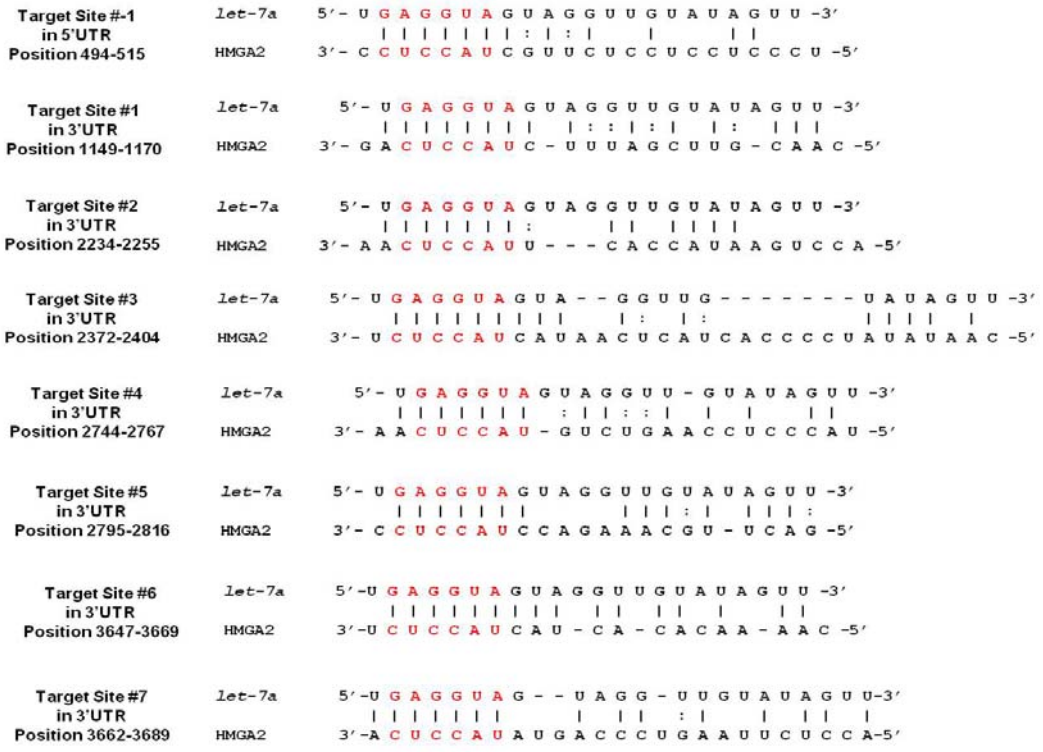

Figure 25. Bioinformatic prediction of let-7 targets in Hmga2 mRNA. **(A)** Schematic representation of Hmga2 gene targets by let-7 miRNA. **(B)** Sequence alignment of let-7a complementary sites in the 5'UTR and 3'UTR of Hmga2 gene. Seed region (nucleotides 2 to 7) is highlighted in red.

With the limited miRNA seed region, other factors must influence target site selection in the context. i.e. the position and context feature that contribute to target site selection and efficiency. AU rich region enhance accessibility to the miRNA complex. In addition, target sites tend to avoid sequence immediately after translation stop codon.

Hmga2 codes for a chromatin-associated protein, which has no intrinsic transcription activity but can regulate transcription by altering the chromatin architecture [129]. Hmga2 is normally expressed at low levels in adult tissues; however, over-expression of Hmga2 has been detected high expression in human tumors [130]. Let-7 family, one of the well-studied of the miRNA families, was first identified in C. elegans [131]. It was reported that let-7 acts as a tumor suppressor gene. Bartel *et al.* reported that the loss of let-7 was associated with oncogenic Hmga2 translocations in various human tumors [128].

4.2 Methods and Materials

4.2.1 SLA-RT-PCR for detection cleavage RNA fragments

Total RNA was prepared by using TRIzol reagent (Invitrogen, Carlbad, CA) and phenol:chloroform according to standard total RNA isolation protocols. RNA was treated with DNaseI to eliminate DNA contamination. RNA was reversed transcribed using the High Capacity Reverse Transcription kit (Applied Biosystem) in combination with a series of stem-loop RT-primers. Briefly, 10 μL RNA (50 ng) was supplemented with 2 μL RT primer (10 μM), 2 μL RT buffer (10 ×), 1 μL multiscribe reverse transcriptase, 0.8 μL dNTP mix (100 mM) in a total reaction volume of 20 μL. To increase reverse

transcription efficiency, a pulsed RT reaction was performed (60 cycles of 18 °C for 1 min and 37 °C for 1 second, followed by 60 cycles of 20 °C for 1min and 37 °C for 1 second, and then 37 °C 30min, 42 °C 20 min, 85 °C 10min).

For each cDNA sample, RT product was diluted 500 fold. PCR reactions were conducted as follows: 95 °C for 5 min followed by 35 cycles of 95 °C for 15 s, 61 °C for 30s, and 37 °C for 30s, then chased for 95°C for 15 s, 58 °C for 2 min, and 37 °C for 2 min.

4.2.2 Western blotting analysis

Proteins were resolved with 7.5% or 15% SDS-polyacrylamide gels and transferred to Immobilon-P transfer membrane (Millipore). Primary antibodies used were rabbit anti-Ago2 (Cell-Signaling), rabbit anti-GW182 (Novus), mouse anti-Hmga2 (Cell-Signaling), rabbit TUTase-2 (Abnova), goat TUTase-3 (Abcam), and mouse anti-β-actin (Clontech).

4.2.3 Let-7 target plasmid construction

Dual let-7 target sequences were cloned into the 3' UTR of the GFP gene in the vector pLJT214. The first let-7 targets and the second let-7 target sequence were cloned directly into the unique NheI-EcoRI and the unique BglII-xhoI restriction sites of the vector, respectively

4.3 Results

4.3.1 Let-7 mediated Hmga2 mRNA cleavage by the influence of Hmga2 mRNA context

Total RNA from H1299 cells was chosen for this analysis. A collection of SL RT primers with 6 nt probe matching along Hmga2 let-7 target sequence were designed to detect the accumulation of cleaved mRNA fragments around 8 let-7 target sites. PCR amplicons were analyzed on agarose electrophoresis gels in the order of let-7 miRNA target sequence at 3' - 5' direction. Amplicon intensity of each PCR reaction represented the relative abundance of 5' fragment detected by a SL-RT primer respectively. We detected these 8 predicted let-7 target sites have different cleavage efficiency, indicating the other characteristics except 7 nt seed match help specify targeting. Importantly, the context feature of target sites within an mRNA has been associated with how well it is recognized and regulated by the miRISC, which may help explain the variable efficiency in let-7 cleavage Hmga2 target mRNA.

The predicted 1# target site in 3'UTR, which is in the 15nt from stop codon, could no longer cleaved by let-7 (**Figure 27**). It reaches the same conclusion that targets sites tend to avoid sequence immediately after the translational stop codon, which is bound by the ribosome. It suggested that miRISC might utilize the translation machinery to scan mRNAs, as miRISC was found to be associated with ribosomal factors and was displaced by the ribosome when the stop codon approached the ribosome A site. In addition, the predicted -1# target site in 5'UTR can be cleaved by let-7 with the reduced efficacy (**Figure 26**). The majority of miRNA target sites are reported in the 3'UTR of mRNAs, which are more effective than those in either 5' UTRs or ORF. The reduced efficacy of

miRNA target sites in 5'UTR or ORF may be attributed to displacement of the miRISC by ribosomes in 5'UTR and ORF, as miRISC passes from the cap to the start codon and finally to stop codon by translocating ribosomes.

We detected the accumulation of let-7 cleaved 5' fragments around target sites -1# -7# (**Figure 26-33**). SLA-RT-PCR revealed similar pattern around miRNA target sites, which have elevated bands at central bulge, 3' complimentary pairing region, 3' adjacent and 5' adjacent region. Seed region is the only region without cleaved 5' RNA fragment accumulation. However, the target mRNA cleavage mechanisms in these regions are different. Ago2 retains the ability to catalyze site-specific miRNA directed endonucleolytic target cleavage, which requires the Watson–Crick pairing between miRNA and target. The accumulation on 3' adjacent region is because the let-7 target sites block 3'-5' degradation, and the increased band on 5' adjacent region is due to the 3'-5' degradation caused from the 3' complimentary pairing region.

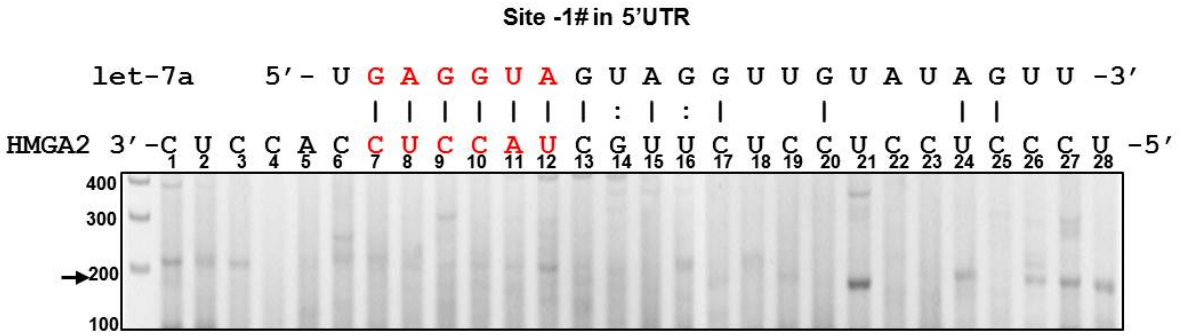

SLA-RT primers list and detected corresponding RNA fragment

	5'- UGAGGUAGUAGGUUGUAUAGUU -3' 3'-CUCCACCUCCAUCGUUCUCCUCCUCCCUUCGCU-5' ||||||	HMGA2 Target
	Stem loop RT probe (5'-3')	RNA Fragment Detected(3'-5')
C1	SL- GAGGTG	CUCCACCUCCAUCGUUCUCCUCCUCCCUUCGC
U2	SL- AGGTGG	UCCACCUCCAUCGUUCUCCUCCUCCCUUCGC
C3	SL- GGTGGA	CCACCUCCAUCGUUCUCCUCCUCCCUUCGC
C4	SL- GTGGAG	CACCUCCAUCGUUCUCCUCCUCCCUUCGC
A5	SL- TGGAGG	ACCUCCAUCGUUCUCCUCCUCCCUUCGC
C6	SL- GGAGGT	CCUCCAUCGUUCUCCUCCUCCCUUCGC
C7	SL- GAGGTA	CUCCAUCGUUCUCCUCCUCCCUUCGC
U8	SL- AGGTAG	UCCAUCGUUCUCCUCCUCCCUUCGC
C9	SL- GGTAGC	CCAUCGUUCUCCUCCUCCCUUCGC
C10	SL- GTAGCA	CAUCGUUCUCCUCCUCCCUUCGC
A11	SL- TAGCAA	AUCGUUCUCCUCCUCCCUUCGC
U12	SL- AGCAAG	UCGUUCUCCUCCUCCCUUCGC
C13	SL- GCAAGA	CGUUCUCCUCCUCCCUUCGC
G14	SL- CAAGAG	GUUCUCCUCCUCCCUUCGC
U15	SL- AAGAGG	UUCUCCUCCUCCCUUCGC
U16	SL- AGAGGA	UCUCCUCCUCCCUUCGC
C17	SL- GAGGAG	CUCCUCCUCCCUUCGC
U18	SL- AGGAGG	UCCUCCUCCCUUCGC
C19	SL- GGAGGA	CCUCCUCCCUUCGC
C20	SL- GAGGAG	CUCCUCCCUUCGC
U21	SL- AGGAGG	UCCUCCCUUCGC
C22	SL- GGAGGG	CCUCCCUUCGC
C23	SL- GAGGGA	CUCCCUUCGC
U24	SL- AGGGAA	UCCCUUCGC
C25	SL- GGGAAG	CCCUUCGC
C26	SL- GGAAGC	CCUUCGC
C27	SL- GAAGCG	CUUCGC
U28	SL- AAGCGA	UUCGC

Figure 26. Detection of let-7 miRNA directed Hmga2 cleavage at target site 1# in 5' UTR by SLA-RT-PCR. All PCR products were run in agarose gels and mapped to the

position expected to let-7-directed Hmga2 cleavage. The expected PCR size was marked with arrow at the left side of agarose gel. miRNA and target site seed region was highlighted with red. Each SLA-RT primer and corresponding RNA cleaved fragment which could be detected was illustrated in the table.

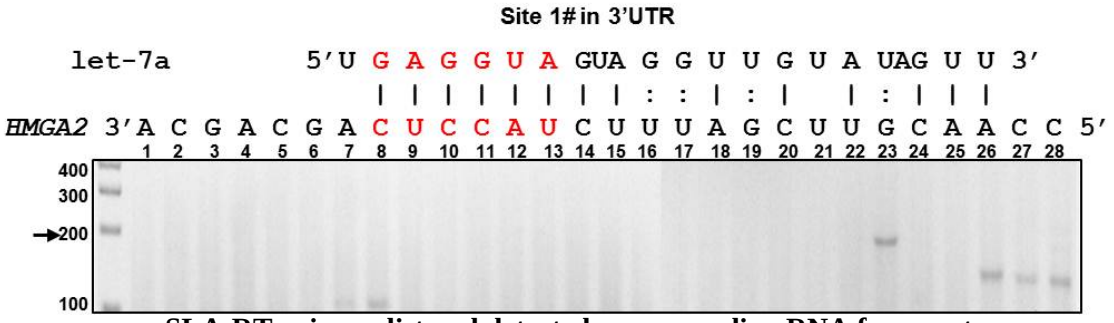

SLA-RT primers list and detected corresponding RNA fragment

	5'- UGAGGUAGUAGGUUGUAUAGUU -3' ||||||||::|:| |:||| 3'-ACGACGACUCCAUCUUUAGCUUGCAACCGCGG-5' ||||||	HMGA2 Target
	Stem loop RT probe (5'-3')	RNA Fragment Detected(3'-5')
A1	SL- TGCTGC	ACGACGACUCCAUCUUUAGCUUGCAACCGCGG
C2	SL- GCTGCT	CGACGACUCCAUCUUUAGCUUGCAACCGCGG
G3	SL- CTGCTG	GACGACUCCAUCUUUAGCUUGCAACCGCGG
A4	SL- TGCTGA	ACGACUCCAUCUUUAGCUUGCAACCGCGG
C5	SL- GCTGAG	CGACUCCAUCUUUAGCUUGCAACCGCGG
G6	SL- CTGAGG	GACUCCAUCUUUAGCUUGCAACCGCGG
A7	SL- TGAGGT	ACUCCAUCUUUAGCUUGCAACCGCGG
C8	SL- GAGGTA	CUCCAUCUUUAGCUUGCAACCGCGG
U9	SL- AGGTAG	UCCAUCUUUAGCUUGCAACCGCGG
C10	SL- GGTAGA	CCAUCUUUAGCUUGCAACCGCGG
C11	SL- GTAGAA	CAUCUUUAGCUUGCAACCGCGG
A12	SL- TAGAAA	AUCUUUAGCUUGCAACCGCGG
U13	SL- AGAAAT	UCUUUAGCUUGCAACCGCGG
C14	SL- GAAATC	CUUUAGCUUGCAACCGCGG
U15	SL- AAATCG	UUUAGCUUGCAACCGCGG
U16	SL- AATCGA	UUAGCUUGCAACCGCGG
U17	SL- ATCGAA	UAGCUUGCAACCGCGG
A18	SL- TCGAAC	AGCUUGCAACCGCGG
G19	SL- CGAACG	GCUUGCAACCGCGG
C20	SL- GAACGT	CUUGCAACCGCGG
U21	SL- AACGTT	UUGCAACCGCGG
U22	SL- ACGTTG	UGCAACCGCGG
G23	SL- CGTTGG	GCAACCGCGG
C24	SL- GTTGGC	CAACCGCGG
A25	SL- TTGGCG	AACCGCGG
A26	SL- TTGGCG	ACCGCGG
C27	SL- TGGCGC	CCGCGG

C28	SL- GGCGCC	CGCGG

Figure 27. Detection of let-7 miRNA directed Hmga2 cleavage at target site 1# in 3' UTR by SLA-RT-PCR. All PCR products were run in agarose gels and mapped to the position expected to let-7-directed Hmga2 cleavage. The expected PCR size was marked with arrow at the left side of agarose gel. miRNA and target site seed region was highlighted with red. Each SLA-RT primer and corresponding RNA cleaved fragment which could be detected was illustrated in the table.

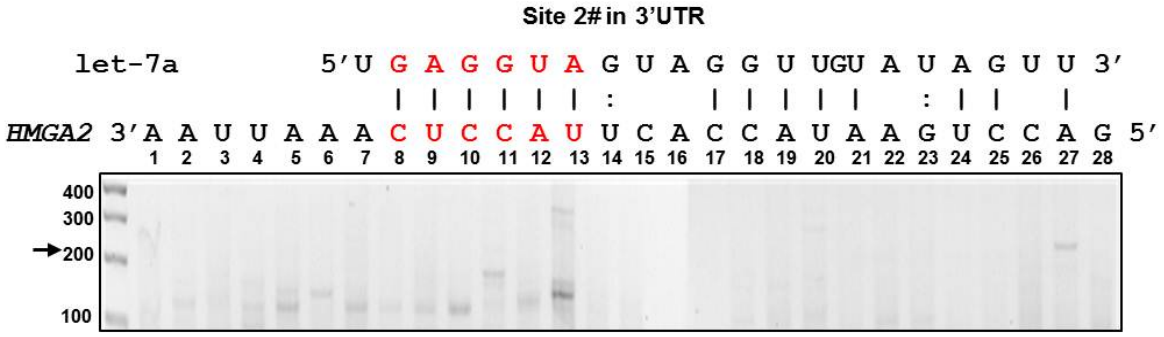

SLA-RT primers list and detected corresponding RNA fragment

	5'- UGAGGUAGUAGGUUGUAUAGUU -3' 3'-AAUUAAACUCCAUUCACCAUAAGUCCAGAAAGU-5' ||||||	HMGA2 Target
	Stem loop RT probe (5'-3')	RNA Fragment Detected(3'-5')
A1	SL-TTAATT	AAUUAAACUCCAUUCACCAUAAGUCCAGAAAG
A2	SL-TAATTT	AUUAAACUCCAUUCACCAUAAGUCCAGAAAG
U3	SL-AATTTG	UUAAACUCCAUUCACCAUAAGUCCAGAAAG
U4	SL-ATTTGA	UAAACUCCAUUCACCAUAAGUCCAGAAAG
A5	SL-TTTGAG	AAACUCCAUUCACCAUAAGUCCAGAAAG
A6	SL-TTGAGG	AACUCCAUUCACCAUAAGUCCAGAAAG
A7	SL-TGAGGT	ACUCCAUUCACCAUAAGUCCAGAAAG
C8	SL-GAGGTA	CUCCAUUCACCAUAAGUCCAGAAAG
U9	SL-AGGTAA	UCCAUUCACCAUAAGUCCAGAAAG
C10	SL-GGTAAG	CCAUUCACCAUAAGUCCAGAAAG
C11	SL-GTAAGT	CAUUCACCAUAAGUCCAGAAAG
A12	SL-TAAGTG	AUUCACCAUAAGUCCAGAAAG
U13	SL-AAGTGG	UUCACCAUAAGUCCAGAAAG
U14	SL-AGTGGT	UCACCAUAAGUCCAGAAAG
C15	SL-GTGGTA	CACCAUAAGUCCAGAAAG
A16	SL-TGGTAT	ACCAUAAGUCCAGAAAG
C17	SL-GGTATT	CCAUAAGUCCAGAAAG
C18	SL-GTATTC	CAUAAGUCCAGAAAG
A19	SL-TATTCA	AUAAGUCCAGAAAG
U20	SL-ATTCAG	UAAGUCCAGAAAG

A21	SL-TTCAGG	AAGUCCAGAAAG
A22	SL-TCAGGT	AGUCCAGAAAG
G23	SL-CAGGTC	GUCCAGAAAG
U24	SL-AGGTCT	UCCAGAAAG
C25	SL-GGTCTT	CCAGAAAG
C26	SL-GTCTTT	CAGAAAG
A27	SL-TCTTTC	AGAAAG
G28	SL-CTTTCA	GAAAG

Figure 28. Detection of let-7 miRNA directed Hmga2 cleavage at target site 2# in 3' UTR by SLA-RT-PCR. All PCR products were run in agarose gels and mapped to the position expected to let-7-directed Hmga2 cleavage. The expected PCR size was marked with arrow at the left side of agarose gel. miRNA and target site seed region was highlighted with red. Each SLA-RT primer and corresponding RNA cleaved fragment which could be detected was illustrated in the table.

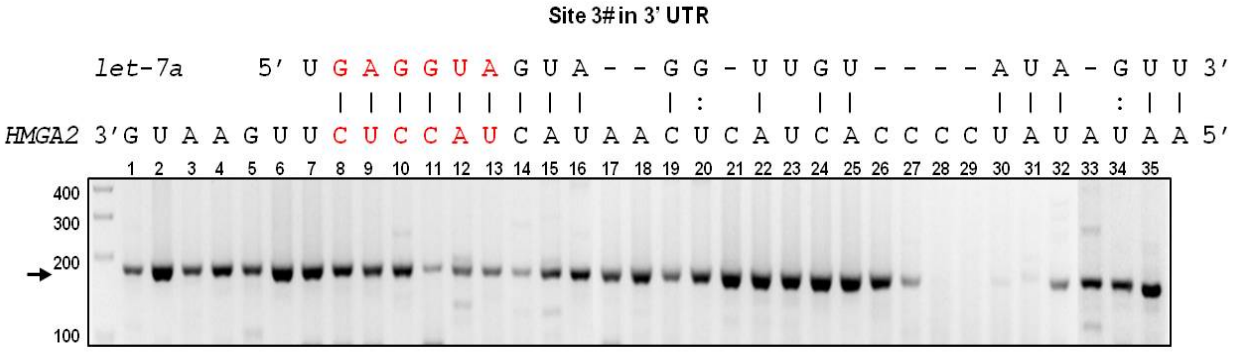

SLA-RT primers list and detected corresponding RNA fragment

	5'- UGAGGUAGUA--GG-UUGU----AUAGUU3' 3'-GUAAGUUCUCCAUCAUAACUCAUCACCCCUAUAUA-5'	HMGA2 Target
	Stem loop RT probe (5'-3')	RNA Fragment Detected(3'-5')
G1	SL-CATTCA	GUAAGUUCUCCAUCAUAACUCAUCACCCCUAUAUA
U2	SL-ATTCAA	UAAGUUCUCCAUCAUAACUCAUCACCCCUAUAUA
A3	SL-TTCAAG	AAGUUCUCCAUCAUAACUCAUCACCCCUAUAUA
A4	SL-TCAAGA	AGUUCUCCAUCAUAACUCAUCACCCCUAUAUA
G5	SL-CAAGAG	GUUCUCCAUCAUAACUCAUCACCCCUAUAUA
U6	SL-AAGAGG	UUCUCCAUCAUAACUCAUCACCCCUAUAUA
U7	SL-AGAGGT	UCUCCAUCAUAACUCAUCACCCCUAUAUA
C8	SL-GAGGTA	CUCCAUCAUAACUCAUCACCCCUAUAUA
U9	SL-AGGTAG	UCCAUCAUAACUCAUCACCCCUAUAUA
C10	SL-GGTAGT	CCAUCAUAACUCAUCACCCCUAUAUA
C11	SL-GTAGTA	CAUCAUAACUCAUCACCCCUAUAUA
A12	SL-TAGTAT	AUCAUAACUCAUCACCCCUAUAUA

U13	SL-AGTATT	UCAUAACUCAUCACCCCUAUAUA
C14	SL-GTATTG	CAUAACUCAUCACCCCUAUAUA
A15	SL-TATTGA	AUAACUCAUCACCCCUAUAUA
U16	SL-ATTGAG	UAACUCAUCACCCCUAUAUA
A17	SL-TTGAGT	AACUCAUCACCCCUAUAUA
A18	SL-TGAGTA	ACUCAUCACCCCUAUAUA
C19	SL-GAGTAG	CUCAUCACCCCUAUAUA
U20	SL-AGTAGT	UCAUCACCCCUAUAUA
C21	SL-GTAGTG	CAUCACCCCUAUAUA
A22	SL-TAGTGG	AUCACCCCUAUAUA
U23	SL-AGTGGG	UCACCCCUAUAUA
C24	SL-GTGGGG	CACCCCUAUAUA
A25	SL-TGGGGA	ACCCCUAUAUA
C26	SL-GGGGAT	CCCCUAUAUA
C27	SL-GGGATA	CCCUAUAUA
C28	SL-GGATAT	CCUAUAUA
C29	SL-GATATA	CUAUAUA
U30	SL-ATATAT	UAUAUA
A31	SL-TATATT	AUAUA
U32	SL-ATATTG	UAUA
A33	SL-ATATTG	AUA
U34	SL-TATTGC	UA
A35	SL-ATTGCA	A

Figure 29. Detection of let-7 miRNA directed Hmga2 cleavage at target site 3# in 3' UTR by SLA-RT-PCR. All PCR products were run in agarose gels and mapped to the position expected to let-7-directed Hmga2 cleavage. The expected PCR size was marked with arrow at the left side of agarose gel. miRNA and target site seed region was highlighted with red. Each SLA-RT primer and corresponding RNA cleaved fragment which could be detected was illustrated in the table.

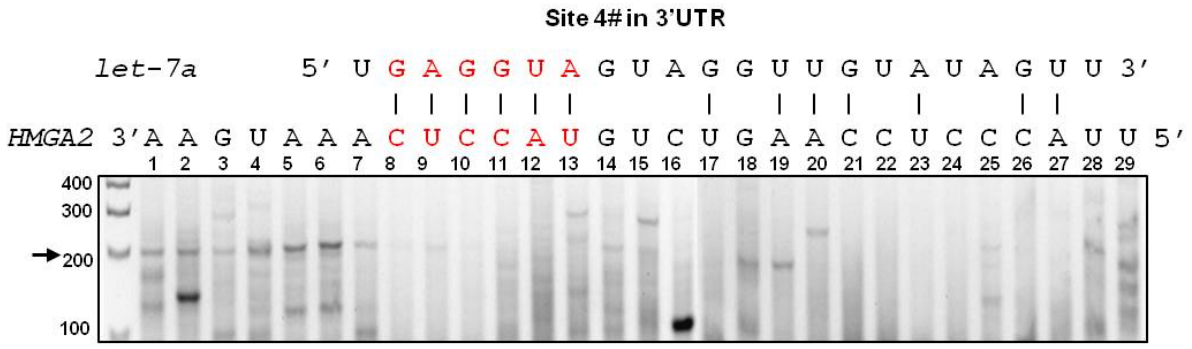

SLA-RT primers list and detected corresponding RNA fragment

	5'- UGAGGUAGUAGGUUGUAUAGUU -3' 3'-AAGUAAACUCCAUGUCUGAACCUCCCAUU-5' HMGA2 Target
	Stem loop RT probe (5'-3')	RNA Fragment Detected(3'-5')
A1	SL- TTCATT	AAGUAAACUCCAUGUCUGAACCUCCCAUU
A2	SL- TCATTT	AGUAAACUCCAUGUCUGAACCUCCCAUU
G3	SL- CATTTG	GUAAACUCCAUGUCUGAACCUCCCAUU
U4	SL- ATTTGA	UAAACUCCAUGUCUGAACCUCCCAUU
A5	SL- TTTGAG	AAACUCCAUGUCUGAACCUCCCAUU
A6	SL- TTGAGG	AACUCCAUGUCUGAACCUCCCAUU
A7	SL- TGAGGT	ACUCCAUGUCUGAACCUCCCAUU
C8	SL- GAGGTA	CUCCAUGUCUGAACCUCCCAUU
U9	SL- AGGTAC	UCCAUGUCUGAACCUCCCAUU
C10	SL- GGTACA	CCAUGUCUGAACCUCCCAUU
C11	SL- GTACAG	CAUGUCUGAACCUCCCAUU
A12	SL- TACAGA	AUGUCUGAACCUCCCAUU
U13	SL- ACAGAC	UGUCUGAACCUCCCAUU
G14	SL- CAGACT	GUCUGAACCUCCCAUU
U15	SL- AGACTT	UCUGAACCUCCCAUU
C16	SL- GACTTG	CUGAACCUCCCAUU
U17	SL- ACTTGG	UGAACCUCCCAUU
G18	SL- CTTGGA	GAACCUCCCAUU
A19	SL- TTGGAG	AACCUCCCAUU
A20	SL- TGGAGG	ACCUCCCAUU
C21	SL- GGAGGG	CCUCCCAUU
C22	SL- GAGGGT	CUCCCAUU
U23	SL- AGGGTA	UCCCAUU
C24	SL- GGGTAA	CCCAUU
C25	SL- GGTAAT	CCAUU
C26	SL- GTAATA	CAUU
A27	SL- TAATAT	AUU
U28	SL- AATATT	UU
U29	SL- ATATTT	U

Figure 30. Detection of let-7 miRNA directed Hmga2 cleavage at target site 4# in 3' UTR by SLA-RT-PCR. All PCR products were run in agarose gels and mapped to the position expected to let-7-directed Hmga2 cleavage. The expected PCR size was marked with arrow at the left side of agarose gel. miRNA and target site seed region was highlighted with red. Each SLA-RT primer and corresponding RNA cleaved fragment which could be detected was illustrated in the table.

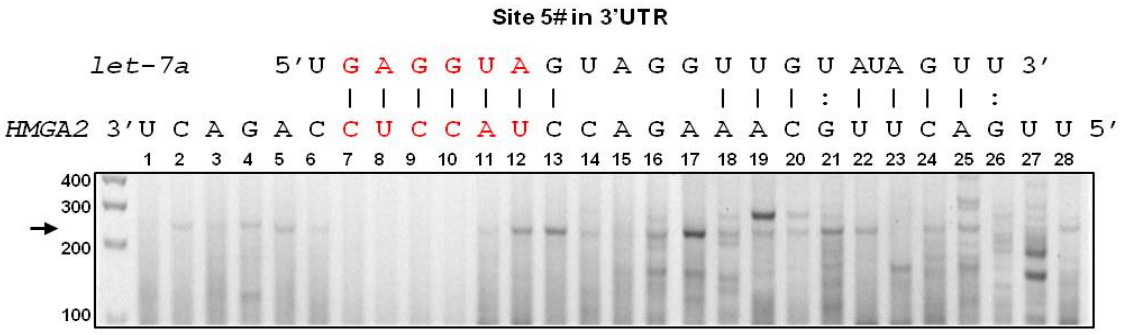

SLA-RT primers list and detected corresponding RNA fragment

	5'- UGAGGUAGUAGGUUGUAUAGUU -3' ||||||| |||:||||: 3'-UCAGACCUCCAUCCAGAAACGUUCAGUU-5' ||||||	HMGA2 Target
	Stem loop RT probe (5'-3')	RNA Fragment Detected(3'-5')
U1	SL- AGTCTG	UCAGACCUCCAUCCAGAAACGUUCAGUU
C2	SL- GTCTGG	CAGACCUCCAUCCAGAAACGUUCAGUU
A3	SL- TCTGGA	AGACCUCCAUCCAGAAACGUUCAGUU
G4	SL- CTGGAG	GACCUCCAUCCAGAAACGUUCAGUU
A5	SL- TGGAGG	ACCUCCAUCCAGAAACGUUCAGUU
C6	SL- GGAGGT	CCUCCAUCCAGAAACGUUCAGUU
C7	SL- GAGGTA	CUCCAUCCAGAAACGUUCAGUU
U8	SL- AGGTAG	UCCAUCCAGAAACGUUCAGUU
C9	SL- GGTAGG	CCAUCCAGAAACGUUCAGUU
C10	SL- GTAGGT	CAUCCAGAAACGUUCAGUU
A11	SL- TAGGTC	AUCCAGAAACGUUCAGUU
U12	SL- AGGTCT	UCCAGAAACGUUCAGUU
C13	SL- GGTCTT	CCAGAAACGUUCAGUU
C14	SL- GTCTTT	CAGAAACGUUCAGUU
A15	SL- TCTTTG	AGAAACGUUCAGUU
G16	SL- CTTTGC	GAAACGUUCAGUU
A17	SL- TTTGCA	AAACGUUCAGUU
A18	SL- TTGCAA	AACGUUCAGUU
A19	SL- TGCAAG	ACGUUCAGUU
C20	SL- GCAAGT	CGUUCAGUU
G21	SL- CAAGTC	GUUCAGUU
U22	SL- AAGTCA	UUCAGUU
U23	SL- AGTCAA	UCAGUU

C24	SL- GTCAAT	CAGUU
A25	SL- TCAATT	AGUU
G26	SL- CAATTA	GUU
U27	SL- AATTAG	UU
U28	SL- ATTAGT	U

Figure 31. Detection of let-7 miRNA directed Hmga2 cleavage at target site 5# in 3' UTR by SLA-RT-PCR. All PCR products were run in agarose gels and mapped to the position expected to let-7-directed Hmga2 cleavage. The expected PCR size was marked with arrow at the left side of agarose gel. miRNA and target site seed region was highlighted with red. Each SLA-RT primer and corresponding RNA cleaved fragment which could be detected was illustrated in the table.

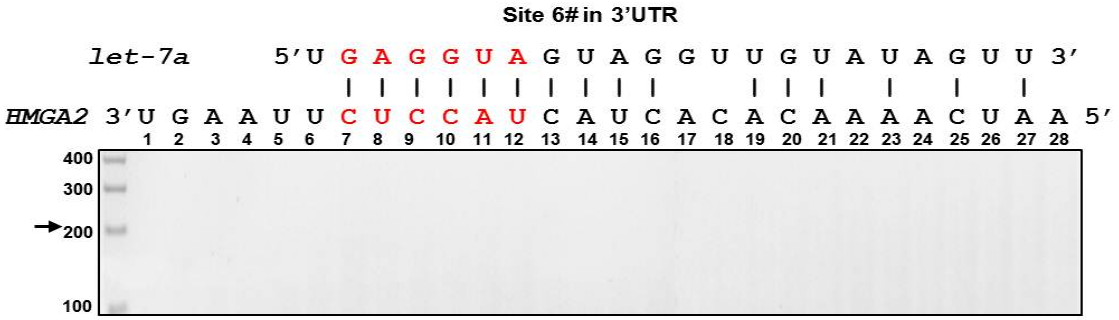

SLA-RT primers list and detected corresponding RNA fragment

	5'- UGAGGUAGUAGGUUGUAUAGUU -3' 3'-UGAAUUCUCCAUCAUCACACAAAACUAA-5'	HMGA2 Target
	Stem loop RT probe (5'-3')	RNA Fragment Detected(3'-5')
U1	SL- ACTTAA	UGAAUUCUCCAUCAUCACACAAAACUAA
G2	SL- CTTAAG	GAAUUCUCCAUCAUCACACAAAACUAA
A3	SL- TTAAGA	AAUUCUCCAUCAUCACACAAAACUAA
A4	SL- TAAGAG	AUUCUCCAUCAUCACACAAAACUAA
U5	SL- AAGAGG	UUCUCCAUCAUCACACAAAACUAA
U6	SL- AGAGGT	UCUCCAUCAUCACACAAAACUAA
C7	SL- GAGGTA	CUCCAUCAUCACACAAAACUAA
U8	SL- AGGTAG	UCCAUCAUCACACAAAACUAA
C9	SL- GGTAGT	CCAUCAUCACACAAAACUAA
C10	SL- GTAGTA	CAUCAUCACACAAAACUAA
A11	SL- TAGTAG	AUCAUCACACAAAACUAA
U12	SL- AGTAGT	UCAUCACACAAAACUAA
C13	SL- GTAGTG	CAUCACACAAAACUAA
A14	SL- TAGTGT	AUCACACAAAACUAA
U15	SL- AGTGTG	UCACACAAAACUAA
C16	SL- GTGTGT	CACACAAAACUAA

A17	SL- TGTGTT	ACACAAAACUAA
C18	SL- GTGTTT	CACAAAACUAA
A19	SL- TGTTTT	ACAAAACUAA
C20	SL- GTTTTG	CAAAACUAA
A21	SL- TTTTGA	AAAACUAA
A22	SL- TTTGAT	AAACUAA
A23	SL- TTGATT	AACUAA
A24	SL- TGATTG	ACUAA
C25	SL- GATTGT	CUAA
U26	SL- ATTGTA	UAA
A27	SL- TTGTAC	AA
A28	SL- TGTACA	A

Figure 32. Detection of let-7 miRNA directed Hmga2 cleavage at target site 6# in 3' UTR by SLA-RT-PCR. All PCR products were run in agarose gels and mapped to the position expected to let-7-directed Hmga2 cleavage. The expected PCR size was marked with arrow at the left side of agarose gel. miRNA and target site seed region was highlighted with red. Each SLA-RT primer and corresponding RNA cleaved fragment which could be detected was illustrated in the table.

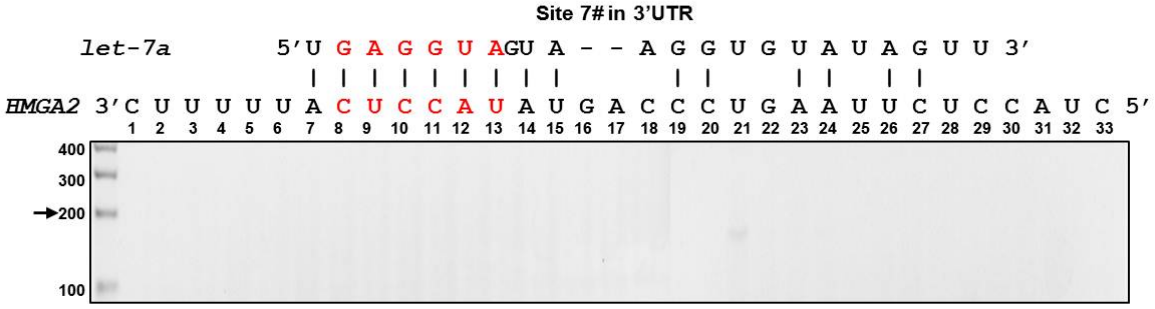

SLA-RT primers list and detected corresponding RNA fragment

	5'- UGAGGUAGUA--GGUUGUAUAGUU -3' 3'-CUUUUUACUCCAUAUGACCCUGAAUUCUCCAUC-5'	HMGA2 Target
	Stem loop RT probe (5'-3')	RNA Fragment Detected(3'-5')
C1	SL- GAAAAA	CUUUUUACUCCAUAUGACCCUGAAUUCUCCAUC
U2	SL- AAAAAT	UUUUUACUCCAUAUGACCCUGAAUUCUCCAUC
U3	SL- AAAATG	UUUUACUCCAUAUGACCCUGAAUUCUCCAUC
U4	SL- AAATGA	UUUACUCCAUAUGACCCUGAAUUCUCCAUC
U5	SL- AATGAG	UUACUCCAUAUGACCCUGAAUUCUCCAUC
U6	SL- ATGAGG	UACUCCAUAUGACCCUGAAUUCUCCAUC
A7	SL- TGAGGT	ACUCCAUAUGACCCUGAAUUCUCCAUC
C8	SL- GAGGTA	CUCCAUAUGACCCUGAAUUCUCCAUC
U9	SL- AGGTAT	UCCAUAUGACCCUGAAUUCUCCAUC
C10	SL- GGTATA	CCAUAUGACCCUGAAUUCUCCAUC
C11	SL- GTATAC	CAUAUGACCCUGAAUUCUCCAUC
A12	SL- TATACT	AUAUGACCCUGAAUUCUCCAUC

U13	SL- ATACTG	UAUGACCCUGAAUUCUCCAUC
A14	SL- TACTGG	AUGACCCUGAAUUCUCCAUC
U15	SL- ACTGGG	UGACCCUGAAUUCUCCAUC
G16	SL- CTGGGA	GACCCUGAAUUCUCCAUC
A17	SL- TGGGAC	ACCCUGAAUUCUCCAUC
C18	SL- GGGACT	CCCUGAAUUCUCCAUC
C19	SL- GGACTT	CCUGAAUUCUCCAUC
C20	SL- GACTTA	CUGAAUUCUCCAUC
U21	SL- ACTTAA	UGAAUUCUCCAUC
G22	SL- CTTAAG	GAAUUCUCCAUC
A23	SL- TTAAGA	AAUUCUCCAUC
A24	SL- TAAGAG	AUUCUCCAUC
U25	SL- AAGAGG	UUCUCCAUC
U26	SL- AGAGGT	UCUCCAUC
C27	SL- GAGGTA	CUCCAUC
U28	SL- AGGTAG	UCCAUC
C29	SL- GGTAGT	CCAUC
C30	SL- GTAGTA	CAUC
A31	SL- TAGTAG	AUC
U32	SL- AGTAGT	UC
C33	SL- GTAGTG	C

Figure 33. Detection of let-7 miRNA directed Hmga2 cleavage at target site 7# in 3' UTR by SLA-RT-PCR. All PCR products were run in agarose gels and mapped to the position expected to let-7-directed Hmga2 cleavage. The expected PCR size was marked with arrow at the left side of agarose gel. miRNA and target site seed region was highlighted with red. Each SLA-RT primer and corresponding RNA cleaved fragment which could be detected was illustrated in the table.

4.3.2 U-Tract added onto the exposed 3' end of the cleaved 5'-fragment of Hmga2 target

RISC-generated products are eventually degraded by exoribonucleases: Xrn1, a 5'-3′ exonuclease, and exosome, a 3-5′multisubunit exonuclease. Interestingly, we recognized an unexpected blank out in seed region, which do not have 3'-5'degradation. We then asked if there is 3' end modification at the end of seed region after cleavage by let-7, which block 3'- 5' degradation in the seed region. Nontemplated oligouridine were post-transcriptionally added to miRNA cleaved 5' fragments as reported by Shen [132]. To

test if oligouridines were added to the 5’ fragments accumulated around let-7 target sites on Hmga2 mRNA, we modified SL-RT primers with addition of a number of adenosines at the 5’ end of primer probe to match possible nontemplated oligouridines at the 3’ end of cleaved RNA fragments (**Figure 34**).

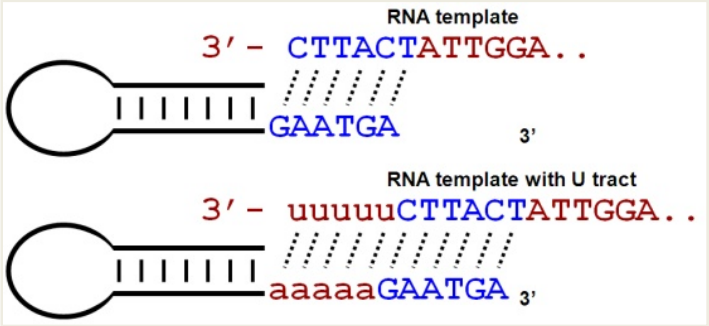

Figure 34. SLA-RT primers with addition of a number of adenosines at the 5’ end to detect possible nontemplated oligouridines at the 3’ end of cleaved RNA fragments.

Total RNA from H1299 cells were tested with two sets of oligouridine detecting SL-RT primers: SLA-RT primers and SLA-8U+RT primers (**Figure 35-39**). 8U-RT-PCR bands increased in 3’ adjacent region, the end in seed region, and the 3’ complimentary pairing region. These U sequences were not found in the genome, so they must have been added after cleavage by let-7. The weak amplicon blocks in unmodified form in **Figure 26-33** disappeared from oligouridylated groups (**Figure 35-39**). The drastically increased RNA fragments in various length of oligouridylated form over unmodified form indicated that oligouridine modification triggered accumulation rather than immediate degradation of miRNA cleaved RNA fragments.

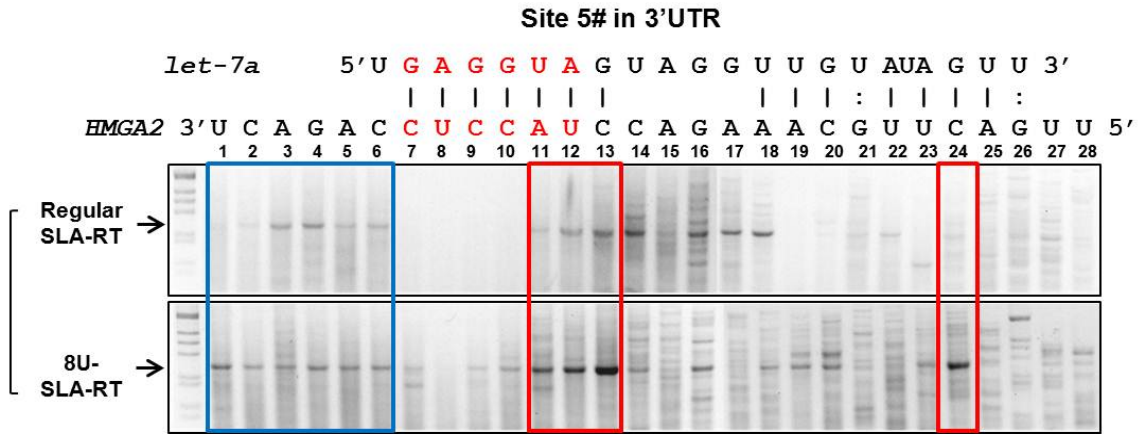

SLA-RT primers and 8U-SLA-RT primers list

	5'- UGAGGUAGUAGGUUGUAUAGUU -3' 3'-UCAGACCUCCAUCCAGAAACGUUCAGUU-5' HMGA2 Target	
	Regular Stem loop RT probe (5'–3')	8U-Stem loop RT probe (5'–3')
U1	SL- AGTCTG	SL- AAAAAAAAGTCTG
C2	SL- GTCTGG	SL- AAAAAAAAGTCTGG
A3	SL- TCTGGA	SL- AAAAAAAATCTGGA
G4	SL- CTGGAG	SL- AAAAAAAACTGGAG
A5	SL- TGGAGG	SL- AAAAAAAATGGAGG
C6	SL- GGAGGT	SL- AAAAAAAAGGAGGT
C7	SL- GAGGTA	SL- AAAAAAAAGAGGTA
U8	SL- AGGTAG	SL- AAAAAAAAAGGTAG
C9	SL- GGTAGG	SL- AAAAAAAAGGTAGG
C10	SL- GTAGGT	SL- AAAAAAAAGTAGGT
A11	SL- TAGGTC	SL- AAAAAAAATAGGTC
U12	SL- AGGTCT	SL- AAAAAAAAAGGTCT
C13	SL- GGTCTT	SL- AAAAAAAAGGTCTT
C14	SL- GTCTTT	SL- AAAAAAAAGTCTTT
A15	SL- TCTTTG	SL- AAAAAAAATCTTTG
G16	SL- CTTTGC	SL- AAAAAAAACTTTGC
A17	SL- TTTGCA	SL- AAAAAAAATTTGCA
A18	SL- TTGCAA	SL- AAAAAAAATTGCAA
A19	SL- TGCAAG	SL- AAAAAAAATGCAAG
C20	SL- GCAAGT	SL- AAAAAAAAGCAAGT
G21	SL- CAAGTC	SL- AAAAAAAACAAGTC
U22	SL- AAGTCA	SL- AAAAAAAAAAGTCA
U23	SL- AGTCAA	SL- AAAAAAAAAGTCAA
C24	SL- GTCAAT	SL- AAAAAAAAGTCAAT
A25	SL- TCAATT	SL- AAAAAAAATCAATT
G26	SL- CAATTA	SL- AAAAAAAACAATTA
U27	SL- AATTAG	SL- AAAAAAAAAATTAG
U28	SL- ATTAGT	SL- AAAAAAAAATTAGT

Figure 35. let-7 miRNA directed uridylation of cleavage fragment at target site 5# in 3'UTR. All PCR products were run in agarose gels and mapped to the position expected to let-7-directed Hmga2 cleavage. RNA was tested with two sets of SLA-RT primers: SLA-RT primers and SLA-8U-RT primers, which listed in the table. 8U-RT-PCR bands increased in 3' adjacent region (highlighted with blue), the end in seed region (highlighted with red), and the 3' complimentary pairing region (highlighted with red). The expected PCR size was marked with arrow at the left side of agarose gel. miRNA and target site seed region was highlighted with red.

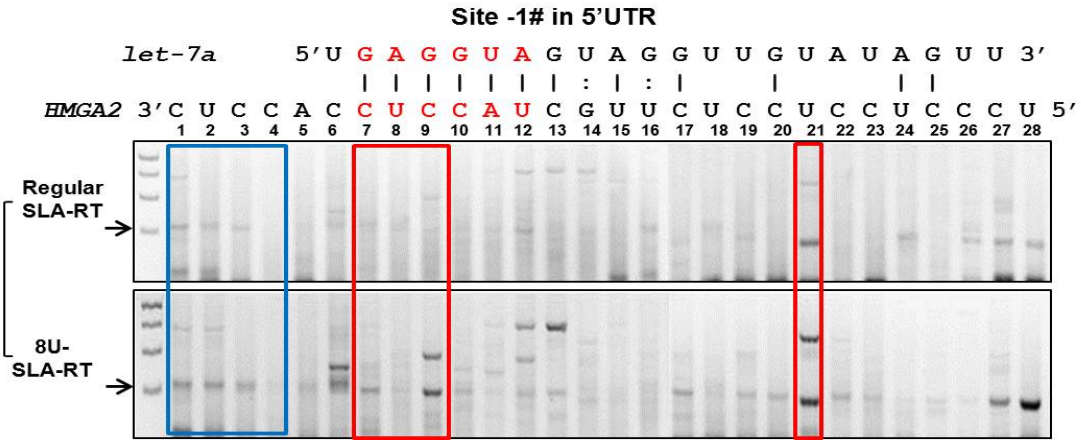

SLA-RT primers and 8U-SLA-RT primers list

	5'- UGAGGUAGUAGGUUGUAUAGUU -3' 3'-CUCCACCUCCAUCGUUCUCCUCCUCCCUUCGCU-5'	HMGA2 Target
	Regular Stem loop RT probe (5'-3')	8U-Stem loop RT probe (5'-3')
C1	SL- GAGGTG	SL-AAAAAAAAGAGGTG
U2	SL- AGGTGG	SL-AAAAAAAAAGGTGG
C3	SL- GGTGGA	SL-AAAAAAAAGGTGGA
C4	SL- GTGGAG	SL-AAAAAAAAGTGGAG
A5	SL- TGGAGG	SL-AAAAAAAATGGAGG
C6	SL- GGAGGT	SL-AAAAAAAAGGAGGT
C7	SL- GAGGTA	SL-AAAAAAAAGAGGTA
U8	SL- AGGTAG	SL-AAAAAAAAAGGTAG
C9	SL- GGTAGC	SL-AAAAAAAAGGTAGC
C10	SL- GTAGCA	SL-AAAAAAAAGTAGCA
A11	SL- TAGCAA	SL-AAAAAAAATAGCAA
U12	SL- AGCAAG	SL-AAAAAAAAAGCAAG
C13	SL- GCAAGA	SL-AAAAAAAAGCAAGA
G14	SL- CAAGAG	SL-AAAAAAAACAAGAG
U15	SL- AAGAGG	SL-AAAAAAAAAAGAGG
U16	SL- AGAGGA	SL-AAAAAAAAAGAGGA
C17	SL- GAGGAG	SL-AAAAAAAAGAGGAG
U18	SL- AGGAGG	SL-AAAAAAAAAGGAGG
C19	SL- GGAGGA	SL-AAAAAAAAGGAGGA
C20	SL- GAGGAG	SL-AAAAAAAAGAGGAG

U21	SL- AGGAGG	SL-AAAAAAAAGGAGG
C22	SL- GGAGGG	SL-AAAAAAAGGAGGG
C23	SL- GAGGGA	SL-AAAAAAAGAGGGA
U24	SL- AGGGAA	SL-AAAAAAAAGGGAA
C25	SL- GGGAAG	SL-AAAAAAAGGGAAG
C26	SL- GGAAGC	SL-AAAAAAAGGAAGC
C27	SL- GAAGCG	SL-AAAAAAAGAAGCG
U28	SL- AAGCGA	SL-AAAAAAAAAGCGA

Figure 36. let-7 miRNA directed uridylation of cleavage fragment at target site -1# in 5'UTR. All PCR products were run in agarose gels and mapped to the position expected to let-7-directed Hmga2 cleavage. RNA was tested with two sets of SLA-RT primers: SLA-RT primers and SLA-8U-RT primers, which listed in the table. 8U-RT-PCR bands increased in 3' adjacent region (highlighted with blue), the end in seed region (highlighted with red), and the 3' complimentary pairing region (highlighted with red). The expected PCR size was marked with arrow at the left side of agarose gel. miRNA and target site seed region was highlighted with red.

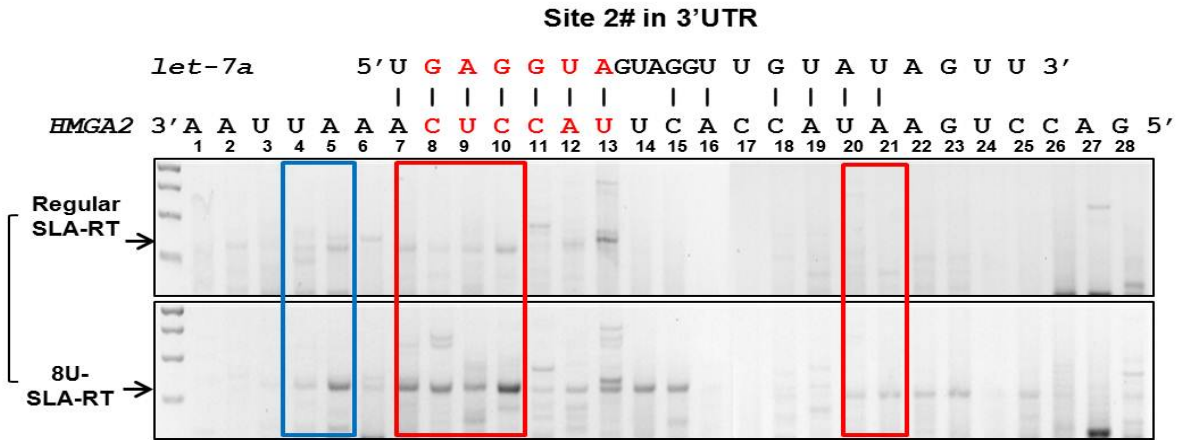

SLA-RT primers and 8U-SLA-RT primers list

	5'- UGAGGUAGUAGGUUGUAUAGUU -3' 3'-AAUUAAACUCCAUUCACCAUAAGUCCA-5' HMGA2 Target	
	Regular Stem loop RT probe (5'-3')	8U-Stem loop RT probe (5'-3')
A1	SL-TTAATT	SL-AAAAAAAATTAATT
A2	SL-TAATTT	SL-AAAAAAAATAATTT
U3	SL-AATTTG	SL-AAAAAAAAAATTTG
U4	SL-ATTTGA	SL-AAAAAAAAATTTGA
A5	SL-TTTGAG	SL-AAAAAAAATTTGAG
A6	SL-TTGAGG	SL-AAAAAAAATTGAGG
A7	SL-TGAGGT	SL-AAAAAAAATGAGGT

C8	SL-GAGGTA	SL-AAAAAAAAGAGGTA
U9	SL-AGGTAA	SL-AAAAAAAAAGGTAA
C10	SL-GGTAAG	SL-AAAAAAAAGGTAAG
C11	SL-GTAAGT	SL-AAAAAAAAGTAAGT
A12	SL-TAAGTG	SL-AAAAAAAATAAGTG
U13	SL-AAGTGG	SL-AAAAAAAAAAGTGG
U14	SL-AGTGGT	SL-AAAAAAAAAGTGGT
C15	SL-GTGGTA	SL-AAAAAAAAGTGGTA
A16	SL-TGGTAT	SL-AAAAAAAATGGTAT
C17	SL-GGTATT	SL-AAAAAAAAGGTATT
C18	SL-GTATTC	SL-AAAAAAAAGTATTC
A19	SL-TATTCA	SL-AAAAAAAATATTCA
U20	SL-ATTCAG	SL-AAAAAAAATTCAG
A21	SL-TTCAGG	SL-AAAAAAAATTCAGG
A22	SL-TCAGGT	SL-AAAAAAAATCAGGT
G23	SL-CAGGTC	SL-AAAAAAAACAGGTC
U24	SL-AGGTCT	SL-AAAAAAAAAGGTCT
C25	SL-GGTCTT	SL-AAAAAAAAGGTCTT
C26	SL-GTCTTT	SL-AAAAAAAAGTCTTT
A27	SL-TCTTTC	SL-AAAAAAAATCTTTC
G28	SL-CTTTCA	SL-AAAAAAAACTTTCA

Figure 37. let-7 miRNA directed uridylation of cleavage fragment at target site 2# in 3'UTR. All PCR products were run in agarose gels and mapped to the position expected to let-7-directed Hmga2 cleavage. RNA was tested with two sets of SLA-RT primers: SLA-RT primers and SLA-8U-RT primers, which listed in the table. 8U-RT-PCR bands increased in 3' adjacent region (highlighted with blue), the end in seed region (highlighted with red), and the 3' complimentary pairing region (highlighted with red). The expected PCR size was marked with arrow at the left side of agarose gel. miRNA and target site seed region was highlighted with red.

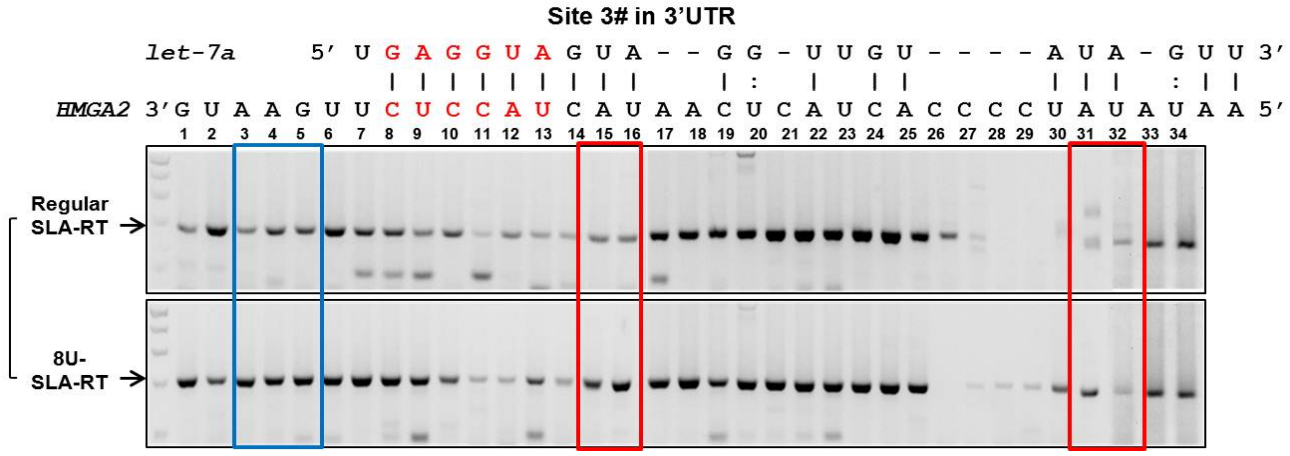

SLA-RT primers and 8U-SLA-RT primers list

	5’- UGAGGUAGUA--GG-UUGU----AUAGUU3’ ||||||||| |: | || ||| | 3’-GUAAGUUCUCCAUCAUAACUCAUCACCCCUAUAUA-5’ ||||||	HMGA2 Target
	Regular Stem loop RT probe (5’–3’)	8U-Stem loop RT probe (5’–3’)
G1	SL-CATTCA	SL-AAAAAAAACATTCA
U2	SL-ATTCAA	SL-AAAAAAAAATTCAA
A3	SL-TTCAAG	SL-AAAAAAAATTCAAG
A4	SL-TCAAGA	SL-AAAAAAAATCAAGA
G5	SL-CAAGAG	SL-AAAAAAAACAAGAG
U6	SL-AAGAGG	SL-AAAAAAAAAAGAGG
U7	SL-AGAGGT	SL-AAAAAAAAAGAGGT
C8	SL-GAGGTA	SL-AAAAAAAAGAGGTA
U9	SL-AGGTAG	SL-AAAAAAAAAGGTAG
C10	SL-GGTAGT	SL-AAAAAAAAGGTAGT
C11	SL-GTAGTA	SL-AAAAAAAAGTAGTA
A12	SL-TAGTAT	SL-AAAAAAAATAGTAT
U13	SL-AGTATT	SL-AAAAAAAAAGTATT
C14	SL-GTATTG	SL-AAAAAAAAGTATTG
A15	SL-TATTGA	SL-AAAAAAAATATTGA
U16	SL-ATTGAG	SL-AAAAAAAAATTGAG
A17	SL-TTGAGT	SL-AAAAAAAATTGAGT
A18	SL-TGAGTA	SL-AAAAAAAATGAGTA
C19	SL-GAGTAG	SL-AAAAAAAAGAGTAG
U20	SL-AGTAGT	SL-AAAAAAAAAGTAGT
C21	SL-GTAGTG	SL-AAAAAAAAGTAGTG
A22	SL-TAGTGG	SL-AAAAAAAATAGTGG
U23	SL-AGTGGG	SL-AAAAAAAAAGTGGG
C24	SL-GTGGGG	SL-AAAAAAAAGTGGGG
A25	SL-TGGGGA	SL-AAAAAAAATGGGGA
C26	SL-GGGGAT	SL-AAAAAAAAGGGGAT
C27	SL-GGGATA	SL-AAAAAAAAGGGATA
C28	SL-GGATAT	SL-AAAAAAAAGGATAT
C29	SL-GATATA	SL-AAAAAAAAGATATA
U30	SL-ATATAT	SL-AAAAAAAAATATAT
A31	SL-TATATT	SL-AAAAAAAATATATT
U32	SL-ATATTG	SL-AAAAAAAAATATTG
A33	SL-ATATTG	SL-AAAAAAAAATATTG
U34	SL-TATTGC	SL-AAAAAAAATATTGC
A35	SL-ATTGCA	SL-AAAAAAAAATTGCA

Figure 38. let-7 miRNA directed uridylation of cleavage fragment at target site 3# in 3’UTR. All PCR products were run in agarose gels and mapped to the position expected to let-7-directed Hmga2 cleavage. RNA was tested with two sets of SLA-RT primers: SLA-RT primers and SLA-8U-RT primers, which listed in the table. 8U-RT-PCR bands increased in 3’ adjacent region (highlighted with blue), the end in seed region

(highlighted with red), and the 3' complimentary pairing region (highlighted with red). The expected PCR size was marked with arrow at the left side of agarose gel. miRNA and target site seed region was highlighted with red.

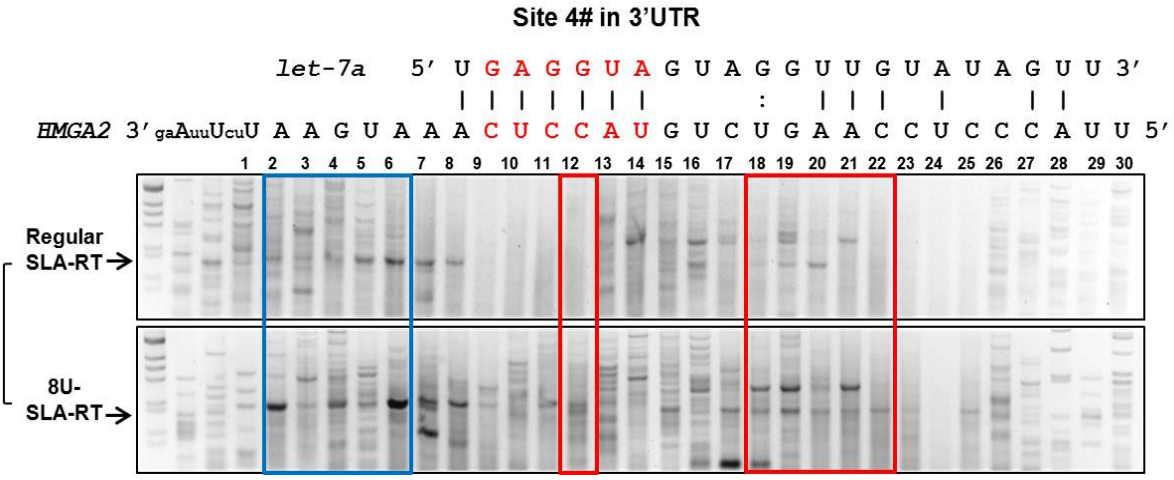

SLA-RT primers and 8U-SLA-RT primers list

	5'- UGAGGUAGUAGGUUGUAUAGUU -3' 3'-AAGUAAACUCCAUGUCUGAACCUCCCAUU-5' HMGA2 Target	
	Regular Stem loop RT probe (5'-3')	8U-Stem loop RT probe (5'-3')
A1	SL- TTCATT	SL- AAAAAAAATTCATT
A2	SL- TCATTT	SL- AAAAAAAATCATTT
G3	SL- CATTTG	SL- AAAAAAAACATTTG
U4	SL- ATTTGA	SL- AAAAAAAAATTTGA
A5	SL- TTTGAG	SL- AAAAAAAATTTGAG
A6	SL- TTGAGG	SL- AAAAAAAATTGAGG
A7	SL- TGAGGT	SL- AAAAAAAATGAGGT
C8	SL- GAGGTA	SL- AAAAAAAAGAGGTA
U9	SL- AGGTAC	SL- AAAAAAAAAGGTAC
C10	SL- GGTACA	SL- AAAAAAAAGGTACA
C11	SL- GTACAG	SL- AAAAAAAAGTACAG
A12	SL- TACAGA	SL- AAAAAAAATACAGA
U13	SL- ACAGAC	SL- AAAAAAAAACAGAC
G14	SL- CAGACT	SL- AAAAAAAACAGACT
U15	SL- AGACTT	SL- AAAAAAAAAGACTT
C16	SL- GACTTG	SL- AAAAAAAAGACTTG
U17	SL- ACTTGG	SL- AAAAAAAAACTTGG
G18	SL- CTTGGA	SL- AAAAAAAACTTGGA
A19	SL- TTGGAG	SL- AAAAAAAATTGGAG
A20	SL- TGGAGG	SL- AAAAAAAATGGAGG
C21	SL- GGAGGG	SL- AAAAAAAAGGAGGG

C22	SL- GAGGGT	SL- AAAAAAAAGAGGGT
U23	SL- AGGGTA	SL- AAAAAAAAAGGGTA
C24	SL- GGGTAA	SL- AAAAAAAAGGGTAA
C25	SL- GGTAAT	SL- AAAAAAAAGGTAAT
C26	SL- GTAATA	SL- AAAAAAAAGTAATA
A27	SL- TAATAT	SL- AAAAAAAATAATAT
U28	SL- AATATT	SL- AAAAAAAAAATATT
U29	SL- ATATTT	SL- AAAAAAAAATATTT

Figure 39. let-7 miRNA directed uridylation of cleavage fragment at target site 4# in 3'UTR. All PCR products were run in agarose gels and mapped to the position expected to let-7-directed Hmga2 cleavage. RNA was tested with two sets of SLA-RT primers: SLA-RT primers and SLA-8U-RT primers, which listed in the table. 8U-RT-PCR bands increased in 3' adjacent region (highlighted with blue), the end in seed region (highlighted with red), and the 3' complimentary pairing region (highlighted with red). The expected PCR size was marked with arrow at the left side of agarose gel. miRNA and target site seed region was highlighted with red.

A terminal U tail on RNA is known to serve as a ''mark'' for 5'- 3' degradation. Certain types of mRNA, such as histone mRNA [133] and RNA interference cleavage products [132] are uridylated before degradation. This oligo U tract is recognized by the Lsm1–7 complex, which then appears to feed the transcript into the standard mRNA decay pathways [134].

The next obvious question was which enzyme is responsible for uridylation after cleaved by miRNAs. We examined whether terminal uridylyl transferase (TUTase) might be responsible for the addition of an oligo U tail to RISC-generated RNA fragments. Knocking down TUTase 3 erases the accumulation of U-tract added fragments to background level. Knocking down TUTase 2 decreased uridylylized 5' fragment only in the seed region (**Figure 40**)

A

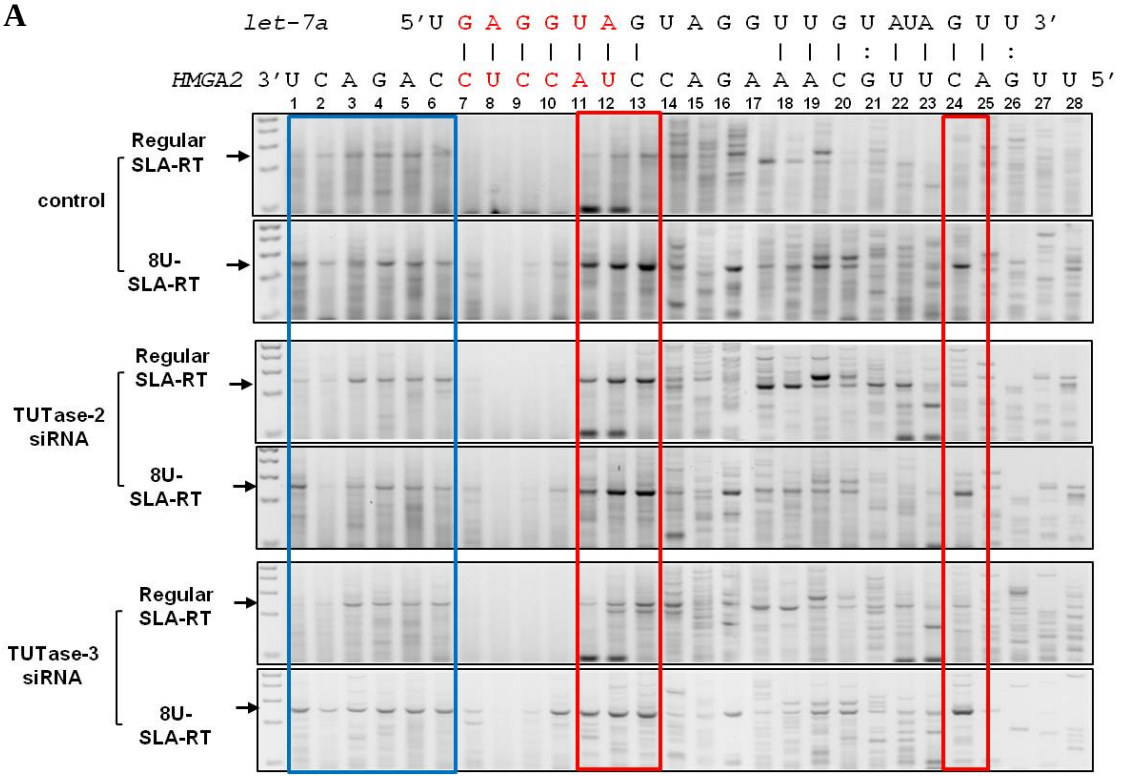

B **SLA-RT primers and 8U-SLA-RT primers list**

	5′- UGAGGUAGUAGGUUGUAUAGUU -3′ ||||||| |||:||||: 3′-UCAGACCUCCAUCCAGAAACGUUCAGUU-5′ ||||||	HMGA2 Target
	Regular Stem loop RT probe (5′-3′)	8U-Stem loop RT probe (5′-3′)
U1	SL- AGTCTG	SL- AAAAAAAAGTCTG
C2	SL- GTCTGG	SL- AAAAAAAAGTCTGG
A3	SL- TCTGGA	SL- AAAAAAAATCTGGA
G4	SL- CTGGAG	SL- AAAAAAAACTGGAG
A5	SL- TGGAGG	SL- AAAAAAAATGGAGG
C6	SL- GGAGGT	SL- AAAAAAAAGGAGGT
C7	SL- GAGGTA	SL- AAAAAAAAGAGGTA
U8	SL- AGGTAG	SL- AAAAAAAAAGGTAG
C9	SL- GGTAGG	SL- AAAAAAAAGGTAGG
C10	SL- GTAGGT	SL- AAAAAAAAGTAGGT
A11	SL- TAGGTC	SL- AAAAAAAATAGGTC
U12	SL- AGGTCT	SL- AAAAAAAAAGGTCT
C13	SL- GGTCTT	SL- AAAAAAAAGGTCTT
C14	SL- GTCTTT	SL- AAAAAAAAGTCTTT
A15	SL- TCTTTG	SL- AAAAAAAATCTTTG
G16	SL- CTTTGC	SL- AAAAAAAACTTTGC
A17	SL- TTTGCA	SL- AAAAAAAATTTGCA

A18	SL- TTGCAA	SL- AAAAAAAATTGCAA
A19	SL- TGCAAG	SL- AAAAAAAATGCAAG
C20	SL- GCAAGT	SL- AAAAAAAAGCAAGT
G21	SL- CAAGTC	SL- AAAAAAAACAAGTC
U22	SL- AAGTCA	SL- AAAAAAAAAAGTCA
U23	SL- AGTCAA	SL- AAAAAAAAAGTCAA
C24	SL- GTCAAT	SL- AAAAAAAAGTCAAT
A25	SL- TCAATT	SL- AAAAAAAATCAATT
G26	SL- CAATTA	SL- AAAAAAAACAATTA
U27	SL- AATTAG	SL- AAAAAAAAAATTAG
U28	SL- ATTAGT	SL- AAAAAAAAATTAGT

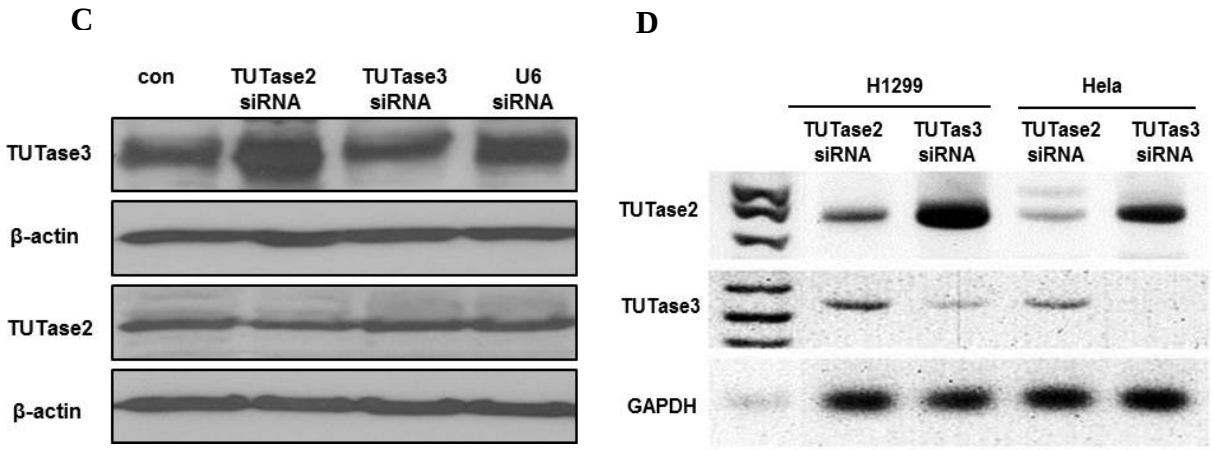

Figure 40. Effects of 3' terminal TUTases on the addition of uridine residues to the 3'-ends of let-7 cleaved mRNA fragments. **(A)** Effects of uridylation of target site 5# after treatment with TUTase2 siRNA and TUTase3 siRNA. The uridized sites at 3' adjacent region (highlighted with blue), the end in seed region (highlighted with red), and the 3' complimentary pairing region (highlighted with red) 3' adjacent region (highlighted with blue), the end in seed region (highlighted with red), and the 3' complimentary pairing region (highlighted with red). Knocking down TUTase 3 erases the accumulation of U-tract added fragments to background level. Knocking down TUTase 2 decreased uridylylized 5' fragment only in the seed region. The expected PCR size was marked with arrow at the left side of agarose gel. miRNA and target site seed region was highlighted with red. **(B)** The specific SL-RT primer and corresponding detected cleavage RNA fragment was illustrated in the table. **(C)** Western blotting analysis and **(D)** RT-PCR analysis of TUTase 2 and TUTase 3 after treatment with TUTase2 siRNA and TUTase3 siRNA. TUTase2 siRNA inhibited TUTase2 expression, and TUTase3 siRNA inhibited TUTase3 expression.

One possible explanation for observed miRNA cleavage pattern is that the retention of miRISC on its miRNA sites hampers mRNA 3'-5' degradation and the 3'-5' partially degraded mRNA fragments are further uridylylized by TUTase 3 recruited by miRISCs at 2 and 3 nt of 3' adjacent region.

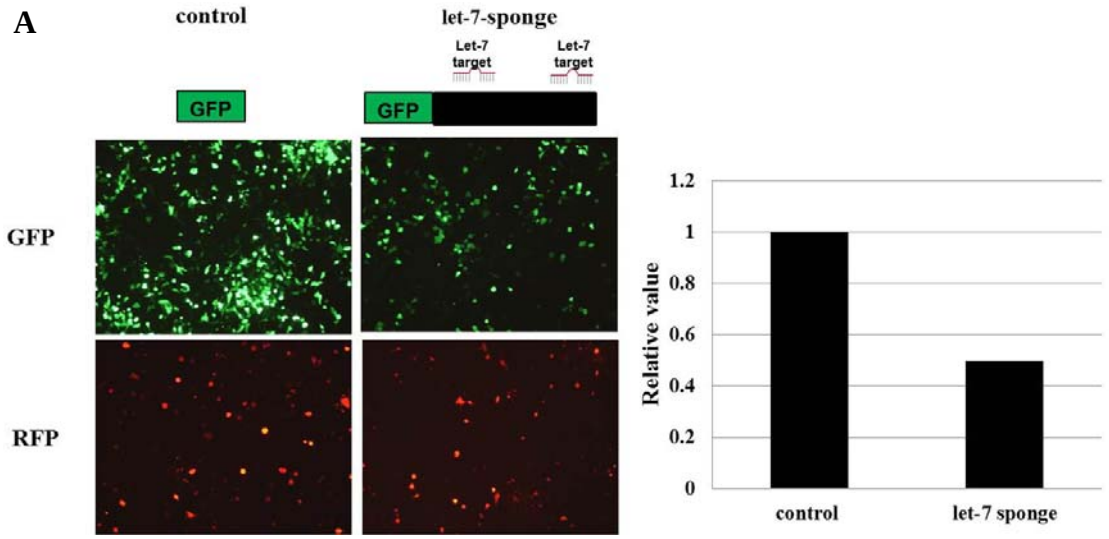

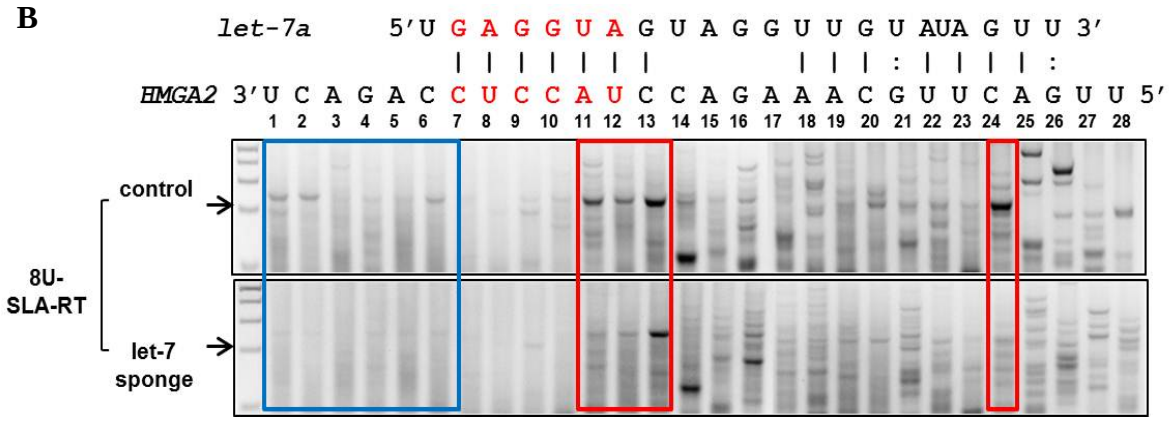

C **SLA-RT primers and 8U-SLA-RT primers list**

	5’- UGAGGUAGUAGGUUGUAUAGUU -3’ ||||||| |||:||||: 3’-UCAGACCUCCAUCCAGAAACGUUCAGUU-5’ |||||| HMGA2 Target	
	Regular Stem loop RT probe (5’-3’)	8U-Stem loop RT probe (5’-3’)
U1	SL- AGTCTG	SL- AAAAAAAAGTCTG
C2	SL- GTCTGG	SL- AAAAAAAAGTCTGG
A3	SL- TCTGGA	SL- AAAAAAAATCTGGA
G4	SL- CTGGAG	SL- AAAAAAAACTGGAG
A5	SL- TGGAGG	SL- AAAAAAAATGGAGG
C6	SL- GGAGGT	SL- AAAAAAAAGGAGGT
C7	SL- GAGGTA	SL- AAAAAAAAGAGGTA
U8	SL- AGGTAG	SL- AAAAAAAAAGGTAG
C9	SL- GGTAGG	SL- AAAAAAAAGGTAGG
C10	SL- GTAGGT	SL- AAAAAAAAGTAGGT
A11	SL- TAGGTC	SL- AAAAAAAATAGGTC
U12	SL- AGGTCT	SL- AAAAAAAAAGGTCT
C13	SL- GGTCTT	SL- AAAAAAAAGGTCTT
C14	SL- GTCTTT	SL- AAAAAAAAGTCTTT
A15	SL- TCTTTG	SL- AAAAAAAATCTTTG
G16	SL- CTTTGC	SL- AAAAAAAACTTTGC
A17	SL- TTTGCA	SL- AAAAAAAATTTGCA
A18	SL- TTGCAA	SL- AAAAAAAATTGCAA
A19	SL- TGCAAG	SL- AAAAAAAATGCAAG
C20	SL- GCAAGT	SL- AAAAAAAAGCAAGT
G21	SL- CAAGTC	SL- AAAAAAAACAAGTC
U22	SL- AAGTCA	SL- AAAAAAAAAAGTCA
U23	SL- AGTCAA	SL- AAAAAAAAAGTCAA
C24	SL- GTCAAT	SL- AAAAAAAAGTCAAT
A25	SL- TCAATT	SL- AAAAAAAATCAATT
G26	SL- CAATTA	SL- AAAAAAAACAATTA
U27	SL- AATTAG	SL- AAAAAAAAAATTAG
U28	SL- ATTAGT	SL- AAAAAAAAATTAGT

Figure 41. Let-7 sponge inhibited let-7 directed uridylation and cleavage activity of Hmga2 mRNA. **(A)** let-7 sponge plasmid was constructed with GFP with two let-7 target sites in 3’UTR. After transfection in H1299 cells, the GFP expression was dramatically down-regulated compared with GFP expression plasmid, which indicated that the let-7 sponge exhausted let-7 miRNA in H1299 cells. H1299 cells were co-transfected with RFP expression plasmid as transfection efficiency control. **(B)** After transfected with let-7 sponge, the intensity of uridized PCR band was reduced compared to control group, which indicated the let-7 directed uridized acitivity was inhibited by let-7 sponge. The expected PCR size was marked with arrow at the left side of agarose gel. miRNA and

target site seed region was highlighted with red. **(C)** The specific SL-RT primer and 8U-SL-RT primers were illustrated in the table.

Looking for Hmga2 is the true target of let-7; we conducted let-7 depletion by transfected H1299 cells with let-7 sponge plasmid. When let-7 was depleted by let-7 sponge, the cleavage and uridylation activity on target site 5# was inhibited, suggesting that the cleavage and uridylation activity is caused by let-7 (**Figure 30**).

4.3.3 Cooperativity between adjacent target sites, blocking 3'-5' degradation caused by the adjacent target sites

Based on our observations of le-7 targets on Hmga2, we hypothesized that when the two miRNA sites were close together, miRNA will work cooperatively. Several earlier studies have examined cooperative down-regulation via multiple miRNA target sites. Grimson *et al.* observed that siRNA cooperatively silenced a reporter bearing two target sites spaced 8-40 nt apart in 3'UTR. Expanding the distance to 56 nt disrupted the cooperative function [135].

We noticed one notable exception: when target site 6# and target site 7# are too close, in which the 5' end of target site 7# is in the 3' end of target site 6#, the cleavage activity is dramatically reduced (**Figure 32-33**). One possible explanation is that if the sites are too close there may be steric hindrance resulting in reduced function as we observed with the 9 base spacing versus a single site.

To characterize how different target RNA context influence RISC-mediated target recognition and cleavage, we made plasmid PLJT214, which has two identical copies of let-7 target sequence inserted at the 3' UTR of GFP reporter plasmid, 262 bp apart (**Figure 42**). Due to the identical target sequences were used in this plasmid constructs, the different patterns and effectiveness of cleavage for the copies in tandem can only be explained by the influence of mRNA context. The secondary structure was determined by using the Mfold algorithm. Target site T1 cleavage and uridylation activity are much efficient that target site T2, which may be explained by the position and secondary structure of target site T1 is more optimistically for let-7 than target site T2.

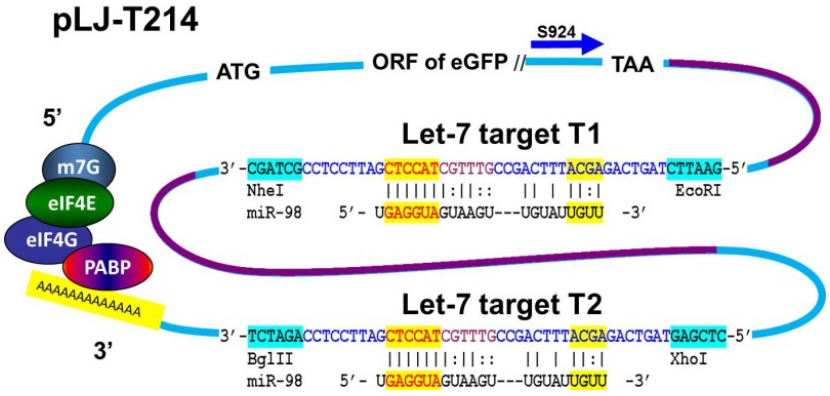

Figure 42. Schematic representation of plasmid PLJT214 construction. Plasmid pLJT214 contain dual miR-98 target sequences added to the 3' UTR of GFP transcript.

A

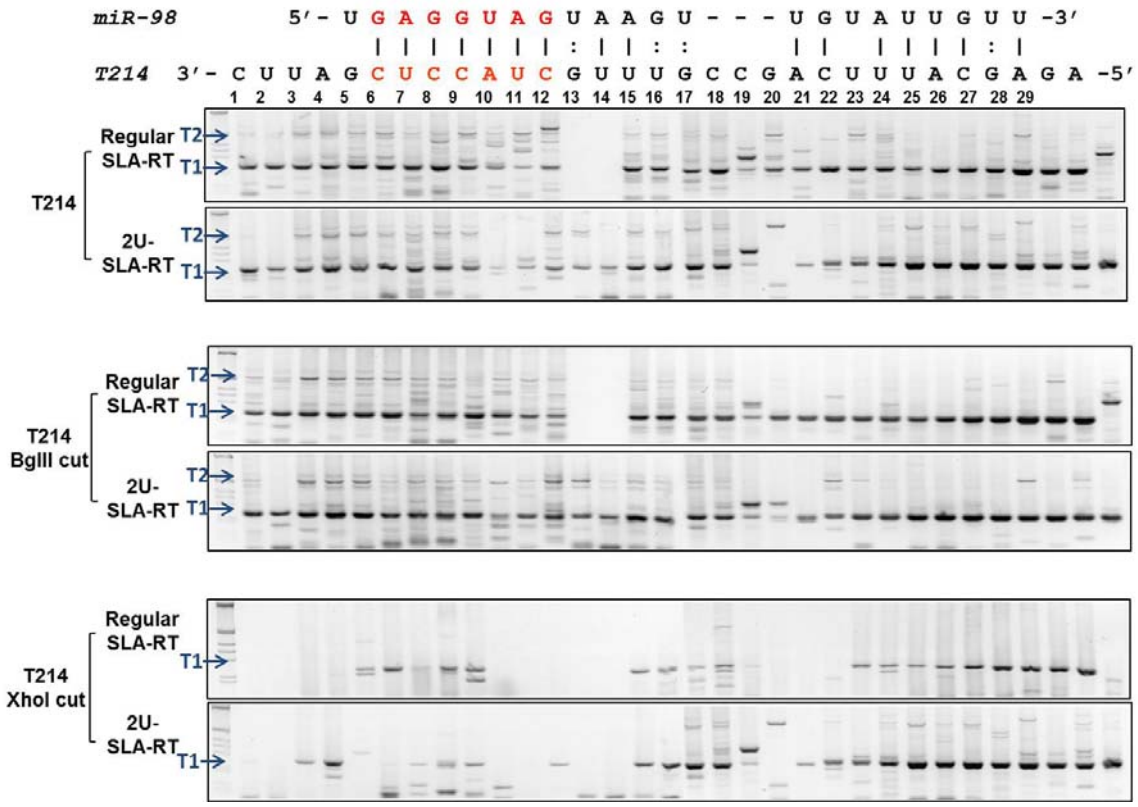

B

	5′- UGAGGUAGUAAGU---UGUAUUGUU -3′ ||||||:||: || | ||:| 3′-CUUAGCUCCAUCGUUUGCCGACUUUACGAG-5′ ||||||	PLJT214 Target
	Regular Stem loop RT probe (5′-3′)	8U-Stem loop RT probe (5′-3′)
C1	SL- GAATCG	SL- GAATCG
U2	SL- AATCGA	SL- AATCGA
U3	SL- ATCGAG	SL- ATCGAG
A4	SL- TCGAGG	SL- TCGAGG
G5	SL- CGAGGT	SL- CGAGGT
C6	SL- GAGGTA	SL- GAGGTA
U7	SL- AGGTAG	SL- AGGTAG
C8	SL- GGTAGC	SL- GGTAGC
C9	SL- GTAGCA	SL- GTAGCA
A10	SL- TAGCAA	SL- TAGCAA
U11	SL- AGCAAA	SL- AGCAAA
C12	SL- GCAAAC	SL- GCAAAC
G13	SL- CAAACG	SL- CAAACG
U14	SL- AAACGG	SL- AAACGG
U15	SL- AACGGC	SL- AACGGC
U16	SL- ACGGCT	SL- ACGGCT
G17	SL- CGGCTG	SL- CGGCTG
C18	SL- GGCTGA	SL- GGCTGA
C19	SL- GCTGAA	SL- GCTGAA

G20	SL- CTGAAA	SL- CTGAAA
A21	SL- TGAAAT	SL- TGAAAT
C22	SL- GAAATG	SL- GAAATG
U23	SL- AAATGC	SL- AAATGC
U24	SL- AATGCT	SL- AATGCT
U25	SL- ATGCTC	SL- ATGCTC
A26	SL- TGCTCT	SL- TGCTCT
C27	SL- GCTCTA	SL- GCTCTA
G28	SL- CTCTAC	SL- CTCTAC
A29	SL- TCTACG	SL- TCTACG

Figure 43. Cooperativity between two adjacent target sites. **(A)** Plasmid PLJT214 was cut by BglII to delete polyA tale, and cut by xhoI to delete target site T2. PLJT214, PLJT214 cut by BglII, and PLJT214 cut by xhoI were transfected into H1299 cells individually, and then SLA-RT-PCR detected the cleavage fragment and uridized fragment. The expected PCR size for detecting target site 1# cleavage fragment was labeled with T1, and for target site 2# was labeled with T2 with arrow at the left side of agarose gel. miRNA and target site seed region was highlighted with red. After cutting by xhoI, target site T2 cleavage and uridylation activity was totally gone, in addition, target site T1 cleavage and uridylation activity was also dramatically reduced. **(B)** The specific SL-RT primer and corresponding detected cleavage RNA fragment was illustrated in the table.

Furthermore, PLJT214 was cut by BglII to delete polyA tale, and cut by xhoI to delete target site T2. After cutting by xhoI, target site T2 cleavage and uridylation activity was totally gone, in addition, target site T1 cleavage and uridylation activity was also dramatically reduced (**Figure 43**). One possible explanation could be target site T1 and target site T2 function cooperatively.

4.4.4 Ago2 and GW182 are required for mediating miRNA targets cleavage and degradation

The existence of a link between the miRNA pathway and mRNA decay is supported by the observation that mammalian Agos, miRNAs and miRNA targets colocalize to cytoplasmic foci know as P-bodies. Following this endonucleolytic cleavage by Ago2, the resulting mRNA fragments are added oligo U by TUTase, which handed over to the general 5'-3' mRNA-decay machinery. Strikingly, all proteins that function in the 5'-3' mRNA-decay pathway have now been shown to localize to P bodies.

GW182 have been shown to be associated with miRISC and required for miRNA-mediated gene silencing. GW182 is localized to P bodies that are cytoplasmic messenger ribonucleoprotein (mRNP) aggregates containing mRNA decay factors, translational repressors and untranslated mRNAs. It is known that the oligo U tailored RNA fragments can be recognized by GW182 and subject to further degradation in P body.

We further tested if depletion of Ago2 and GW182 impair miRNA directed target cleavage and degradation. We knockdown Ago2 and GW182 in H1299 cells and carried out SLA-RT-PCR on target site 5# (**Figure 44A**). Ago 2 and GW182 was efficiently inhibited, which was confirmed by the western blotting (**Figure 44B**). When Ago2 and GW182 were depleted, Hmga2 target site 5# cleavage and degradation products decreased, which indicates that let-7 directed cleavage and uridylation activity are dependent on Ago2 and GW182.

A

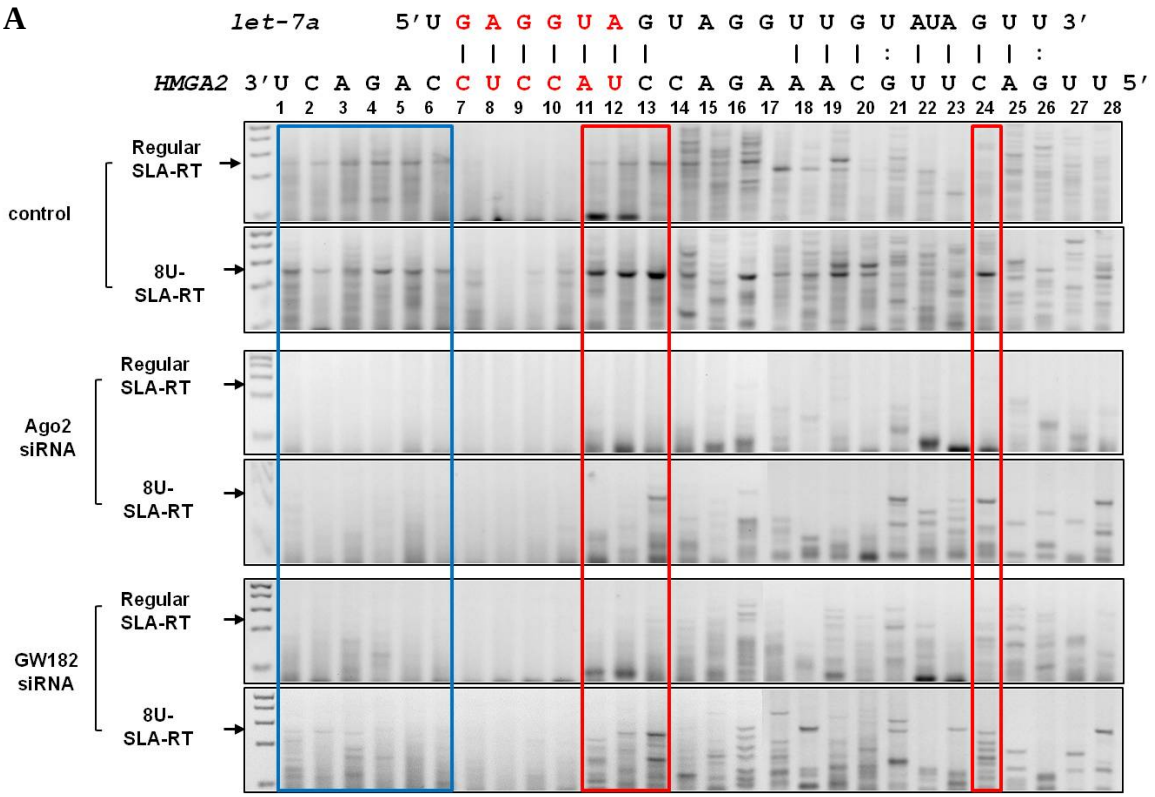

B

	5′- UGAGGUAGUAGGUUGUAUAGUU -3′ 3′-UCAGACCUCCAUCCAGAAACGUUCAGUU-5′	HMGA2 Target
	Regular Stem loop RT probe (5′-3′)	8U-Stem loop RT probe (5′-3′)
U1	SL- AGTCTG	SL- AAAAAAAAGTCTG
C2	SL- GTCTGG	SL- AAAAAAAAGTCTGG
A3	SL- TCTGGA	SL- AAAAAAAATCTGGA
G4	SL- CTGGAG	SL- AAAAAAAACTGGAG
A5	SL- TGGAGG	SL- AAAAAAAATGGAGG
C6	SL- GGAGGT	SL- AAAAAAAAGGAGGT
C7	SL- GAGGTA	SL- AAAAAAAAGAGGTA
U8	SL- AGGTAG	SL- AAAAAAAAAGGTAG
C9	SL- GGTAGG	SL- AAAAAAAAGGTAGG
C10	SL- GTAGGT	SL- AAAAAAAAGTAGGT
A11	SL- TAGGTC	SL- AAAAAAAATAGGTC
U12	SL- AGGTCT	SL- AAAAAAAAAGGTCT
C13	SL- GGTCTT	SL- AAAAAAAAGGTCTT
C14	SL- GTCTTT	SL- AAAAAAAAGTCTTT

A15	SL- TCTTTG	SL- AAAAAAAATCTTTG
G16	SL- CTTTGC	SL- AAAAAAAACTTTGC
A17	SL- TTTGCA	SL- AAAAAAAATTTGCA
A18	SL- TTGCAA	SL- AAAAAAAATTGCAA
A19	SL- TGCAAG	SL- AAAAAAAATGCAAG
C20	SL- GCAAGT	SL- AAAAAAAAGCAAGT
G21	SL- CAAGTC	SL- AAAAAAAACAAGTC
U22	SL- AAGTCA	SL- AAAAAAAAAAGTCA
U23	SL- AGTCAA	SL- AAAAAAAAAGTCAA
C24	SL- GTCAAT	SL- AAAAAAAAGTCAAT
A25	SL- TCAATT	SL- AAAAAAAATCAATT
G26	SL- CAATTA	SL- AAAAAAAACAATTA
U27	SL- AATTAG	SL- AAAAAAAAAATTAG
U28	SL- ATTAGT	SL- AAAAAAAAATTAGT

C

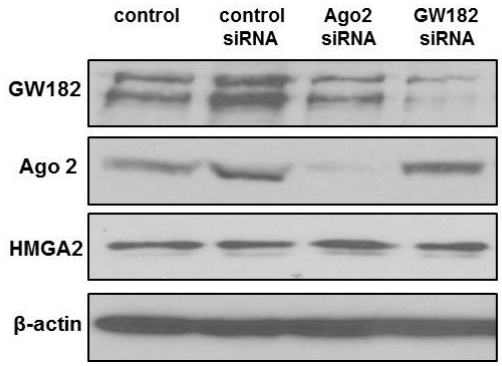

Figure 44. Knocking down Ago2 and GW182 inhibit Hmga2 cleavage and degradation activity directed by let-7 miRNA**. (A)** Agarose gel electrophoresis of SLA-RT-PCR products of target site 5# after Ago 2 and GW182 inhibition. The cleaved fragments product (detected by SLA-RT) and uridized fragments product (detected by 8U-SLA-RT) were inhibited after Ago2 inhibition and GW182 inhibition. The uridized region includes 3' adjacent region (highlighted with blue), the end in seed region (highlighted with red), and the 3' complimentary pairing region (highlighted with red). The expected PCR size was marked with arrow at the left side of agarose gel. miRNA and target site seed region was highlighted with red. **(B)** The specific SLA-RT primer and corresponding detected cleavage RNA fragment was illustrated in the table. **(C)** Western blotting analysis of Ago2 and GW182 after H1299 treated with Ago2 siRNA and GW182 siRNA. Ago2 siRNA inhibited Ago2 expression, and GW182 siRNA inhibited GW182 expression.

4.4.5 TUSC2 mRNA cleavage by miRNAs detected by SLA-RT-PCR

It has been confirmed that TUSC2 3'UTR played an important role in down-regulating TUSC2 expression, which suggested miRNA may target on TUSC2 3'UTR. Target Scan software (http://www.targetscan.org/) predicted TUSC2 mRNA have hundreds of miRNA targets (**Figure 45**), which cannot be true and needs to be verified by SLA-RT-PCR in physiological conditions. Random SL-RT primer was designed first for screen the potential miRNA target on TUSC2, which has six random nucleotides at the 3'end of SLA-RT-primer (**Figure 46**).

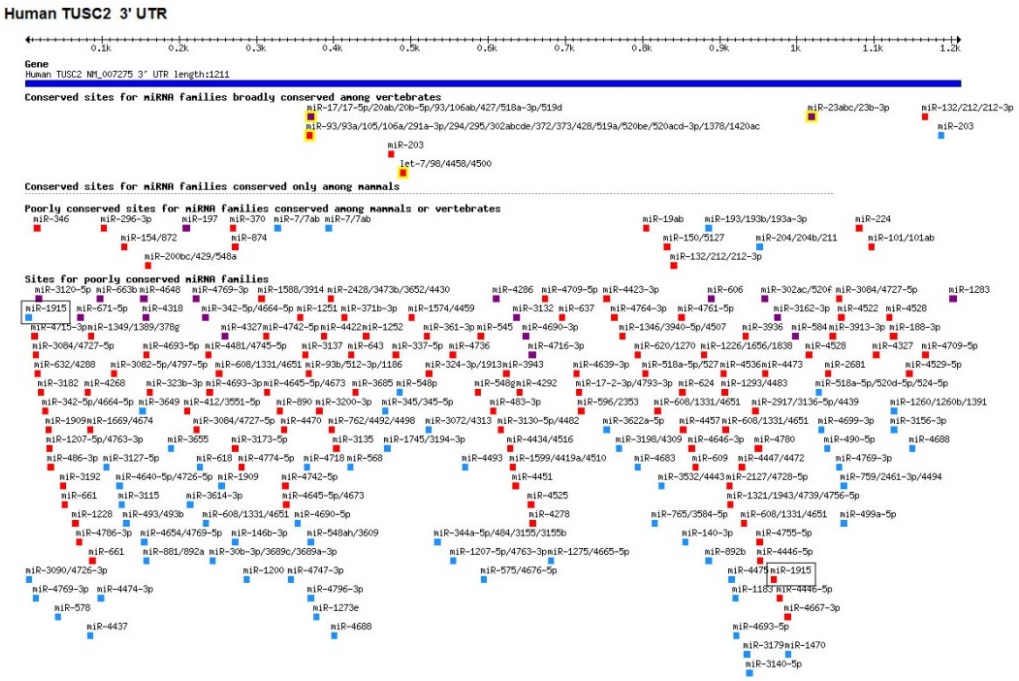

Figure 45. miRNA targets on TUSC2 predicted by Target Scan Software (http://www.targetscan.org/). It predicted TUSC2 mRNA have hundreds of miRNA targets. miRNAs highlighted with purple predicted that target RNA have exact match to positions 2-8 of the mature miRNA (the seed + position 8) followed by an 'A' . miRNAs highlighted with red predicted that target RNA have an exact match to positions 2-8 of the mature miRNA. miRNAs highlighted with blue predicted that target RNA have an exact match to positions 2-7 of the mature miRNA (the seed) followed by an 'A'.

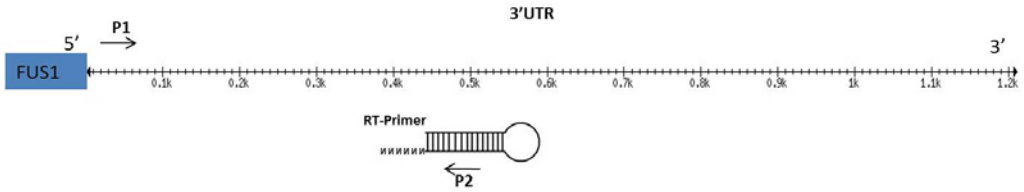

Figure 46. SL-RT-PCR for screen miRNA targets cleavage fragments on TUSC2. SL-RT-primer with six random nucleotides at 3'end was designed for screen cleavage fragments.

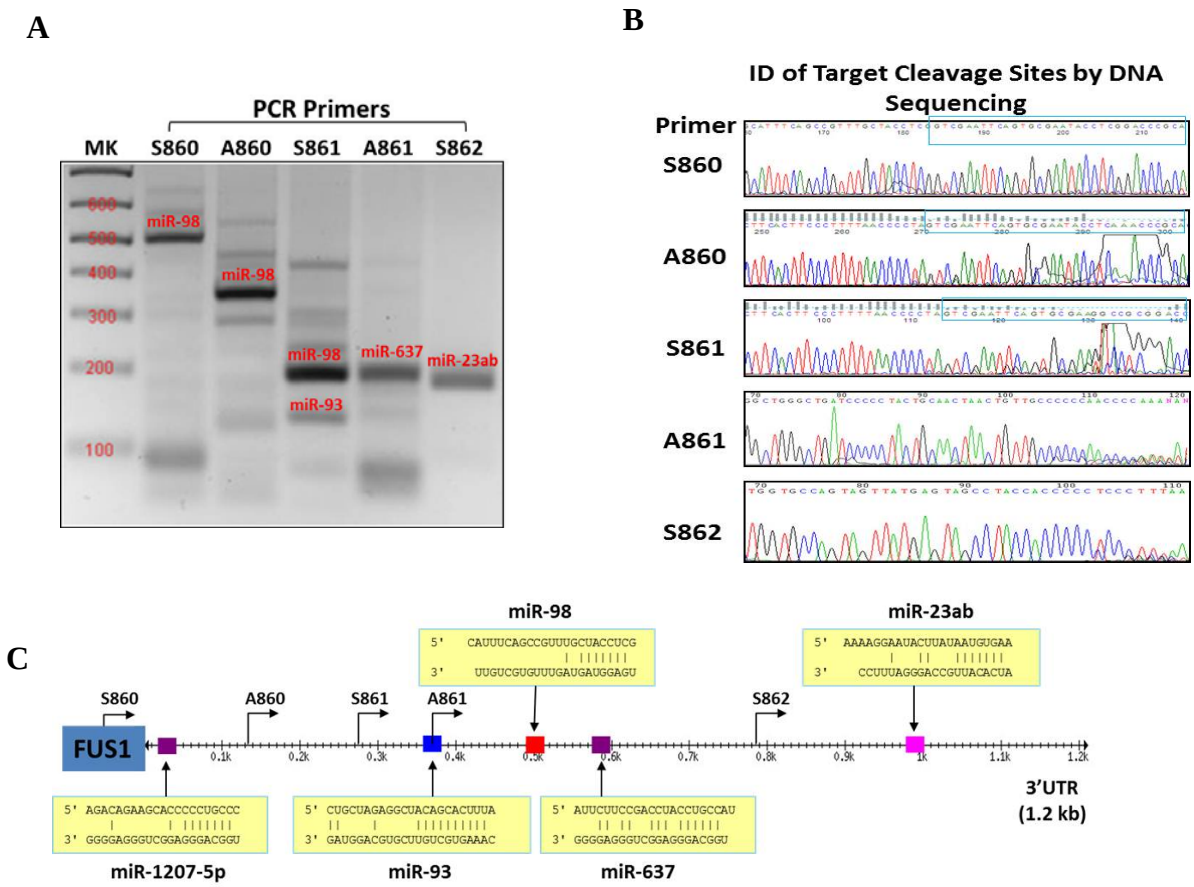

Figure 47. Random SL-RT-PCR detected cleavage fragments on TUSC2. **(A)** Agarose gel analysis of SL-RT-PCR product, the predicted miRNAs targets according to cleavage fragments size and PCR primers were labeled. **(B)** DNA sequence verification of cleavage fragments. The SL-RT primers were highlighted with blue. **(C)** Illustrations of miRNAs targeted at TUSC2. The PCR primers and miRNAs are mapped at 3'UTR according to the specific sizes.

SL-RT-PCR with six random nucleotides at 3'end of SL-RT primer detected several cleavage fragments. According to fragments size and predicted potential targets, miR-98, miR-93, miR-637 and miR-23ab may direct TUSC2 cleavage. All cleavage fragments are verified by DNA sequence (**Figure 47**).

It was reported that squamous metaplasia and dysplasia express significantly lower levels of TUSC2 than normal and hyperplastic bronchial epithelia. SL-RT-PCR was used to screen different miRNA targets among different lung cell lines. The results showed that H1299 and H322 cells have miR-98 directed cleavage fragments, which cannot be detected in A549 cells and HBE cells (**Figure 48**).

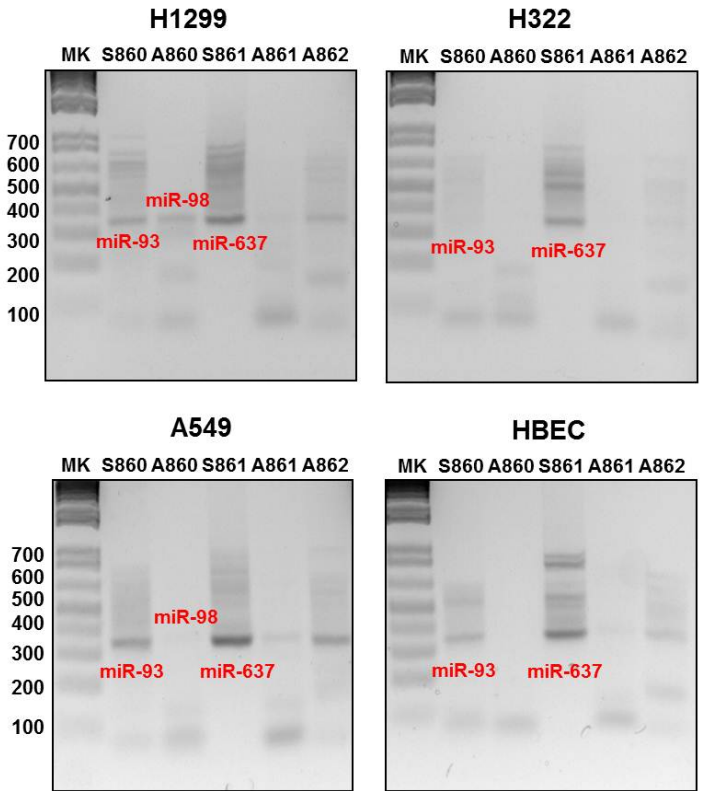

Figure 48. SL-RT-PCR detection of miRNAs directed mRNA cleavage fragments in H1299, H322, A549 and HBEC cells. The predicted miRNAs targets according to cleavage fragments size and PCR primers were labeled. H1299 and H322 cells have miR-98 directed cleavage fragments, which cannot be detected in A549 cells and HBE cells.

Previous report confirmed an authentic miR-98 target on TUSC2 mRNA 3' UTR and overexpressed miR-98 decreased TUSC2 mRNA level [86]. A collection of SLA-RT primers with 6 nt probe matching along TUSC2 miR-98 target sequence were designed to detect the accumulation of cleaved mRNA fragments around this site (**Figure 49**). Amplicon intensity from each RT-PCR reaction represented the relative abundance of 5' RNA fragment detected by a unique SL-RT primer respectively. PCR amplicons were analyzed on agarose electrophoresis gels in the order of miR-98 target sequence at 3'-5' direction. 5' RNA fragment abundance around the endogenous TUSC2 miR-98 target were represented as intensity of PCR amplicons ranging from 232 bp to 200 bp (**Figure 49B**). SLA-RT-PCR results showed the cleaved target sites are at C8, G31, A32, T33, G34 around miR-98 target sites.

A

	TUSC2 mRNA 3’–UCCUUAGCUCCAUCGUUUGCCGACUUUACGAGACUGAUCCCCAAUUUUCCCUUCA-5’ |||||
	Regular Stem loop RT probe (5’–3’)
1	SL-AGGAAT
2	SL-AATCGA
3	SL-ATCGAG
4	SL-TCGAGG
5	SL-CGAGGT
6	SL-GAGGTA
7	SL-AGGTAG
8	SL-GGTAGC
9	SL-GTAGCA
10	SL-TAGCAA
11	SL-AGCAAA
12	SL-GCAAAC
13	SL-CAAACG
14	SL-AAACGG
15	SL-AACGGC
16	SL-ACGGCT
17	SL-CGGCTG
18	SL-GGCTGA
19	SL-GCTGAA
20	SL-CTGAAA
21	SL-TGAAAT
22	SL-GAAATG
23	SL-AAATGC
24	SL-AATGCT
25	SL-ATGCTC
26	SL-TGCTCT
27	SL-GCTCTG
28	SL-CTCTGA
29	SL-TCTGAC
30	SL-CTGACT
31	SL-TGACTA
32	SL-GACTAG
33	SL-ACTAGG
34	SL-CTAGGG
35	SL-GGGGTT
36	SL-GTTAAA
37	SL-AGGGAA

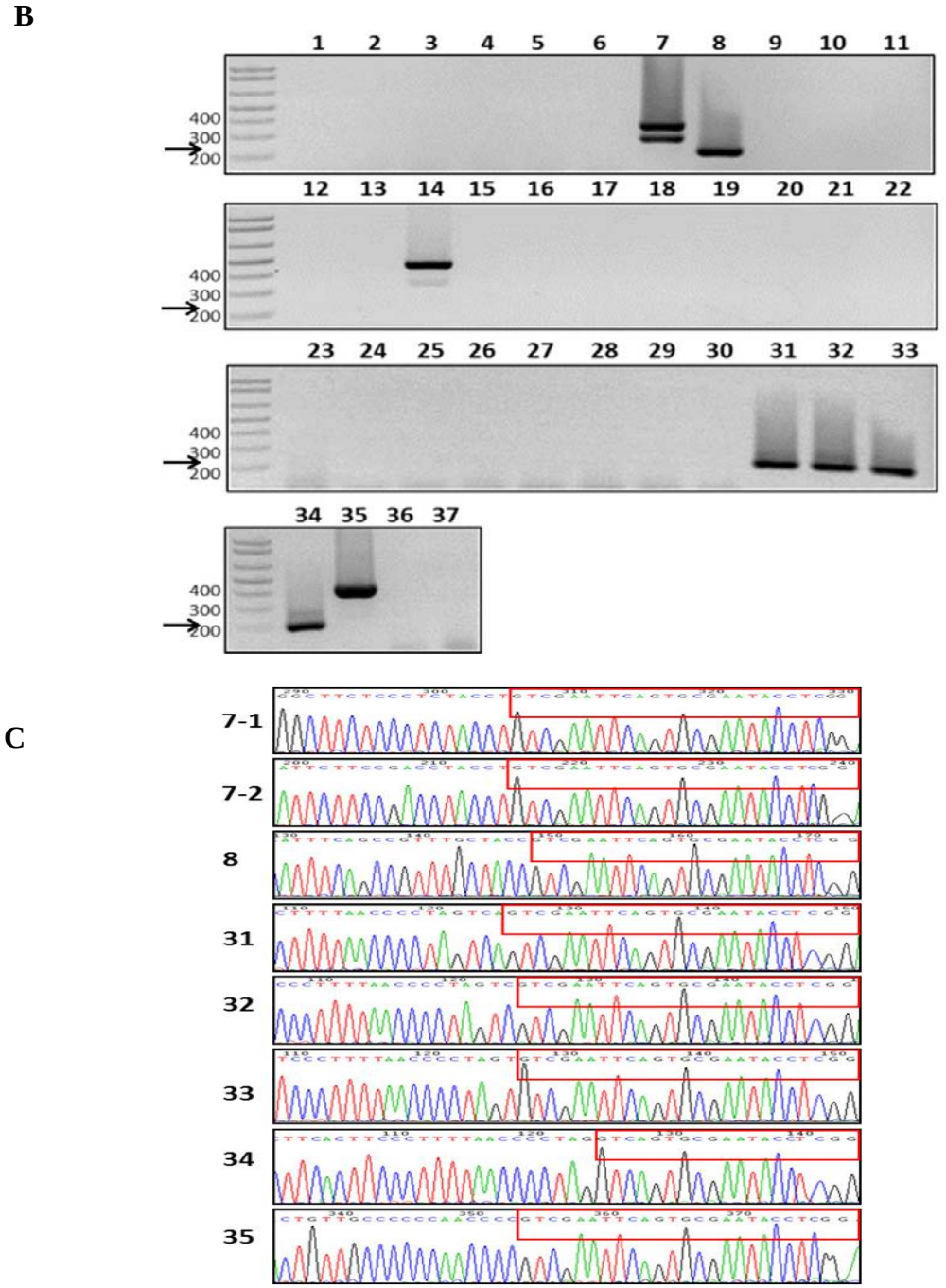

Figure 49. SLA-RT-PCR detection of miR-98 directed TUSC2 cleavage fragments. **(A)** SLA-RT primers design for detecting miR-98 directed cleavage fragments. **(B)** SLA-RT-PCR products were run in agarose gels and mapped to the position expected to miR-98-directed TUSC2 cleavage. The expected PCR size was marked with arrow at the left side of agarose gel. Predicted target site region were highlighted with red. **(C)** DNA sequence confirmation of miR-98 directed cleavage fragments. The SL-RT primers were highlighted with red.

A collection of SLA-RT primers were designed to detect the accumulation of cleaved mRNA fragments around miR-637 target site (**Figure 49A**). SLA-RT-PCR results showed the cleaved target sites are at C6, C10 and T13 around miR-637 target sites.

A

	TUSC2 mRNA 3′–UUGACCCCCAAGCCCCCAACCCCCCGUUGUCAAUCAACGUCAUCCCCCUAGUC-5′ ||||||
	Regular Stem loop RT probe (5′–3′)
1	SL-GGTTCG
2	SL-GTTCGG
3	SL-TTCGGG
4	SL-CGGGGT
5	SL-GGGTTG
6	SL-GGTTGG
7	SL-GTTGGG
8	SL-GGGGCA
9	SL-GGGCAA
10	SL-GGCAAC
11	SL-GCAACA
12	SL-CAACAG
13	SL-AACAGT
14	SL-ACAGTT
15	SL-CAGTTA
16	SL-AGTTAG
17	SL-GTTAGT
18	SL-TTAGTT
19	SL-TAGTTG
20	SL-AGTTGC
21	SL-GTTGCA
22	SL-TTGCAG
23	SL-TGCAGT
24	SL-GCAGTA
25	SL-CAGTAG
26	SL-AGTAGG
27	SL-GATCAG

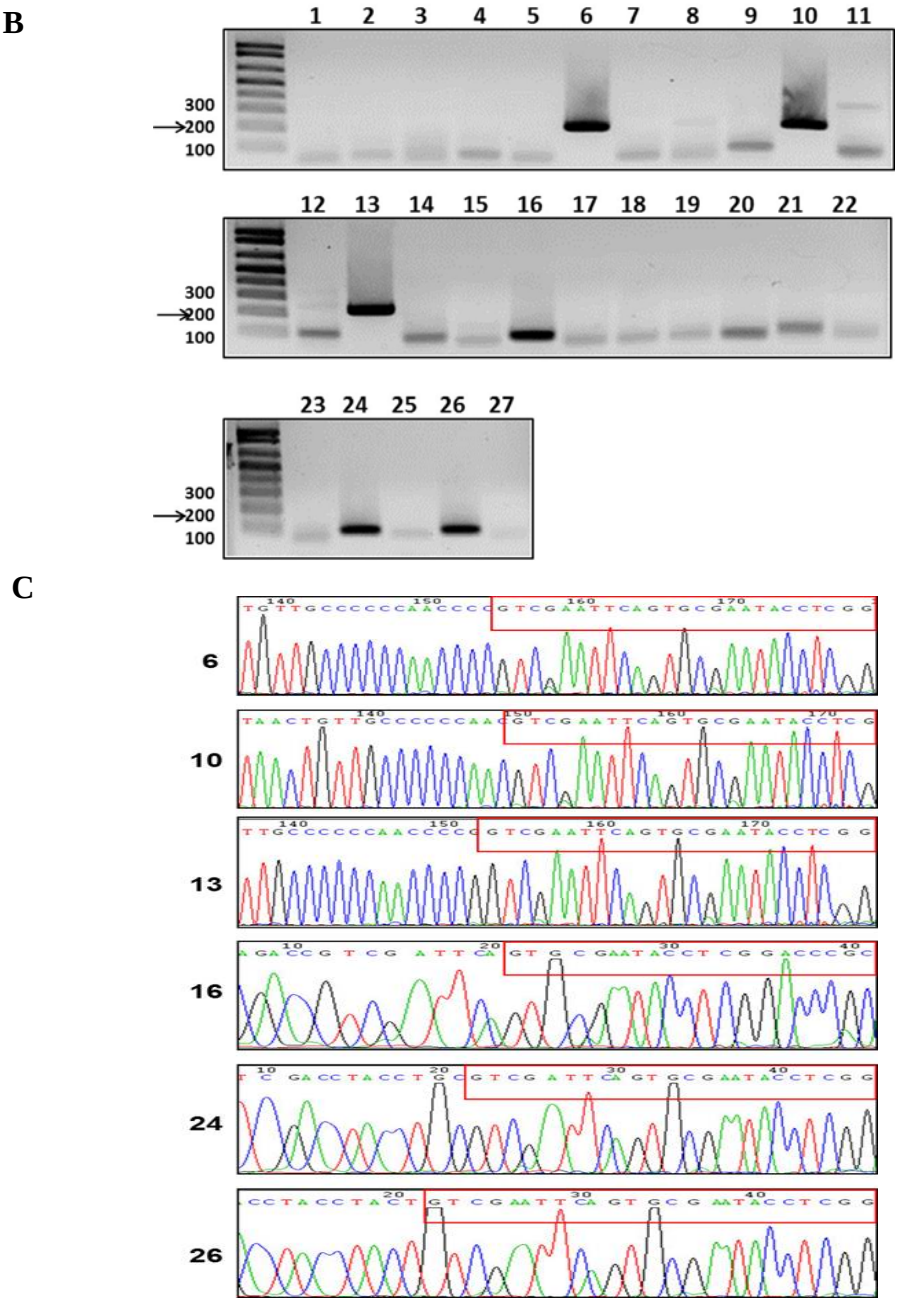

Figure 50. SLA-RT-PCR detection of miR-637 directed TUSC2 cleavage fragments. (A) SLA-RT primers design for detecting miR-637 directed cleavage fragments. (B) SLA-RT-PCR products were run in agarose gels and mapped to the position expected to miR-637-directed TUSC2 cleavage. The expected PCR size was marked with arrow at the left side of agarose gel. Predicted target site region were highlighted with red. (C) DNA sequence confirmation of miR-637 directed cleavage fragments. The SL-RT primers sequences were highlighted with red.

To further confirm the effects of these miRNAs on TUSC2 protein expression, we co-transfected H1299 cells TUSC2-3'UTR construct and miR-93 inhibitor, miR-98 inhibitor, miR-197 inhibitor, miR-637 inhibitor and miR-1207-5p inhibitor. As shown in **Figure 51**, miR-98 inhibitor and miR-93 inhibitor increase the TUSC2 expression. In summary, these results indicate that miR-93, miR-98, miR-637 down-regulate TUSC2 expression through directed TUSC2 mRNA cleavage and degradation.

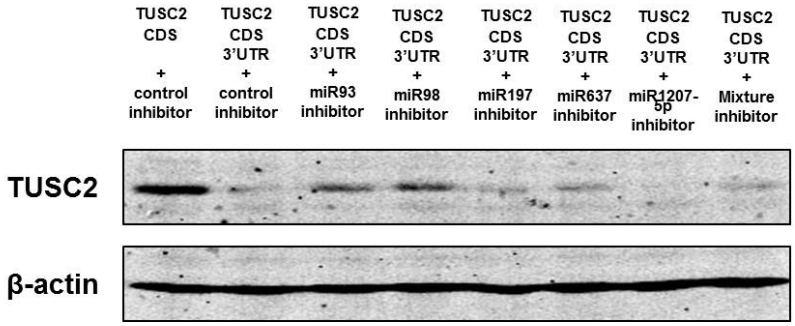

Figure 51. Expression of TUSC2 after treated with miRNA inhibitors. H1299 cell was co-transfected with TUSC2 expression construct and miR-93 inhibitor, miR-98 inhibitor, miR-197 inhibitor, miR-637 inhibitor, miR-1207-5p inhibitor. MiR-93 inhibitor and miR-98 inhibitor increase TUSC2 expression.

4.5 Discussion

We have shown here that miRNA-directed endonucleolytic cleavage on mRNA was the initiation step of miRNA mediated gene silence. The cleaved RNA fragments were mostly oligouridylated at their 3'-termini and accumulated for RNA 5' – 3' decay later. The portion of RNA fragments escaped oligouridine modification were subject to 3' – 5' decay pathway and would be intercepted by other miRISCs stationed on their target sites at 5' end. After shedding off exonucleases, RNA fragments were added with oligouridine at their 3' termini. In this process, miRISC performed two activities - endonucleolytic

cleavage on mRNA targets and oligouridylation of cleaved 5' RNA fragments. Oligouridylation of RNA fragments played important role in stabilizing RNA for accumulation and in converting RNA decay mode from 3' - 5' to 5' - 3'. It would avoid the problematic degradation of mRNA at 3'- 5' direction which processed opposite the 5' - 3' flow of translation apparatus. In case of mRNA in active translation, RNA fragment accumulation, other than degradation, gives time for translation to complete. This eliminated the possible adverse consequences of truncated proteins which might be produced with mRNA 3' - 5' decay pathway [127]. The delayed action on mRNA degradation desynchronized the lineage relationship of mRNA and protein abundance which contributed to the conflicted observation in many miRNA functionality tests [138, 139].

P-bodies are hubs for transient RNA species and played important role in miRNA mediated gene silence. All the components for miRNA machinery, including Agos, miRNA, GW182, Lsm1-7, XRN1, DCP1, CDP2, and Ccr4-Not complex can be found in P-bodies [90]. Blocking miRNA silencing pathways at any step prevented P-body formation, indicating that P bodies arise as a consequence of silencing [141-143]. The miRNA cleaved fragments are accumulated in oligouridylated form which could be recognized by cytoplasmic heptameric Lsm1-7 complex to facilitate the formation of P-bodies. The accumulated RNA fragments in P-bodies are eventually degraded through RNA 5' - 3' decay pathway. Our results shed light on current knowledge of mature mRNA degradation initiated by Ccr4-Not complex-deadenylation pathway which is, in our opinion, too general to address tissue-specific mRNA half-lives. miRNA expression profiling revealed that miRNAs were specific to tissue differentiation, physiological and

pathogenic events [144, 145]. The micro-scale, leak-some and accumulative cleavage activities of miRNA on target transcripts make them primary candidates for tissue and event-specific mRNA half-life determinates in mammalian cells. The target site cleavage efficiency by miRNA could be determined by target mRNA context which influence the association and dissociation of the miRISC.

As currently available miRNA-target prediction algorithms do not take these issues into account, it is conceivable that many proposed miRNA-target interactions occur only in very specific contexts. Hence, the general applicability of proposed concepts of miRNA functions that are based on the genome-wide prediction of seed-based miRNA-target interactions need to be assessed cautiously. Without knowing these context determinants, experimentalists face a difficult challenge. Where should they begin when seeking to understand the molecular mechanisms of phenotypes arising from miRNA knockdown or ectopic expression studies?

In this study, we tried to use the new developed SLA-RT-PCR method to identify the miRNA target sites at TUSC2 3'TUR. It was reported by Lee *et al.* [146] that miR-378 could target TUSC2 3'UTR and repress the TUSC2 expression, leading to enhanced cell survival, tumor growth, and angiogenesis in human NSCLC cells. Another group in UT southwestern also reported that the 3'UTR of TUSC2 is a target of other miRNAs including miR-93, miR-98, and miR-197 [136]. Down-regulation of TUSC2 expression in both SCLC and NSCLC cell lines and primary tumors correlates with elevated miR-93 and miR-197 expression [136].

The SLA-RT-PCR verified that miR-98, miR-93 and miR-637 directed TUSC2 cleaved and degraded. H1299 and H322 cells have miR-98 directed cleavage fragments, which cannot be detected in A549 cells and HBE cells. The level of TUSC2 3'UTR-mediated down-regulation of TUSC2 gene and protein expression is significantly higher in lung cancer cells than in normal bronchial epithelial cells, which was might be attributable to miR-98 targets in 3'UTR.

Our studies elucidated the mechanism that mammalian miRNA regulating target mRNA degradation. These findings warrant further investigation to identify the precise miRNA targets in mammalians in endogenous context. Our findings also demonstrated that different miRNAs targeted at TUSC2 in different lung cell lines, which imply that these miRNA can be used as potential therapeutic targets by effectively blocking the interaction of miRNAs and TUSC2 targets to re-activate TUSC2 expression and restore its tumor suppression function in tumor cells.

Reference

1. Frith, M.C., Pheasant, M., Mattick, J.S. (2005) The amazing complexity of the human transcriptome. Eur. J. Hum. Genet.:13, 894–897
2. Consortium (2004) Finishing the euchromatic sequence of the human genome. Nature: 431, 931–945.
3. Bashirullah, A., Cooperstock, R.L., Lipshitz, H.D. (2001) Spatial and temporal control of RNA stability. Proc Natl Acad Sci USA.98: 7025–7028.
4. van der Velden, A.W., Thomas, A.A. (1999) The role of the 5' untranslated region of an mRNA in translation regulation during development. Int J Biochem Cell Biol.31:87–106.
5. Jansen, R.P. (2001) mRNA localization: message on the move. Nat Rev Mol Cell Biol.2:247–256
6. Brown, C.E., Sachs, A.B. (1998) Poly(A) tail length control in *Saccharomyces cerevisiae* occurs by message-specific deadenylation. Mol Cell Biol.; 18:6548–6559
7. Bagga, S., Bracht, J., Hunter, S., Massirer, K., Holtz, J., Eachus, R., Pasquinelli, A.E., (2005) Regulation by let-7 and lin-4 miRNAs results in target mRNA degradation. Cell 122:553-556
8. Ainger, K., Avossam, D., Diana, A.S., Barry, C., Barbarese, E., Carson, J.H. (1997) Transport and localization elements in myelin basic protein mRNA. J Cell Biol. 138:1077–1087.

9. Vilela, C., Ramirez, C.V., Linz, B., Rodrigues-Pousada, C., McCarthy, J.E. (1999) Post-termination ribosome interactions with the 5' UTR modulate yeast mRNA stability. EMBO J.18:3139–3152.

10. Rodriguez, A., Griffiths-Jones, S., Ashurst, J.L. and Bradley, A. (2004) Identification of mammalian microRNA host genes and transcription units. Genome Res., 14, 1902–1910

11. Rodriguez, A., Griffiths-Jones, S., Ashurst, J.L. and Bradley, A. (2004) Identification of mammalian microRNA host genes and transcription units. Genome Res., 14, 1902–1910.

12. Zamore, P.D. and Haley, B. (2005) Ribo-gnome: the big world of small RNAs. Science, 309, 1519–1524.

13. Croce, C.M. and Calin, G.A. (2005) miRNAs, cancer, and stem cell division. Cell, 122, 6–7.

14. Giraldez, A.J., Cinalli, R.M., Glasner, M.E., Enright, A.J., Thomson, J.M., Baskerville, S., Hammond, S.M., Bartel, D.P. and Schier, A.F. (2005) MicroRNAs regulate brain morphogenesis in zebrafish. Science, 308, 833–838.

15. Lee, R.C., Ambros, V. (2001) An extensive class of small RNAs in Caenorhabditis elegans. Science 294:862-864

16. Lee, R.C., Feinbaum R.L. and Ambros V. (1993) The C. elegans Heterochronic gene lin-4 encodes small RNAs with antisense complementarity to lin-14. Cell 75: 843-845

17. Rhoades, M.W., Reinhart, B.J., Lim, L.P., Burge, C.B., Bartel, B., Bartel, D.P. (2002) Prediction of plant microRNA targets. Cell 110 (4):513-520

18. Bartel, D.P. (2009) MicroRNAs: Target Recognition and regulatory Functions. Cell 136: 215-233

19. Guo, H.l., Ingolia, N.T., Weissman, J.S., Bartel, D.P. (2010) Mammalian microRNAs predominantly act to decrease target mRNA levels. Nature 466: 835–840

20. Behm-Ansmant, I. (2006) mRNA degradation by miRNAs and GW182 requires both CCR4:NOT deadenylase and DCP1:DCP2 decapping complexes. *Genes Dev.* **20**, 1885–1898

21. Liu, J., Rivas, F.V., Wohlschlegel, J., Yates, J.R., Parker, R., Hannon ,G.J. (2005) A role for the P-body component GW182 in microRNA function. *Nature Cell Biol.* **7**, 1261–1266.

22. Jakymiw, A. (2005). Disruption of GW bodies impairs mammalian RNA interference. *Nature Cell Biol.* **7**, 1267–1274

23. Jinek, M., Fabian, M.R., Coyle, S.M., Sonenberg, N. & Doudna, J.A. (2010) Structural insights into the human GW182-PABC interaction in microRNA-mediated deadenylation. Nat. Struct. Mol. Biol. 17, 238–240

24. Giraldez AJ, Mishima Y, Rihel J, Grocock RJ, Van Dongen S, Inoue K, Enright AJ, Schier AF. (2006). Zebrafish MiR-430 promotes deadenylation and clearance of maternal mRNAs. *Science* **312**, 75–79

25. Giraldez AJ, Mishima Y, Rihel J, Grocock RJ, Van Dongen S, Inoue K, Enright AJ, Schier AF. (2006) Differential regulation of germline mRNAs in soma and germ cells by zebrafish *miR-430*. *Curr. Biol.* **16**, 2135–2142

26. Bachellerie JP, Cavaillé J, Hüttenhofer A. (2002) The expanding snoRNA world. Biochimie, 84: 775–790

27. Kiss AM, Jády BE, Bertrand E, Kiss T. (2004) Human box H/ACA pseudouridylation guide RNA machinery. Mol. Cell. Biol., 24 : 5797–5807

28. Mattick, J.S. (2004) RNA regulation: a new genetics? Nat. Rev. Genet., 5, 316–323.

29. Smith, N.G., Brandstrom, M. and Ellegren, H. (2004) Evidence for turnover of functional non-coding DNA in mammalian genome evolution. Genomics, 84, 806–813.

30. Bejerano, G., Pheasant, M., Makunin, I., Stephen, S., Kent, W.J., Mattick, J.S. and Haussler, D. (2004) Ultraconserved elements in the human genome. Science, 304, 1321–1325

31. Simons, C., Pheasant, M., Makunin, I.V. and Mattick, J.S. (2006) Transposon-free regions in mammalian genomes. Genome Res., 16, 164–172.

32. van Nimwegen, E. (2003) Scaling laws in the functional content of genomes. Trends Genet., 19, 479–484.

33. Clemson CM, Hutchinson JN, Sara SA, Ensminger AW, Fox AH, Chess A, Lawrence JB (2009) An architectural role for a nuclear noncoding RNA: NEAT1 RNA is essential for the structure of paraspeckles. Mol Cell 33:717–726.

34. Sasaki YTF, Ideue T, Sano M, Mituyama T, Hirose T (2009) MEN ε/β noncoding RNAs are essential for structural integrity of nuclear paraspeckles. Proc Natl Acad Sci 106:2525–2530.

35. Sunwoo H, Dinger ME, Wilusz JE, Amaral PP, Mattick JS, Spector DL.(2009) MEN ε/β nuclear-retained non-coding RNAs are up-regulated upon muscle differentiation and are essential components of paraspeckles. Genome Res 19:347–359

36. Butcher, S.E. and Brow, D.A. (2005) Towards understanding the catalytic core structure of the spliceosome. Biochem. Soc. Trans., 33

37. Kwek, K.Y., Murphy, S., Furger, A., Thomas, B., O'Gorman, W., Kimura, H., Proudfoot, N.J. and Akoulitchev, A. (2002) U1 snRNA associates with TFIIH and regulates transcriptional initiation. Nat. Struct. Biol., 9, 800–805.

38. O'Gorman, W., Thomas, B., Kwek, K.Y., Furger, A. and Akoulitchev, A. (2005) Analysis of U1 snRNA interaction with cyclin H. J. Biol. Chem., 280, 36920–36925.

39. Bernstein, E. and Allis, C.D. (2005) RNA meets chromatin. Genes Dev., 19, 1635–1655

40. Vulliamy, T., Marrone, A., Goldman, F., Dearlove, A., Bessler, M., Mason, P.J. and Dokal, I. (2001) The RNA component of telomerase is mutated in autosomal dominant dyskeratosis congenita. Nature, 413, 432–435

41. Esquela-Kerscher, A.， Slack, F. J. (2006) OncomiRs — microRNAs with a role in cancer. Nature Rev. Cancer **6**, 259–269.

42. Calin, G. A. (2002) Frequent deletions and down-regulation of micro-RNA genes miR15 and miR16 at 13q14 in chronic lymphocytic leukemia. Proc. Natl Acad. Sci. USA **99**, 15524–15529.

43. Davalos, V. （2011） Dynamic epigenetic regulation of the microRNA‐200 family mediate epithelial and mesenchymal transitions in human tumorigenesis. Oncogene 383.

44. Krutzfeldt, J., Rajewsky, N., (2005) Braich R. Silencing of microRNAs in vivo with ‘antagomirs’. Nature 438: 685–689

45. Ma, L., Reinhardt, F., Pan, E., Soutschek, J., Bhat, B., Marcusson, E.G., Teruya-Feldstein, J., Bell, G.W., Weinberg, R.A. (2010) Therapeutic silencing of miR‐10b inhibits metastasis in a mouse mammary tumor model. Nature Biotech. 28, 341–347.

46. Kota, J., Chivukula, R.R., O'Donnell, K.A., Wentzel, E.A., Montgomery, C.L., Hwang, H.W., Chang, T.C., Vivekanandan, P., Torbenson, M., Clark, K.R., Mendell, J.R., Mendell, J.T. (2009) Therapeutic microRNA delivery suppresses tumorigenesis in a murine liver cancer model. Cell 137: 1005–1017

47. Sobczak, K., Krzyzosiak, W.J., (2002) Structural determinants of BRCA1 translational regulation. J. Biol. Chem 10:1074.

48. The ENCODE Project Consortium. Identification and analysis of functional elements in 1% of the human genome by the ENCODE pilot project. Nature 447,799–816 (2007).

49. Medina, P. P., Nolde, M., Slack, F. J. (2010) OncomiR addiction in an in vivo model of microRNA-21‐induced pre‐B‐cell lymphoma. Nature 467: 86–90

50. Lujambio, A., Portela, A., Liz, J., Melo, S. A., Rossi, S., Spizzo, R., Croce, C.M., Calin, G.A. and Esteller M. (2010). CpG island hypermethylationassociated silencing of non-coding RNAs transcribed from ultraconserved regions in human cancer. Oncogene 29: 6390–6401

51. Minna, J.D., Fong. K., Zochbauer-Muller, S., Gazdar, A.F. (2002) Molecular pathogenesis of lung cancer and potential translational applications. Cancer J 8(Suppl 1):S41–S46

52. Sekido, Y., Fong, K.M., Minna, J.D. (2003) Molecular genetics of lung cancer. Ann Rev Med 54:73–87

53. Wistuba, I.I., Gazdar, A.F., Minna, J.D. (2001) Molecular genetics of small cell lung carcinoma. Semin Oncol 28:3–13

54. Lerman, M.I., Minna, J.D. (2000) The 630-kb lung cancer homozygous deletion region on human chromosome 3p21. 3: identification and evaluation of the resident

candidate tumor suppressor genes. The International Lung Cancer Chromosome 3p21. 3 Tumor Suppressor Gene Consortium. Cancer Res 60:6116–6133

55. Zabarovsky, E.R., Lerman, M.I., Minna, J.D. (2002) Tumor suppressor genes on chromosome 3p involved in the pathogenesis of lung and other cancers. Oncogene 21:6915– 6935

56. Ji, L., Nishizaki, M., Gao, B., Burbee, D., Kondo, M., Kamibayashi, C., Xu, K., Yen, N., Atkinson, E.N., Fang, B., Lerman, M.I., Roth, J.A., Minna, J.D. 2002. Expression of several genes in the human chromosome 3p21.3 homozygous deletion region by an adenovirus vector results in tumor suppressor activities in vitro and in vivo. Cancer Res 62:2715–2720

57. Ji, L., Minna, J.D., Roth, J.A. 2005. 3p21.3 tumor suppressor cluster: prospects for translational applications. Future Oncol 1:79 –92

58. Uno, F., Sasaki, J., Nishizaki, M., Carboni, G., Xu, K., Atkinson, E.N., Kondo, M., Minna, J.D., Roth, J.A., Ji, L. 2004. Myristoylation of the FUS1 protein is required for tumor suppression in human lung cancer cells. Cancer Res 64:2969 –2976

59. Kondo, M., Ji, L., Kamibayashi, C., Tomizawa, Y., Randle, D., Seiko, Y., Yokota, J., Kashuba, V., Zabarovsky, E., Kuzmin, I., Lerman, M., Roth, J., Minna, JD. 2001. Overexpression of candidate tumor suppressor gene FUS1 isolated from the 3p21. 3 homozygous deletion region leads to G1 arrest and growth inhibition of lung cancer cells. Oncogene 20: 6258–6262

60. Prudkin, L., Behrens, C., Liu, D.D., Zhou, X., Ozburn NC, Bekele BN, Minna JD, Moran C, Roth JA, Ji L, Wistuba II. 2008. Loss and reduction of FUS1 protein expression is a frequent phenomenon in the pathogenesis of lung cancer. Clin Cancer Res 14: 41– 47

61. Lin, J., Sun, T., Ji, L., Deng, W., Roth, J.A., Minna, J.D., Arlinghaus, R. 2007. Oncogenic activation of c-Abl in non-small cell lung cancer cells lacking FUS1 expression: inhibition of c-Abl by the tumor suppressor gene product FUS1. Oncogene 26:6989-96

62. Deng, W.G., Wu, G., Ueda, K., Xu, K., Roth, J.A., Ji, L. 2008. Enhancement of antitumor activity of cisplatin in human lung cancer cells by tumor suppressor TUSC2. Cancer Gene Ther 15(1): 29-39

63. Mignone, F., Gissi, C., Liuni, S., Pesole, G. 2002. Untranslated regions of mRNAs. Genome Biol: 3-4

64. Gray, N.K., and Wickens, M.P. 1998. Control of translation initiation in animals. Annu Rev Cell Dev Biol. 14, 399–458

65. Wickens, M., Anderson, P., Jackson, R.J. (1997) Life and death in the cytoplasm: messages from the 3' end. Curr Opin Genet Dev 7: 220–232

66. Hershey, J.W.B. and Merrick, W.C. (2000) Pathway and mechanism of initiation of protein synthesis. In Translational Control of Gene Expression. 33-88. Cold Spring Harbour Laboratory Press.

67. Kozak, M. (1984) Point mutations close to the AUG initiator codon affect the efficiency of translation of rat preproinsulin in vivo. Nature 308 (5956): 241–246

68. Baulcombe, D.C. and Zamore, P.D. 2010. Welcome to silence. Silence 1: 1.

69. Ghildiyal, M. and Zamore, P.D. 2009. Small silencing RNAs: an expanding universe. Nat Rev Genet 10: 94-108.

70. Du, T. and Zamore, P.D. 2007. Beginning to understand microRNA function. Cell research 17: 661-663.

71. Zamore, P.D. and Haley, B. 2005. Ribo-gnome: the big world of small RNAs. Science 309:1519-1524.

72. Ambros, V. 2008. The evolution of our thinking about microRNAs. Nat Med 14: 1036-1040.

73. Bartel, D.P. 2004. MicroRNAs: genomics, biogenesis, mechanism, and function. Cell 116: 281-297.

74. Bartel, D.P. 2009.MicroRNAs: target recognition and regulatory functions. Cell 136: 215-233.

75. Ambros, V. 2004. The functions of animal microRNAs. Nature 431: 350-355.

76. Berezikov, E. 2011. Evolution of microRNA diversity and regulation in animals. Nat Rev Genet 12: 846-860.

77. Calin GA and Croce, C.M. 2006. MicroRNA signatures in human cancers. Nat Rev Cancer 6: 857-866.

78. Du, T. and Zamore, P.D. 2005. microPrimer: the biogenesis and function of microRNA. Development 132: 4645-4652.

79. Hutvagner, G. and Zamore, P.D. 2002. A microRNA in a multiple-turnover RNAi enzyme complex. Science 297: 2056-2060.

80. Berezikov, E., Robine, N., Samsonova, A., Westholm, J.O., Naqvi, A., Hung, J.H., Okamura, K., Dai, Q., Bortolamiol-Becet, D., Martin, R. Zhao, Y.J., Zamore, P.D., Hannon, G.J., Marra M.A., Weng, Z.P., Perrimon, N., Lai, E.C. 2011. Deep annotation of Drosophila melanogaster microRNAs yields insights into their processing, modification, and emergence. Genome Res 21: 203-215.

81. Friedlander, M.R., Chen, W., Adamidi, C., Maaskola, J., Einspanier, R., Knespel, S. and Rajewsky, N. 2008. Discovering microRNAs from deep sequencing data using miRDeep. Nat Biotechnol 26: 407-415.

82. Berezikov, E., Cuppen, E. and Plasterk, R.H. 2006. Approaches to microRNA discovery. Nat Genet 38: Suppl, S2-7.

83. Brennecke, J. and Cohen, S.M. 2003. Towards a complete description of the microRNA complement of animal genomes. Genome Biol 4: 228.

84. Krichevsky, A.M., King, K.S., Donahue, C.P., Khrapko, K. and Kosik, K.S. 2003. A microRNA array reveals extensive regulation of microRNAs during brain development. RNA 9: 1274-1281.

85. Liu, C.G., Calin, G.A., Meloon, B., Gamliel, N., Sevignani, C., Ferracin, M., Dumitru, C.D., Shimizu, M., Zupo, S., Dono, M., Alder, H., Bullrich, F., Negrini,

M., Croce, C.M. 2004. An oligonucleotide microchip for genome-wide microRNA profiling in human and mouse tissues. Proc Natl Acad Sci U S A 101: 9740-9744.

86. Lu, J., Getz, G., Miska, E.A., Alvarez-Saavedra, E., Lamb, J., Peck, D., Sweet-Cordero, A., Ebert, B.L., Mak, R.H., Ferrando, A.A., Downing, J.R., Jacks, T., Horvitz H.R., Golub T.R. 2005. MicroRNA expression profiles classify human cancers. Nature 435: 834-838.

87. Nelson, P.T., Baldwin, D.A., Scearce, L.M., Oberholtzer, J.C., Tobias, J.W. and Mourelatos, Z. 2004. Microarray-based, high-throughput gene expression profiling of microRNAs. Nat Methods 1: 155-161.

88. Neely, L.A., Patel, S., Garver, J., Gallo, M., Hackett, M., McLaughlin, S., Nadel, M., Harris, J., Gullans, S. and Rooke, J. 2006. A single-molecule method for the quantitation of microRNA gene expression. Nat Methods 3: 41-46.

89. Palmer, S., Wiegand, A.P., Maldarelli, F., Bazmi, H., Mican, J.M., Polis, M., Dewar, R.L., Planta, A., Liu, S., Metcalf, J.A., Mellors, J.W., Coffin, J.M. 2003. New real-time reverse transcriptase-initiated PCR assay with single-copy sensitivity for human immunodeficiency virus type 1 RNA in plasma. Journal of clinical microbiology 41: 4531-4536.

90. Chen, C., Ridzon, D.A., Broomer, A.J., Zhou, Z., Lee, D.H., Nguyen, J.T., Barbisin, M., Xu, N.L., Mahuvakar, V.R., Andersen, M.R. 2005. Real-time quantification of microRNAs by stem-loop RT-PCR. Nucleic Acids Res 33: e179.

91. Imle, P. 2005. Fluorescence-based fragment size analysis. Methods Mol Biol 311: 139-146.

92. Gee, H.E., Buffa, F.M., Camps, C., Ramachandran, A., Leek, R., Taylor, M., Patil, M., Sheldon, H., Betts, G., Homer, J. et al. (2011) The small-nucleolar RNAs commonly used for microRNA normalisation correlate with tumour pathology and prognosis. British journal of cancer 104: 1168-1177.

93. Abbott, A.L., Alvarez-Saavedra, E., Miska, E.A., Lau, N.C., Bartel, D.P., Horvitz, H.R. and Ambros, V. (2005) The let-7 MicroRNA family members mir-48, mir-84, and mir-241 function together to regulate developmental timing in Caenorhabditis elegans. Developmental cell 9: 403-414.

94. Kozomara, A. and Griffiths-Jones, S. (2011) miRBase: integrating microRNA annotation and deep-sequencing data. Nucleic Acids Res 39: D152-157.

95. Martinez, J., Patkaniowska, A., Urlaub, H., Luhrmann, R. and Tuschl, T. (2002) Single-stranded antisense siRNAs guide target RNA cleavage in RNAi. Cell 110: 563-574.

96. Lim, L.P., Lau, N.C., Garrett-Engele, P., Grimson, A., Schelter, J.M., Castle, J., Bartel, D.P., Linsley, P.S. and Johnson, J.M. (2005) Microarray analysis shows that some microRNAs downregulate large numbers of target mRNAs. Nature 433: 769-773.

97. Lewis, B.P., Shih, I.H., Jones-Rhoades, M.W., Bartel, D.P. and Burge, C.B. (2003) Prediction of mammalian microRNA targets. Cell 115: 787-798

98. Broderick, J.A. and Zamore, P.D. (2011) MicroRNA therapeutics. Gene Ther 18: 1104-1110.

99. Castanotto, D. and Rossi, J.J. (2009) The promises and pitfalls of RNA-interference-based therapeutics. Nature 457: 426-433.

100. Landgraf, P., Rusu, M., Sheridan, R., Sewer, A., Iovino, N., Aravin, A., Pfeffer, S., Rice, A., Kamphorst, A.O., Landthaler, M. et al. (2007) A mammalian microRNA expression atlas based on small RNA library sequencing. Cell 129: 1401-1414.

101. Alvarez-Garcia, I. and Miska, E.A. (2005) MicroRNA functions in animal development and human disease. Development 132: 4653-4662.

102. Polisky, B., Greene, P., Garfin, D.E., McCarthy, B.J., Goodman, H.M. and Boyer, H.W. (1975) Specificity of substrate recognition by the EcoRI restriction endonuclease. Proc Natl Acad Sci U S A 72: 3310-3314.

103. Chandrashekaran, S., Saravanan, M., Radha, D.R. and Nagaraja, V. (2004) Ca(2+)-mediated site-specific DNA cleavage and suppression of promiscuous activity of KpnI restriction endonuclease. J Biol Chem 279: 49736-49740.

104. Ameres, S.L., Horwich, M.D., Hung, J.H., Xu, J., Ghildiyal, M., Weng, Z. and Zamore, P.D. (2010) Target RNA-directed trimming and tailing of small silencing RNAs. Science 328: 1534-1539.

105. Cheloufi, S., Dos Santos, C.O., Chong, M.M. and Hannon, G.J. (2010) A dicer-independent miRNA biogenesis pathway that requires Ago catalysis. Nature 465: 584-589.

106. Janowski, B.A., Huffman, K.E., Schwartz, J.C., Ram, R., Nordsell, R., Shames, D.S., Minna, J.D. and Corey, D.R. (2006) Involvement of AGO1 and AGO2 in mammalian transcriptional silencing. Nature Structural & Molecular Biology 13: 787-792.

107. Broderick, J.A., Salomon, W.E., Ryder, S.P., Aronin, N. and Zamore, P.D. (2011) Argonaute protein identity and pairing geometry determine cooperativity in mammalian RNA silencing. RNA 17: 1858-1869

108. Cenik, E.S. and Zamore, P.D. (2011) Argonaute proteins. Current biology: CB, 21, R446-449.

109. Hutvagner, G. and Simard, M.J. (2008) Argonaute proteins: key players in RNA silencing. Nat Rev Mol Cell Biol 9: 22-32.

110. Behlke, M.A. (2006) Progress towards in vivo use of siRNAs. Molecular therapy : the journal of the American Society of Gene Therapy 13: 644-670.

111. Fromont-Racine, M., Bertrand, E., Pictet, R. and Grange, T. (1993) A highly sensitive method for mapping the 5' termini of mRNAs. Nucleic Acids Res 21: 1683-1684

112. Lee, R.C., Feinbaum R.L. and Ambros V. (1993) The C. elegans Heterochronic gene lin-4 encodes small RNAs with antisense complementarity to lin-14. Cell 75: 843-845

113. Mariana Lagos-Quintana, Rauhut R., Lendeckel W., Tusch T. (2001) Identification of novel genes coding for small expressed RNAs. Science 294: 853-858

114. Nelson, C. L., Lim, L. P., Weinstein, E.G., Bartel, D.P. (2001) An Abundant Class of Tiny RNAs with Probable Regulatory Roles in Caenorhabditis elegans. Science 294: 858-862

115. Lee, R.C., Ambros, V. (2001) An extensive class of small RNAs in Caenorhabditis elegans. Science 294:862-864

116. Schwarz, D.S., and Zamorel, P.D. (2002). Why do miRNAs live in the miRNP? Genes & Development 16 (9):1025–1031

117. Rhoades, M.W., Reinhart, B.J., Lim, L.P., Burge, C.B., Bartel, B., Bartel, D.P. (2002) Prediction of plant microRNA targets. Cell 110 (4):513-520

118. Bartel, D.P. (2009) MicroRNAs: Target Recognition and regulatory Functions. Cell 136: 215-233

119. Lim, L.P., Lau, N.C., Garrett-Engele, P., Grimson, A., Schelter, J.M., Castle, J., Bartel, D.P., Linsley, P.S., and Johnson, J.M. (2005) Microarray analysis shows that some microRNAs downregulate large numbers of target mRNAs. Nature 433: 769–773.

120. Baek, D., Ville´n, J., Shin, C., Camargo, F.D., Gygi, S. P., Bartel, D.P. (2008) The impact of microRNAs on protein output. Nature 455:64-73

121. Guo, H.l., Ingolia, N.T., Weissman, J.S., Bartel, D.P. (2010) Mammalian microRNAs predominantly act to decrease target mRNA levels. Nature 466: 835–840

122. Sasaki, T., Shiohama, A., Minoshima, S., Shimizu N. (2003) Identification of eight members of the Argonaute family in the human genome. Genomics 82: 323–330

123. Liu, J.D., Carmell, M.A., Rivas, F.V., Marsden, C.G., Thomson, J. M., Song, J. J., Hammond, S.M., Joshua-Tor, L., Hannon., G.J. (2004) Argonaute2 is the catalytic engine of mammalian RNAi. Science: 305 (5689) 1437-1441.

124. Eulalio, A., Huntzinger, E., Nishihara, T., Rehwinkel, J., Fauser, M., Izaurralde, E. (2009) Deadenylation is a widespread effect of miRNA regulation. RNA 15: 21–32

125. Yekta, S., I-hung, S., Bartel, D.P. (2004) MicroRNA-directed cleavage of HOXB8 mRNA. Science 304: 594–596

126. Karginov, F.V., Cheloufi, S., Chong, M.M., Stark, A., Smith, A.D., Hannon, G.J. (2010) Diverse endonucleolytic cleavage sites in the mammalian transcriptome depend upon microRNAs, Drosha, and additional nucleases. Mol. Cell 38:781–788.

127. Shin, C., Nam, J.W., Farh, K.K., Chiang, H.R., Shkumatava, A., Bartel,D.P. (2010) Expanding the microRNA targeting code: functional sites with centered pairing. Mol. Cell 38: 789–802.

128. Mayr, C., Hemann, M.T., Bartel, D.P. 2007. Disrupting the pairing between let-7 and Hmga2 enhances oncogenic transformation. Science 315: 1576-1579.

129. Thanos, D., Maniatis, T. (1995) Virus induction of human IFN beta gene expression requires the assembly of an enhanceosome. Cell 83: 1091-1100

130. Schoenberg Fejzo, M., Ashar, H.R., Krauter, K.S., Powell, W.L., Rein, M.S., Weremowicz, S., Yoon, S.J., Kucherlapati, R.S., Chada, K., Morton, C.C. (1996) Translocation breakpoints upstream of the HMGIC gene in uterine leiomyomata suggest dysregulation of this gene by a mechanism different from that in lipomas. Genes Chrom. Cancer 17: 1-6.

131. Reinhart, B.J., Slack, F.J., Basson, M., Pasquinelli, A.E., Bettinger, J.C., Rougvie, A.E., Horvitz, H.R., Ruvkun, G. (2000) The 21-nucleotide let-7 RNA regulates developmental timing in Caenorhabditis elegans. Nature 403(6772):901-6

132. Shen B.Z. and Goodman, H.M. (2004) Uridine addition after microRNA-directed cleavage. Science 306(5698):997

133. Mullen, T.E., Marzluff, W.F. (2008) Degradation of histone mRNA requires oligouridylation followed by decapping and simultaneous degradation of the mRNA both 5' to 3' and 3' to 5'. Genes and Development 22:50–65

134. Song, M.G., Kiledjian, M. (2007) 3' Terminal oligo U-tract-mediated stimulation of decapping. RNA 13:2356–2365

135. Grimson, A., Farh, K.K., Johnston, W.K., Garrett-Engele, P., Lim, L.P, Bartel, D.P. (2007) MicroRNA targeting specificity in mammals: Determinants beyond seed pairing. Mol. Cell 27: 91–105.

136. Du, L., Schageman, J.J., Subauste, M.C., Saber, B., Hammond, S.M., Prudkin, L., Wistuba, I.I., Ji, L., Roth, J.A., Minna, J.D., Pertsemlidis, A. (2009) miR-93, miR-98, and miR-197 regulate expression of tumor suppressor gene FUS1. Mol Cancer Res 7(8):1234-43

137. Bracken, C. P., Szubert, J. M., Mercer, T.R., Dinger, M.E., Thomson, D.W., Mattick, J.S., Michael, M.Z., Goodall, G.J. (2011) Global analysis of the mammalian RNA degradome reveals widespread miRNA-dependent and miRNA-independent endonucleolytic cleavage. Nucleic Acids Research 39 (13): 5658–5668.

138. Djuranovic, S., Nahvi, A., Green, R. (2011) A parsimonious model for gene regulation by miRNAs. Science 331: 550-553

139. Huntzinger, E. and Izaurralde, E. (2011) Gene silencing by microRNAs: contributions of translational repression and mRNA decay. Nature Reviews|Genetics 12:99-110

140. Schoenberg, D.R. and Maquat, L.E. (2012) Regulation of cytoplasmic mRNA decay. Nature Reviews|Genetics 13: 246-259

141. Wu, L., Fan, J., Belasco, J.G. (2006) MicroRNAs direct rapid deadenylation of mRNA. Proc. Natl Acad. Sci. USA 103:4034–4039

142. Eulalio, A., Behm-Ansmant, I., Schweizer D., Izaurralde, E.(2007) P-Body formation is a consequence, not the cause, of RNA-mediated gene silencing. Molecular and cellular biology 27 (11):3970–3981

143. Garneau, N.L., Wilusz, J., Wilusz, C.J. (2007) The highways and byways of mRNA decay. Nature reviews, Molecular cell biology 8:113-126

144. Lu, J., Getz, G., Miska, E.A., Alvarez-Saavedra, E., Lamb, J., Peck, D., Sweet-Cordero, A., Ebert, B.L., Mak, R.H., Ferrando, A.A., Downing, J.R., Jacks, T., Horvitz, H.R., Golub, T.R. (2005) MicroRNA expression profiles classify human cancers. Nature 435:834-838

145. Pritchard, C.C., Cheng, H.H., Tewari, M. (2012) MicroRNA profiling: approaches and considerations. Nature Genetics 13:358-369

146. Lee, D.Y., Deng, Z., Wang, C.H., Yang, B.B. (2007) MicroRNA-378 promotes cell survival,tumor growth, and angiogenesis by targeting SuFu and Fus-1 expression, Proc.Natl. Acad. Sci. USA 104: 20350–20355.

VITA

Jing Lin was born in Jinhua, China on November 10, 1982, the daughter of Yaolong Lin and Jinfang Zhu. After completing her high school at The First High School of Jinhua, Zhejiang, China in 2000, she entered Ningbo University in Ningbo, China. She received the degree of Bachelor of Science with a major in Biology from Ningbo University in July, 2004. For the next two and a half years, she entered Dr. Xiaojun Yan's lab and received the degree of Master Science in Ningbo University in 2007. Then she enrolled in Biomedical Science at Graduate School of Biomedical Science in the University of Texas M.D. Anderson Cancer Center in 2007 (Advisor, Ji Lin Ph.D.).

Permanent address:

Apt 102, Building 6, Lane 1,

Jinhua,

Zhejiang, China, 321000

Publications

Jing Lin, Kai Xu, Jayachandran Gitanjali, Jack A. Roth, Lin Ji, (2011) Regulation of tumor suppressor gene FUS1 expression by the untranslated regions of mRNA in human lung cancer cells, Biochemical and Biophysical Research Communications 410(2):235-241.

Jing Lin, Kai Xu, Jack A. Roth, Lin Ji, Detection of intermediates and end products of microRNA processing in human cells by a novel stem-loop Array RT-PCR. Nuclei Acids Research (submitted)